• U C •

FCTUC FACULDADE DE CIÊNCIAS
E TECNOLOGIA
UNIVERSIDADE DE COIMBRA

Neuroengineering Contributions in Parkinsonic Tremor Characterization Using Accelerometry and Surface Electromyography

Adriana Costa Leal

A thesis submitted for the degree of
Master of Biomedical Engineering
at the University of Coimbra

February 2015

Neuroengineering Contributions in Parkinsonic Tremor Characterization Using Accelerometry and Surface Electromyography

Author:
Adriana Costa Leal

Supervisors:
Prof. Dra. Paula Pascoal-Faria
Prof. Dr. Miguel Castelo-Branco

Dissertation presented to the Faculty of Sciences and Technology of the University of Coimbra to obtain a Master's degree in Biomedical Engineering

Coimbra, 2015

Este trabalho foi desenvolvido em colaboração com:

Faculty of Medicine - University of Coimbra

FMUC FACULDADE DE MEDICINA
UNIVERSIDADE DE COIMBRA

IBILI - Institute for Biomedical Imaging and Life Sciences

ICNAS - Institute of Nuclear Sciences Applied to Health

ICNAS INSTITUTO DE CIÊNCIAS NUCLEARES
APLICADAS À SAÚDE
UNIVERSIDADE DE COIMBRA

Dedico esta tese aos meus pais e ao meu irmão

Abstract

Parkinson's Disease (PD) is associated to a dopaminergic neural loss in the nigrostriatal pathway. Consequently, the temporal organization of motor cortical activity during muscle contraction and movement planning and execution will be affected. Disturbances of the dopaminergic system can lead to widespread motor symptoms such as involuntary oscillatory movements (tremor), bradykinesia, muscle rigidity and postural instability and also cognitive impairments.

Tremor in PD may occur in a rest or posture position or in both situations. Rest and posture tremors can overlap in frequency. It has been reported that, during rest, tremor exists in the 4 to 6 Hz range. Concerning postural tremor, it typically ranges between 5 and 12 Hz, making it difficult to distinguish both types of tremor, because of the overlapping frequencies.

This study presents a quantitative behavioural analysis of rest and posture PD tremor in an functional magnetic resonance imaging (fMRI) noisy environment. It aims to implement algorithms able to characterize the amplitude and frequency of PD tremor when a task comprising rest and postural arm positions was performed. To assess and quantify tremor, both accelerometry and surface electromyography (sEMG) were used, as they are the most common techniques to efficiently detect and quantify tremor in PD patients. Six runs were performed and, in half of them, a superimposed load was placed in the participant's wrist. This preliminary study included three idiopathic PD patients.

Off-line processing started by filtering the sEMG signals to remove fMRI artifacts, particularly high frequency content resulting from the radio frequency (RF) pulses and the harmonic related frequencies originated by the magnetic field gradient applied to acquire the fMRI data. Then, the frequency spectrum was inspected in order to assess the frequency and amplitude changes across resting and postural tremor conditions. Parameters such as peak frequency and power and total power were computed. The envelope of the sEMG signals was also assessed and the area under the envelope was computed for each segment. Tremor and nontremor intervals were determined for each run and each patient and used in a general linear model (GLM) multi-study analysis.

An additional correlation analysis was performed to understand which were the most contributing frequency bands for the signal power. The observed blood oxygen level dependent (BOLD) signal changes could also be correlated with the different frequency ranges, in a voxel-by-voxel analysis.

Our results confirmed that an upper limb postural position is able to considerably increase tremor amplitude when compared to an upper limb rest condition. Plots of frequency in function of amplitude showed a distinct peaks in the 5 to 12 Hz frequency range. Particularly, in one patient peaks around 5 Hz were identified in the postural segments and second peaks were also found in the 10 Hz frequency. The latter were absent in the other two patients. The study of a larger and homogeneous population would clarify if the identified peaks correspond to postural tremor or to re-emergent rest tremor, since they can coexist at this frequency range. Increasing the number of participants will also allow to study the effect of loading, which seems to provoke slight and negligible changes in tremor amplitude (in agreement with what had been reported in some studies in literature).

Using the signal processing methodology developed throughout this thesis to analyse accelerometry and sEMG signals recorded in a fMRI environment it could be possible to distinguish rest from postural tremor. Additionally, concomitant acquisition of functional images of the brain can provide an insight of which regions are activated when different tasks designed to modulate tremor are performed. The combined information provided by the three techniques, accelerometry, sEMG and fMRI can be determinant to characterize and separate PD tremors and identify the correspondent brain generators.

Keywords: Parkinson Disease, Tremor, Accelerometry, Surface Electromyography, Functional Magnetic Resonance Imaging

Resumo

A Doença de Parkinson (DP) está associada a uma perda de neurónios produtores de dopamina no sistema nigroestriatal. Por consequência, a organização temporal da actividade motora cortical durante a contracção muscular e planeamento e execução de movimento vai ser afectada. Distúrbios no sistema dopaminérgico podem levar à manifestação de sintomas motores tais como movimentos oscilatórios involuntários (tremor), bradicinesia, rigidez muscular e instabilidade postural e também défices cognitivos.

O tremor na DP pode ocorrer numa posição de repouso ou de postura, ou em ambas as situações. Os tremores de repouso e postural podem sobrepôr-se na frequência. Vários estudos têm evidenciado que o tremor de repouso se manisfesta no intervalo de 4 a 6 Hz. Por outro lado, o tremor postural revela-se tipicamente na gama de 5 a 12 Hz, o que torna difícil distinguir ambos os tipos de tremor em termos da distribuição de frequências.

Este estudo apresenta uma análise comportamental quantitativa dos tremores de repouso e postural na DP associada a um estudo de imagem por ressonância magnética functional (fMRI em inglês). O objectivo é implementar algoritmos que consigam caracterizar a frequência e amplitude do tremor na DP manifestado quando é realizada uma tarefa em que a posição do braço do participante alterna entre o repouso e a postura. Para avaliar e quantificar o tremor durante a realização da tarefa foram adquiridos simultaneamente sinais de acelerometria e electromiografia de superfície (sEMG). Estas duas técnicas têm sido frequentemente utilizadas para detectar e quantificar o tremor na DP. A tarefa foi realizada seis vezes em cada sessão sendo que em três delas foi adicionado um peso a cada pulso do participante. Este estudo preliminar incluiu três doentes parkinsónicos idiopáticos.

Na análise off-line, os sinais de acelerometria e sEMG foram filtrados removendo assim os artefactos introduzidos pelo pulso de radiofrequências e pelos gradientes de campo magnético aplicados durante a acquisição das imagens funcionais. De seguida, procedeu-se à inspecção do espectro de frequências por forma a avaliar as alterações a nível de amplitude e frequência ao longo da realização da tarefa. Foram calculados parâmetros tais como picos de potência e

frequência correspondente e potência total do espectro para cada um dos segmentos da tarefa (em repouso e na postura). O envelope do sinal foi também avaliado e a área abaixo do envelope foi determinada para cada segmento da tarefa. Foram também determinados os intervalos em que há tremor para cada sinal, sendo essa informação utilizada numa análise multi-estudos que aplica o Modelo Linear Geral (GLM, em inglês). Foi ainda realizada uma análise adicional com o objectivo de perceber quais as bandas de frequência que mais contribuem para a potência do sinal. As gamas de frequência podem também ser correlacionadas com as alterações observadas no sinal BOLD (*Blood Oxygen Level Dependent*).

Os resultados confirmaram que a manutenção dos braços numa posição postural origina um aumento considerável da amplitude do tremor, comparando com a posição de repouso. Os gráficos da frequência em função da amplitude mostraram picos distintos no intervalo de frequências de 5 a 12 Hz. Nomeadamente, num dos doentes foram identificados picos de potência próximos de 5 Hz nos segmentos de postura. Foram ainda identificados segundos picos perto de 10 Hz. Estes últimos estão ausentes nos gráficos dos segmentos de postura para os outros dois doentes. O estudo de uma população maior e homogénea vai esclarecer que tipo de tremor, postural ou reemergente, dá origem aos picos identificados, sendo que ambos os tremores podem co-existir na mesma gama de frequências. Aumentar o número de participantes vai permitir estudar o efeito da introdução de um peso durante a tarefa, o que se verificou que não resultar em alterações consideráveis na amplitude do tremor.

A metodologia de processamento de sinal desenvolvida ao longo desta tese teve como objectivo analisar sinais de acelerometria e electromiografia de superfície adquiridos dentro de um scanner de ressonância magnética. Foram ainda calculados parâmetros que possibilitam a distinção dos tremores de repouso e postural. Adicionalmente, a obtenção simultânea de imagens funcionais pode revelar informação acerca das regiões do cérebro que são activadas quando diferentes tarefas concebidas para modular o tremor são executadas. Combinar a informação fornecida pelas três técnicas, acelerometria, sEMG e fMRI pode ser determinante na caracterização e separação dos tremores da DP e também na identificação dos circuitos cerebrais que os desencadeiam.

Palavras-chave: Doença de Parkinson, Tremor, Acelerometria, Electromiografia de Superfície, Imagem por Ressonância Magnética Funcional

Acknowledgements

Em primeiro lugar, quero expressar os meus agradecimentos aos meus orientadores Dra. Paula Pascoal-Faria e Dr. Miguel Castelo-Branco por todo o apoio e a orientação prestados durante este projeto de investigação.

Um obrigada a todas as pessoas que me foram esclarecendo pequenas e grandes dúvidas ao longo deste empreendimento, nas quais se inclui o Dr. Marco Gomes, o Dr. Miguel Patrício, o Dr. César Teixeira, a Catarina Duarte e o Pedro Vaz.

Agradeço também às instituições acolhedoras do meu projeto, o Instituto Biomédico de Investigação de Luz e Imagem (IBILI) da Faculdade de Medicina da Universidade de Coimbra e o Instituto de Ciências Nucleares Aplicadas à Saúde (ICNAS) da Universidade de Coimbra por oferecerem as condições necessárias ao arranque e desenvolvimento desta tese. Quero ainda agradecer ao Dr. Miguel Morgado pela disponibilidade mostrada para resolução de problemas e aconselhamento durante todo o Mestrado Integrado em Engenharia Biomédica.

Acrescento também que tudo teria sido mais difícil sem a presença constante da Mafalda, do Fábio, do Gonçalo e restantes amigos.

E por fim, o meu maior agradecimento é dirigido aos meus pais e ao meu irmão e a toda a família. Sem eles o meu percurso teria perdido toda a piada!

Muito obrigada a todos!

List of Publications

P. Faria, **A. Leal**, A. Freire, C. Januário, M. Patrício, and M. Castelo-Branco, "Quantication and Modulation of Tremor in Rapid Upper Limb Movements" in The International Conference on Health Informatics SE - 86 (Y.-T. Zhang,ed.), vol. 42 of IFMBE Proceedings, pp. 339342, Springer International Publishing, 2014.

P. Pascoal-Faria, M. Patrício, **A. Leal**, F. Caramelo, A. Freire, C. Januário, and M. Castelo-Branco, "Understanding Tremor in Rapid Upper Limb Movements Using 3D Accelerometers Data", Neuroscience & Medicine, vol. 05, pp. 205213, Oct. 2014.

Review in preparation: "Tremor Modulation in Parkinson's Disease" with contributions from P. Pascoal-Faria, A. Leal, M. Patrício, M. Castelo-Branco and T. Saifee.

Contents

List of Figures

List of Tables

List of Acronyms

APB abductor pollicis brevis

AUC area under the curve

BDI-II Beck Depression Inventory

BOLD blood oxygen level dependent

CWT continuous wavelet transform

DBS Deep Brain Stimulation

DWT Discrete Wavelet Transform

FFT fast Fourier transform

FIR finite impulse response

fMRI functional magnetic resonance imaging

EPI echo-planar imaging

ET Essential Tremor

FT Fourier transform

HRF hemodynamic response function

IIR infinite impulse response

ISEK International Society of Electrophysiology and Kinesiology

GLM general linear model

PD Parkinson's Disease

PA peak amplitude

PF peak frequency

PSD power spectral density

MEM micro electro-mechanical systems

MoCA Montreal Cognitive Assessment

MU motor unit

MVC Maximal Voluntary Contraction

TR repetition time

TE echo time

RF radio frequency

RMS root mean square

sEMG surface electromyography

SENIAM Surface Electromyography for Non-Invasive Assessment of Muscles

STFT short-time Fourier transform

UPDRS Unified Parkinson's Disease Rating Scale

WT Wavelet Transform

Chapter 1

Introduction

1.1 Motivation and Goals

Tremor is a clinical problem which has held the attention of researchers for several years. Specifically, tremor classification has been of major importance to determine a more accurate diagnostic and treatment.[1] In the first instance, tremor is defined as an involuntary movement oscillation, rhythmic and nearly sinusoidal, characterized by particular amplitude and frequency content.[2–4] Classification of the different types of tremor can be achieved by clinical subjective observation, standardized rating scales and signal processing methods.[2,5] However, a lack of standard criteria to differentiate efficiently the different types of tremor still exists because there are features of tremor that need to be better understood. For example, it has been reported a 40% misdiagnosis rate in a Parkinson's Disease (PD) population which presents mixed forms of rest and postural tremors.[6] Thus, the study of tremor is of critical importance to make possible an accurate classification of rest and postural tremor - the latter being present in both PD and Essential Tremor (ET) neurodegenerative disorders - and also improve differential diagnosis.[2,4,7,8]

Classification of tremor depends on the chosen criteria. In other words, the different types of tremor can be divided in two major groups, depending in which circumstances they occur, in rest or action tremor, the latter can include postural and kinetic tremors.[2,4,7,9,10] Tremor can also be classified according to its underlying cause in two main groups: physiological and pathological tremor, the latter including ET and PD which are reported to be the most diagnosed tremor disorders.[4,7,9,11]

Parkinson's disease is considered to be the most suitable clinical model to understand tremor. It is a chronic progressive neurological disorder with

motor and non-motor manifestations that will be responsible for the gradual decrease in quality of live of patients.[5,12,13] It is the second most common progressive neurodegenerative disease. It affects about one million Americans and more than five million subjects worldwide.[14,15] Moreover, it is expected an increase in PD prevalence in the next 20 years caused by population ageing. So the need has been recognized for more suitable methods to deeply and fully understand the triggers and neuronal circuits involved in this brain disease in order to develop suitable treatments, that could help to, at least, optimize patients' quality of life.[12,14]

Parkinson's disease results from disturbances in the dopaminergic system which will affect the function of neuromuscular system, resulting in movement abnormalities that typically include involuntary oscillatory movements (tremor at rest), bradykinesia (slowness of movements), muscle rigidity and postural instability - motor symptoms - accompanied by cognitive impairment, depression and sensory and sleep abnormalities - non-motor symptoms - among others.[4,5,7,12,16] Tremor is present in more than 70% of patients diagnosed with PD.[3,7] Its classic manifestation occurs in stable positions as rest tremor, although postural tremor is also been often seen in PD patients. These two types of tremor can be defined by frequency ranges that overlap - rest tremor occurs in the 4 to 7 Hz and postural tremor manifests in the 4 to 12 Hz frequency range.[10,15,17] Additionally, a re-emerging rest tremor can occur few seconds after patients stand in a postural position, presenting the same tremor frequency range of rest tremor and suggesting that both rest and re-emergent tremors are also triggered by the same pathophysiologic mechanism.[10,11,17,18] Finally, besides the classical rest or postural tremors, other types, such as kinetic tremor can occur in PD patients, depending on how voluntary movements of the limbs are performed.[5,6,8] In fact PD is a rather heterogeneous neurodegenerative disorder, with differences in expression among patients, thus increasing data variability.[11,13] Better characterization of rest and postural tremors is important in order to easily recognize them among the several parkinsonian tremor phenomenologies and reduce the misdiagnosis rate.[18,19]

In this study, tremor will be accessed and quantified using accelerometry and surface electromyography (sEMG). Those are the most reported techniques presented in literature. They are considered to be non painful, non invasive, easy to use and relatively low cost.[2,4,9,10] The acquired signals will then be processed off-line and tremor will be quantified using computational algorithms. Among other parameters, frequency and amplitude are often as-

sessed when studying tremor.[2,19,20]

Also, in previous works of our group[21–23] accelerometers were used to quantify tremor in idiopathic PD and ET patients and in a control cohort. The three groups performed different tasks combining blocks of resting with postural positions[21] and resting with kinetic movement[22,23] (see Procedures[22,23]). In both studies, a load condition was also tested by adding load to patients' wrists during some of the tasks performed. Fourier analysis was used to compute the area under the curve of the frequency versus amplitude. In the rest vs postural task results pointed to a higher tremor variation in the dominant arm (most affected limb). It was observed a statistically significant increase in tremor amplitude only for the unloaded tasks in PD patients comparing to controls.[21] On the other hand, in the rest vs kinetic task, loading allowed a better differentiation between the studied groups.[22,23] In both studies, the results obtained for the area under the curve did not enable to distinguish PD from ET tremor, which presented overlapping results. This work sheds a light on the motivation of this thesis, i.e, it helps to define which factors should be explored in order to understand which are the main causes that can trigger tremor modulation. Based on that, in this study it was decided to assess tremor using both accelerometry and sEMG techniques, to include blocks of resting and postural conditions in the task, to assess the effect of medication withdrawal and loading and finally to implement suitable signal processing algorithms, able to identify and characterize PD tremor. An accurate computation of rest and postural parameters, will improve its differentiation.

The study of tremor modulation can be assessed, simultaneously with accelerometers and sEMG. Adding neuroimaging techniques, namely functional magnetic resonance imaging (fMRI) will be of major importance to understand the neuronal circuits involved in PD tremor modulation and the functional connectivity of the involved brain areas.[5,24–26] Literature reports the existence of a tremor network that includes both basal ganglia and cerebellar circuits. However, tremor has not been associated with a specific generator in the brain. Therefore, fMRI can play an important role in the visualization of the brain regions responsible for triggering tremor.[9,27] The effect of rest and posture tasks on PD tremor will be analysed by correlating the changes in amplitude and frequency, assessed with accelerometry and sEMG, with the blood oxygen level dependent (BOLD) contrast functional images. During acquisition in the fMRI environment, sEMG signal is perturbed by artifacts of high amplitude and frequency that "hide" the real electromyographic signal. Thus, one of the

main purposes of this thesis is to accurately remove artifacts of the signal by developing two different approaches using signal processing methods. Such that critical pre-processing steps are very important for subsequent statistical modelling of the data.

Chapter 2

Tremor Classification

Tremor is a very common movement disorder symptom associated with several unanswered questions, mainly concerning its pathophysiology.[2,27] It is defined as an involuntary, roughly sinusoidal and rhythmic movement of a body part.[6] Amplitude and frequency are the most important neurophysiologic parameters and are widely used in tremor characterization.[2,15] Those parameters can describe the involuntary oscillatory motion manifested by tremor, which pathophysiology varies amongst all types of tremor and therefore still remains unclear.[2,20]

2.1 Tremor classification based on occurrence

In Parkinson's Disease (PD) rest tremor seems to be correlated with the rhythmic activity observed in basal ganglia structures and thalamus. On the other hand, only postural tremor has been reported to be the result of the activity in cerebellum. Therefore, eventually, rest and postural tremors in PD can be modulated by different neural networks.[28]

2.1.1 Rest tremor

Rest tremor can be characterized by a "pill-rolling" tremor which occurs when the body part stands in a relaxed position, completely supported against gravity (e.g., forearm resting on a chair), without any voluntary muscle action.[2,4,7–10,29] Tremor amplitude increases with mental stress (e.g., cognitive task performance such as counting backwards) or when performing an action with another body part (e.g., walking) and decreases when an action is performed by the affected limb or even disappears during sleep.[2,4,5,7,9,15,29] This

tremor has been reported to manifest also as a re-emergent tremor, it diminishes or even vanishes when subject performs any movement of the affected body part and reappears, with the same frequency, a few seconds after that member is kept static in a postural position.[2,4,5,8,10,11,18,27,29,30] Rest tremor is characterized by sinusoidal oscillations and a frequency that ranges between 4 Hz to 7 Hz (see Table 2.1). Re-emergent tremor was reported to present a 5.5 Hz mean frequency.[5] The major cause of rest tremor is idiopathic PD, which in turn is the most common cause of parkinsonism. More than 70 % of patients diagnosed with PD manifest rest tremor at disease onset (usually after the age of 60), slowly progressing during the course of the disease.[5,7,9,10,16,29] It was also reported a 68% to 100% prevalence of rest tremor, sometime during the patients' disease course.[17]

2.1.2 Action tremor

Action tremor manifests when performing voluntary muscle contraction.[2,4,7,15] This tremor is the major responsible for patients' motor disability.[17] It is characterized by a higher frequency range than rest tremor and non-harmonically related.[2,11]

Action tremor includes postural, kinetic, intention, isometric and task-specific tremors.[2,7,10,15] Task-specific and intention tremors are considered by some authors as subtypes of kinetic tremor.[2,6] Task-specific tremor can be caused by the execution of certain tasks such as writing or playing a musical instrument. This type of tremor has not gathered consensus in the scientific community in terms of its origin and nature, being considered by some authors as a subtype of essential tremor.[2,4,10] Intention tremor occurs when the subject voluntary and physically interacts with some object, after previous observation (visually guided or target-directed movements). It develops due to the cerebellum lesions and can be identified with a finger-to-nose test.[2,4,7,10] Isometric tremor develops when a muscle contracts against a stationary/fixed object, without moving the affected part (e.g., when making a fist).[2,4,7,10,15] Postural and kinetic tremors will be presented below using more detailed information.

2.1.2.1 Postural tremor

Postural tremor manifests in up to 60% of PD patients and is more prominent and disabling than rest tremor, which encourages its accurate classification.[5,10] It can be observed when the affected limb is positioned on the opposite direc-

Table 2.1: Frequency of rest, postural and action tremors

Tremor / Author	Rest	Postural	Action
Edwards et. al.[29]	3-4 Hz	6-8 Hz	
Massano & Bhatia[31]	3-6 Hz		
Hess et. al.[2]			5-8 Hz
Grimaldi et. al.[9]		4-12 Hz	
Jankovic et.al.[5]	4-6 Hz		
Vaillancourt & Newell[3]		5-12 Hz	
Deuschl et. al.[8]			4-9 Hz
Helmich et. al.[11]			
Buijink et. al.[10]	4-9 Hz		
Elias et. al.[15]	4-7 Hz		

tion of the gravity force during at least 30 seconds (eg. stretching out the arms).[2,4,7,9,10,15] The reported frequency range of postural tremor is 4-12 Hz and its main cause is essential tremor.[9,29] Postural tremor amplitude can increase by adding a load (e.g., when holding a book or glass).[15]

2.1.2.2 Kinetic tremor

Kinetic tremor occurs during positional changes i.e., when some tasks or actions are performed voluntarily by the affected body part (e.g., finger-to-nose test) and takes its maximum value near the target.[4,7,9,15,32] In most reported cases, kinetic tremor frequency ranges from 2 Hz to 7 Hz[9] and is a characteristic of the cerebellar diseases. Its amplitude markedly increases at the onset of voluntary movement.[32] A less severe form of kinetic tremor is present in almost every PD patient[8] although isolated manifestations of this type of tremor rarely occur.[6]

2.2 Tremor classification based in the underlying cause

Tremor can also be divided according to the underlying cause in two main groups, physiological and pathological tremors.

Physiological tremor manifests in healthy subjects and is not disabling or easy to detect. It is prompted by some external factors which include

stress, anxiety, muscular weariness, scary or exciting moments.[4,9,15,26] Worsened symptoms can be caused by excessive consumption of alcoholic drinks, drugs and toxins (caffeine). Tremor disappears when these type of causes are eliminated and does not manifest in daily activities.[4,10] This tremor can be detected in flexion and extension movements, increasing its frequency with muscular fatigue. It can be defined as high-frequency (5-12 Hz range), low-amplitude, mostly postural and bilateral tremor. Physiological hand tremor presents an high-frequency range of 8-12 Hz, with low-amplitude that approximates to a sinusoidal movement.[10,15,20,26,33]

In the following section pathological tremors will be submitted to a deeper characterization.

2.2.1 Pathological tremor

Pathological tremors are generated by a so far unknown mechanism in the central nervous system.[27] They are characterized by a dominant frequency, which remains constant with little variations.[33]

It has been suggested that PD rest tremor and essential tremor share the same direct generator, the cerebello-thalamo-cortical network which, however, is thought to be differently activated, depending on the considered tremor.[11,27]

2.2.1.1 Parkinson's Disease Tremor

Prevalence in PD increases with age, affecting about 100-300 per 100 000 inhabitants over the age of 80[34,35] and consequently decreases in countries with lower life expectancy.[16] This prevalence increases to 1% when considering subjects over the mean age at onset (60 years).[10,14,16] The disease duration from diagnosis to death is 15 years.[35]

The disease is prompted by the loss or degeneration of dopamine-producing neurons in the *substantia nigra pars compacta* and is also characterized by the presence of neuronal Lewy Bodies in those dopaminergic neurons. The *substantia nigra pars compacta* is part of the basal ganglia of the brain. Basal ganglia is responsible for a specific effect on the temporal organization of motor cortical activity during action control. Lewy Bodies consists of cytoplasmic inclusions in the neurons composed of various proteins such as synuclein and ubiquitin. These structures exists in the basal ganglia, brainstem and cortex, increasing in number as the disease progresses. As consequence, the motor control is severely affected. The most potential risk factors are age, family

history and drug history (e.g. contact with pesticides).[5,12,13,16,26,36]

Motor impairments comprise tremor, rigidity, akinesia (or bradykinesia) and postural instability.[5,12] Those symptoms typically arise when dopamine producing neurons degeneration in substantia nigra is up to 50-70%.[12] Akinesia (slowness of movement) includes movement impairment, fatigue and decrease in amplitude of repetitive movement.[5,12] A PD patient can present mainly akinesia and rigidity or instead manifest prominently tremor.[15] It has been observed that patients with tremor at the onset show a slower progression of the disease comparing than those with postural instability.[13]

PD tremor can be manifest in a rest or posture position or in both situations. Thus, it is sometimes difficult to distinguish both types of tremor. Furthermore, the postural position tremor can be very similar to essential tremor, overlapping in frequency. Rest tremor in PD lies in the 4-7 Hz frequency range, while postural tremor frequency ranges from 4-12 Hz.[2,7,20,37] PD tremor diminishes or even disappears when movements are performed.[27] This tremor is typically asymmetric (affects more one side of the body comparing to the other) and unilateral at the onset (progressing to bilateral tremor overtime).[4,7,12,16,38] The writing is small and hardly readable.[4] Alcohol intake has no effect on tremor.[10] Voluntary movements tend to decrease PD tremor.[7]

There are also non-motor symptoms arising in the course of the disease which significantly accounts for patients' impairment. It includes cognitive impairment (dementia), depression, sleep disturbance, sensory symptoms (e.g. pain), fatigue and olfactory disturbances.[5,16,26] Almost 80% of PD patients present olfactory changes, independent of the disease stage and duration.[10]

The severity of PD symptoms is typically assessed using standardized rating scales such as the Unified Parkinson's Disease Rating Scale (UPDRS) and the Hoehn & Yahr scale. UPDRS is the most used clinical test for PD diagnosis, usually based on physician's subjective examinations, that assesses disability and impairment (see Appendix A). Disease severity increases with the scale result.[5,39,40] Hoehn & Yahr staging provides descriptive information about the disease progression stages (see Appendix B).[4,5,16]

Nevertheless, motor and non-motors symptoms vary among patients due to each individual lifestyle and characteristics thus justifying the need for a specific diagnosis.[5] Specific medical and surgical therapies were developed to reduce the impact of those symptoms. Among medical treatments, administration of levodopa and other dopamine agonists are often chosen.[15,16] Tremor response to dopamine administration in PD population has been reported

to be more variable comparing to bradykinesia and rigidity. In fact, some patients report tremor attenuation when submitted to dopaminergic treatment, in other no changes are detected and in other cases the patient presents worsened tremor.[2,6,11,27,28] Among surgical procedures, Deep Brain Stimulation (DBS) is the most used in PD. It is a reversible surgical therapy performed in order to attenuate motor symptoms and reduce drug intake, without brain tissue damage.[12,15] However, besides being expensive, DBS is an invasive procedure that has some risks associated. For example, hardware problems such as electrode infection and fracture can occur.[39]

The accurate diagnosis of PD is reported in 70% of patients in the early stages.[40] It accounts for the need for suitable methods such surface electromyography (sEMG) and kinematic measurements to analyse and characterize tremor and usually improve clinical assessment of the disease.[20,40–42] Those methods can be used in clinical experiments performed during a brief period of time during day (objective measures of tremor or short-term recordings) or can be used to continuously monitor disease features during day (subjective measures or long term recordings).[41] Using objective measures different results can be obtained due to oscillations in PD features severity during day, which makes these momentary disease state evaluation less accurate. On the other hand, subjective measures present some inconveniences such as daily movements as tooth brushing being confused with tremor and specific conditions being required to acquire sEMG signals such as continuous skin suitable properties.[41,42] Based on that and due to the limitations in the long-term acquisition of the signals using the accelerometers and sEMG techniques, short-term recordings were performed.

2.2.1.2 Essential Tremor

It is the most common movement disturbance in clinical practice, with no gender or ethnic group distinction. This mean age of this disease onset is about 45 years. Although ageing is considered a risk factor, Essential Tremor (ET) onset can occur during childhood or in early adulthood.[2,4,10] This type of tremor is more evident in subjects' hands, affecting upper limbs in 95% of the diagnosed cases, but can also be identified in head, lower limbs, speech, face and trunk. It is typically an action tremor, with contributions from either postural or kinetic conditions, the latter presenting higher tremor amplitude. ET is a typical bilateral and symmetrical tremor (both sides of the body are equally affected), occurring in the 4 to 12 Hz range. Roughly 18 % of ET

patients manifest rest tremor.[2,6,10] Applying a load upon the limb does not affect the tremor frequency due to the activation of a fixed central oscillating mechanism.[10] A positive effect of alcohol intake is a way to detect ET.[10]

Misdiagnosis rate in ET patients ranges from 25-50%, and it is often misdiagnosed with PD. Two hypothesis are considered, or this two disorders share a common syndrome or ET patients progress to PD.[4,15,28] Back to 2007, Mansur et.al.,[4] reported that research in ET physiopathology field (autopsies, computed tomography and magnetic resonance imaging scans) reported no signs of abnormality. Thus its pathophysiology still remains unknown.[15]

Chapter 3

Protocol

This chapter presents and describes the inclusion and exclusion criteria, the task performed by the participants, the acquisition setup including all parameters defined to acquire surface electromyography (sEMG) and accelerometric signals, and in the case of sEMG the on-line processing.

3.1 Patient selection and staging

In this study patients were diagnosed with idiopathic Parkinson's Disease (PD). Neurologists have staged PD using standard scales - Unified Parkinson's Disease Rating Scale (UPDRS) Motor score (items 18-31, see Appendix A) and Hoehn & Yahr stages (see Appendix B). To participate in this study subjects had to be over 20 years and present a subsequent DaT-SPECT and structural MRI with no changes. The Edinburgh Handedness Inventory[43] was filled for each participant in order to assess patient's laterality. Inspection of the clinical history, Beck Depression Inventory (BDI-II) and cognitive evaluation using Montreal Cognitive Assessment (MoCA) helped to identify patients with other neurological and psychiatric disorders or medication unrelated to the treatment of the studied conditions and therefore that did not fulfil the inclusion criteria. Subjects who had other possible causes for their tremor such psychogenic or neuropathic tremor or drug-induced tremor/parkinsonism were also excluded. Patients with cephalic tremor did not participate in the study. In sum, subjects that have any other disease liable of interfere with motor function were not included in the study. After giving their informed consent four participants (three patients and one control) were included in this preliminary study, after giving their informed consent. The patient group consisted of three idiopathic PD patients and is characterized in Table 3.1. All patients

Table 3.1: Clinical characteristics of patients with Parkinson's disease

Characteristic \ ID	1	2	3
Age (years)	33	36	71
Gender	F	F	M
Duration of disease (years)	1.5	1	3
MoCA score	27	29	20
BDI-II score	12	10	1
UPDRS Motor score	8	35	22
Hoehn & Yahr stage	1	2	2
Right-handedness (y/n)	y	y	y
Medication withdrawal (y/n)	y	n	y
Rest tremor (y/n)	n	n	y
Dominant arm (l/r)	r	l	l

ID: patient's identification number; UPDRS: Unified Parkinson's Disease Rating Scale; MoCA: Montreal Cognitive Assessment, normative for age and education; BDI-II: Beck Depression Inventory.

revealed an asymmetric tremor. This study and all procedures were reviewed and approved by the Ethics Commissions of the Faculty of Medicine of the University of Coimbra and were conducted in accordance with the declaration of Helsinki. Written informed consent was obtained from all participants.

Until now medication withdrawal has gathered no consensus, in terms of experimental results. Two studies concluded that maintaining medication before experiment lead to a decrease in tremor amplitude[44] and absolute power[45] of rest and postural tremors. On the other hand, Sturman et.al.[46] compared the performance of rest and postural tasks under medication and off treatment. They observed a reduction in rest and postural tremor amplitude and an increase in tremor frequency in the *on* medication condition. Kulisevsky et. al.[45] found that drug intake before task performance influenced differently the dominant tremor frequency which decreased for rest task frequency and increased for postural task.[45] Nonetheless, it was decided that our patients should stop medication 12 h before the beginning of the experiment.

Regarding loading it should be mentioned that its introduction in the protocol was also prompted by the controversial debate concerning its effect in

parkinsonian tremors. Some studies report no significant differences in tremor peak frequency when load is placed in PD patients' wrists or hands during the execution of a postural task compared to the unloaded postural condition.[47,48] Another study, testing the same postural condition with and without load, observed that the first peak frequency had not shifted by adding load, contrarily to the second peak which changed to a lower frequency.[49] Also, Hwang et al.[37] reported no differences in tremor intensity between postural load and unloaded conditions recorded in patients' hands. Finally, Burne et.al.[32] verified that loading had no significant effect in rest tremor amplitude. However the use of a load condition is still controversial[37] since it was recently reported/stated that postural tremor amplitude can increase by adding a load.[15]

3.2 Task description

This study is divided in two separated experiments: one conducted in the out-bore environment, outside the functional magnetic resonance imaging (fMRI) scanner, recording only accelerometric and electromyographic signals and hereafter the in-bore environment, inside the fMRI scanner, simultaneously with the previous techniques.

During both experiments, participant's actions were visually guided. Different ball colours (blue and red) and screen positions were chosen to represent the two arms (left and right, respectively). Those balls were initially placed on the bottom of a 33.8×27.1 cm computer screen (1280×1024 pixels), as can be seen in Figure 3.1. This stimulus was presented using Physicophysics Toolbox Version 3, a free set of Matlab R2010a. Each participant had to follow the balls movement with both arms.

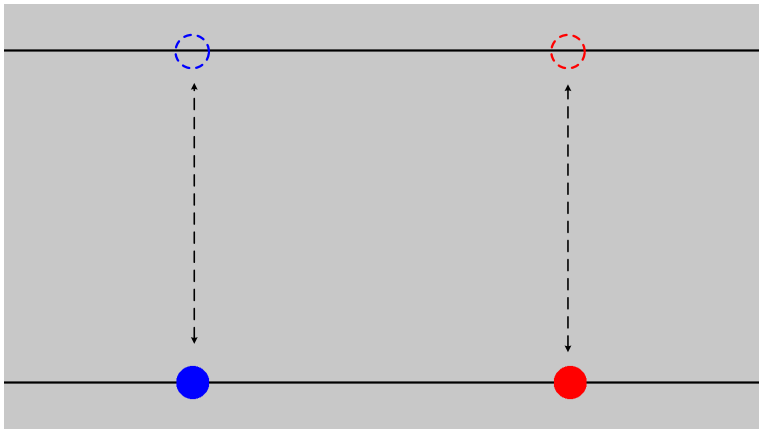

Figure 3.1: Visual guidance to help subjects perform the task.

Each run was composed by 21 segments resulting from the execution of five blocks of four segments and an extra baseline segment added at the end of the run in order to start and end each run with a baseline condition (see Figure 3.2). It results in a 6.50 min single run duration which includes the following segments:

- Six segments started with the participants arms in a relaxed position, placed near the body (rest condition) for 30 s.
- Five segments in which arms started an ascending 6 s movement.
- Five segments in which the arms remained for more 30 s at a shoulder flexion with the elbow at full extension and forearm pronation (posture position).
- Five segments in which arms started a descending 6 s movement back to the rest position.

All subjects were asked to lay down (in supine position) with their hands facing down (see Figure 3.3). Each participant performed runs with and without a 0.5 kg load placed in each wrist (see Table 3.2).

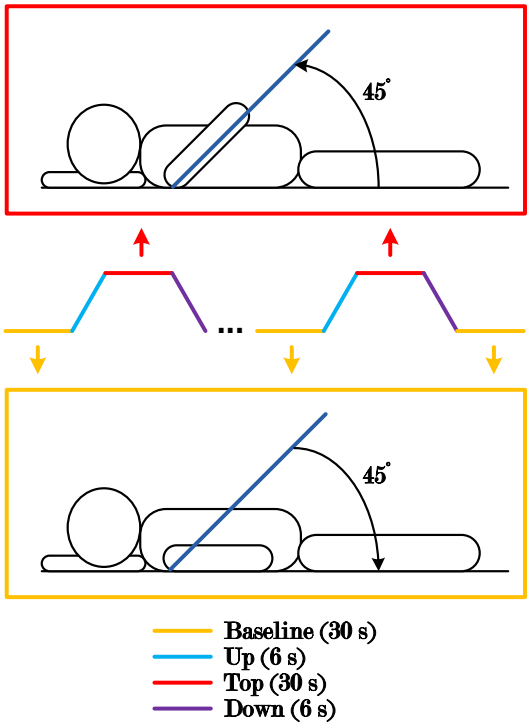

Figure 3.2: Both out-bore and in-bore and in-bore experiment sequence of motor paradigm.

Table 3.2: Load sequence

Run	**1**	**2**	**3**	**4**	**5**	**6**	Time (min)*
In-bore	Unload	Load	Load	Unload	Unload	Load	39
Out-bore	Unload	Load	Unload	Load	-	-	26

* Total task duration.

3.2.1 Out-bore experiment

The out-bore experiment was designed to characterize tremor during rest, posture and ascending and descending arms movement, with loaded and unloaded conditions. Accelerometry and surface sEMG techniques were used to acquire out-bore data, which can be used to control the in-bore artifact removal. The experiment consisted of four runs with and without added load (see Table 3.2).

3.2.2 In-bore experiment

The in-bore experiment shares the first purpose of the out-bore study, i.e., to characterize tremor using a block related design in which rest and postural conditions, with and without added load, are alternated and differences in neural activation are correlated. This experiment also aims to use accelerometer and sEMG data to identify fMRI predictors in order to help to determine the neural basis of tremor. Additionally, it was designed to develop solutions to relate synchronous signals and get further pathophysiological insights in tremor genesis. In this part of the study, in order to increase the statistical power of the fMRI analysis, two runs were added to the out-bore sequence (see Table 3.2), with the same duration as for the out-bore experiment.

3.3 sEMG setup

Disposable Ag/AgCl electrodes compatible with MR environment (disc shape, unshielded, radio-translucent, EL254RT, 7.2 mm diameter housing, 4 mm diameter of the contact area, MRI Touchproof, BIOPAC) were chosen to detect sEMG signals in the abductor pollicis brevis (APB) hand muscle in both arms (see Figure 3.4). This muscle was chosen since PD tremor is frequently associated with the thumb movement towards the index finger - "pill-rolling" rest tremor.[39,50]

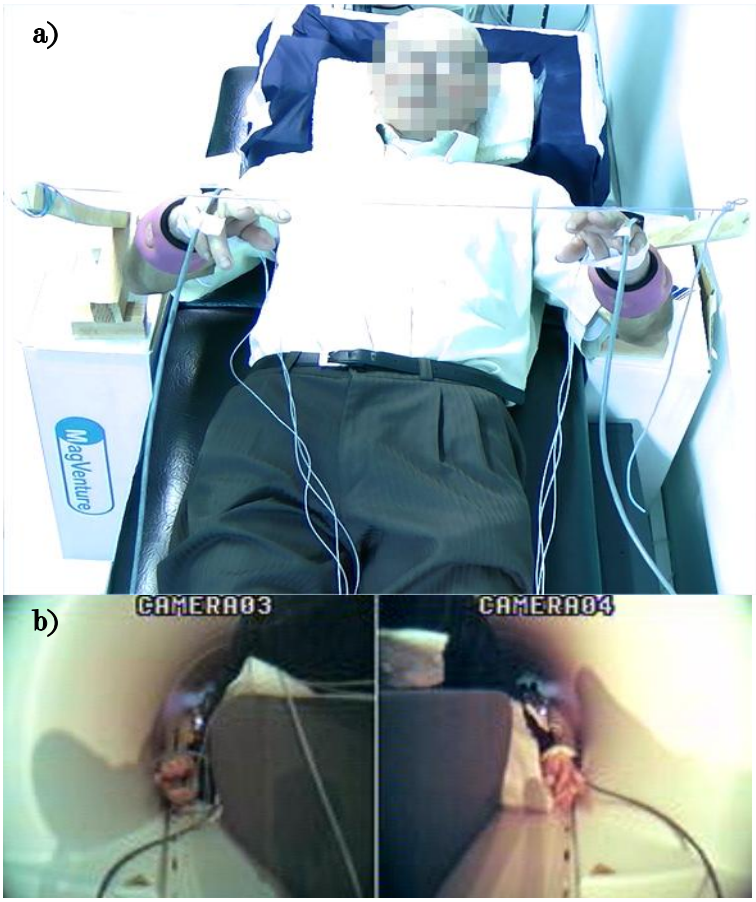

Figure 3.3: a) In the out-bore setup two wooden bars connected with a wire were placed along participants body in order to define arms rising up amplitude of 45˚. All experiment was recorded using a video camera. Loads were added during the task. b) In the in-bore setup patients raised their arms up towards postural position, until the maximum range compatible with the space in the MRI scanner, between 30˚to 40˚. In-bore cameras were used to control the acquisition.

After determination of the proper location in the muscle to attach the electrodes, skin was carefully cleansed with alcohol and abrasive gel (Nuprep, D.O. Weaver and Co) to reduce skin-electrode impedance. This procedure is sufficient since the tasks involves static and slow motion movements and our goal is to quantify parameters such amplitude.[51] Electrodes were filled with sEMG electrode gel (Signa Gel, PARKER) and fixed to the subjects skin using tape.

Inside the scanner, during in-bore experiment, movement artifacts can be produced by the sEMG electrode wires movement. When a subject performs the task, a conductive loop can occur in a non uniform magnetic field as result of the electrode wires movement. In order to reduce the differential effect of the magnetic field, the electrodes were disposed alongside the subject and were fixed to a gutter existing in the scanner in both sides of the body, (see Figure

3.6).[25,52,53]

3.3.1 Analog Filtering

Following the scientific recommendations from the International Society of Electrophysiology and Kinesiology (ISEK) and from Surface Electromyography for Non-Invasive Assessment of Muscles (SENIAM), no hardware filters (e.g. notch filters) able to destroy signal content were applied during sEMG acquisitions. On-line processing consisted in application of only a bandpass amplifier filter (Biopac Systems Inc., Goleta, CA, USA) in order to avoid anti-aliasing effects within sampling.[51,54] sEMG signals were then amplified (differential amplifier, with input impedance of 2 MΩ and total gain 5000).[55]

Signals were also analogically bandpass filtered by applying a lowpass filter at 500 Hz (−20 dB/decade) and a high pass filter at 1 Hz (20 dB/decade), both single pole roll-off.[55] The low frequency cut-off of 1 Hz was set in order to allow detection of the parkinsonian tremor frequencies (rest 4-7 Hz and postural 4-12 Hz tremors, instead of choosing a cut-off frequency in the 5 to 20 Hz range usually indicated to filter sEMG signals.[3,54] The low frequency cut-off of the bandpass filter should also take into account the possibility of removing interferences such as the baseline drift that could be originated by movement or perspiration and should also remove the DC offset, leading the mean of the signal to become nearly or totally zero.[54] On the other hand, the bandpass high frequency cut-off should be set in order to remove high frequency noise and avoid aliasing of the signal. The value of the bandpass high frequency cut-off should be high enough to allow identification of rapid on-off bursts of the sEMG and, typically, should range between 200 - 1000 Hz.[54] In this study, the high frequency cut-off was set to 500 Hz (see Figure 3.4).

International Society of Electrophysiology and Kinesiology (ISEK) and Surface Electromyography for Non-Invasive Assessment of Muscles (SENIAM) recommend a sampling rate of at least twice the cut-off frequency of the analog low pass filter used. However, there are some authors[20,54] that recommend a higher sampling rate of, at least, five times the nominal low pass filter cut-off frequency, in order to avoid aliasing. Analog low pass filters roll off slowly, requiring a higher sampling frequency to prevent significant power at frequencies, well above the cut-off frequency, to be discarded.

Therefore, having set the high frequency cut-off to 500 Hz, a sampling rate of 2000 Hz was used to acquire surface electromyography (sEMG) signals in the out-bore experiment, determining the higher accuracy possible of 2 ms in

time, in the subsequent measurements.[20,54] In-bore, sampling rate was set to 10 000 Hz due to the occurrence of high frequency artifacts caused by the radio frequency field (127.73 MHz/T in our scanner).[52]

3.3.2 Maximum Voluntary Contraction Normalization

Before the beginning of the task, control subjects should perform the Maximal Voluntary Contraction (MVC) for one minute, in the rest, three times, in order to proceed for amplitude normalization of the sEMG signal. The aim is to get unbiased data, which amplitude can be influenced by the detection condition. In other words, signal amplitude can change by changing electrode placement, from subject to subject and also by getting measurements of the same muscle in different days.[51,56] Subject has to maximally move the thumb towards the little finger, in order to obtain effective maximum innervation. This procedure

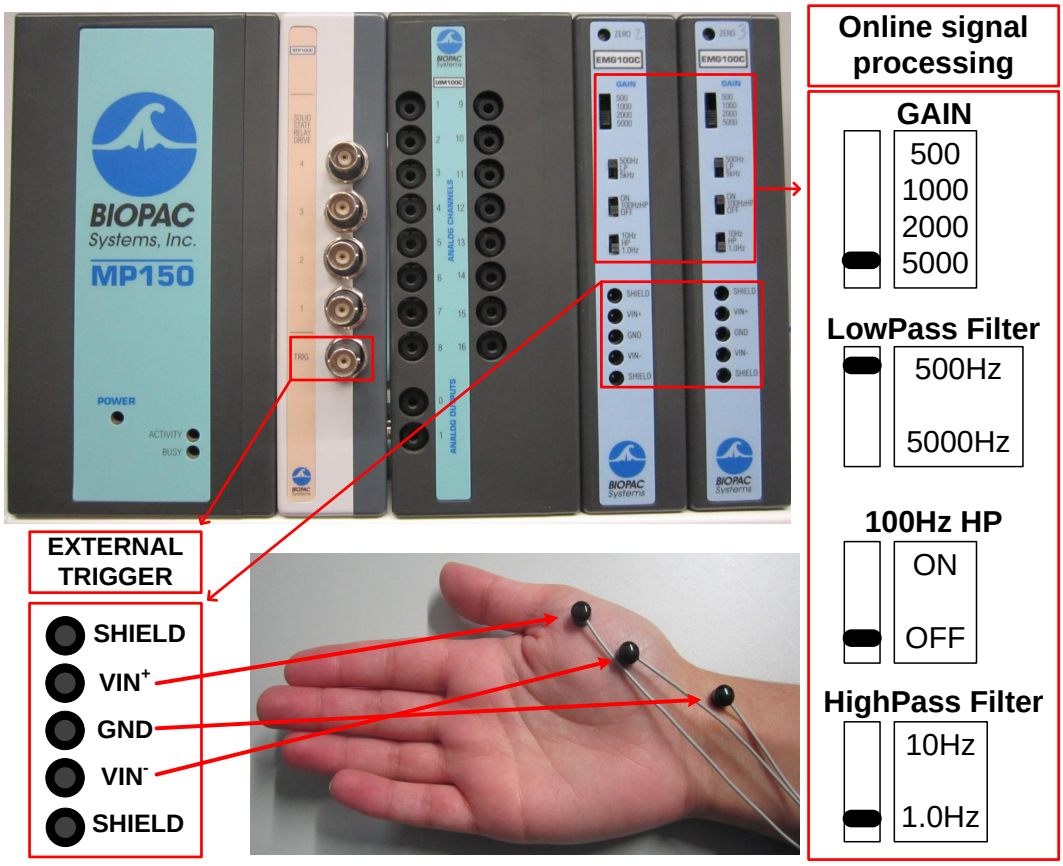

Figure 3.4: MP150 Data Acquisition System is attached to STP100C isolated digital interface which is connected with the UIM100C universal interface module which in turn is connected to two EMG100C electromyogram amplifier modules. The parameters specification is depicted. Interelectrode spacing was set 2 cm from center to center in order to obtain information about a sufficient number of motor units (MUs).[40] The ground electrode was placed in the subjects' wrist bone.

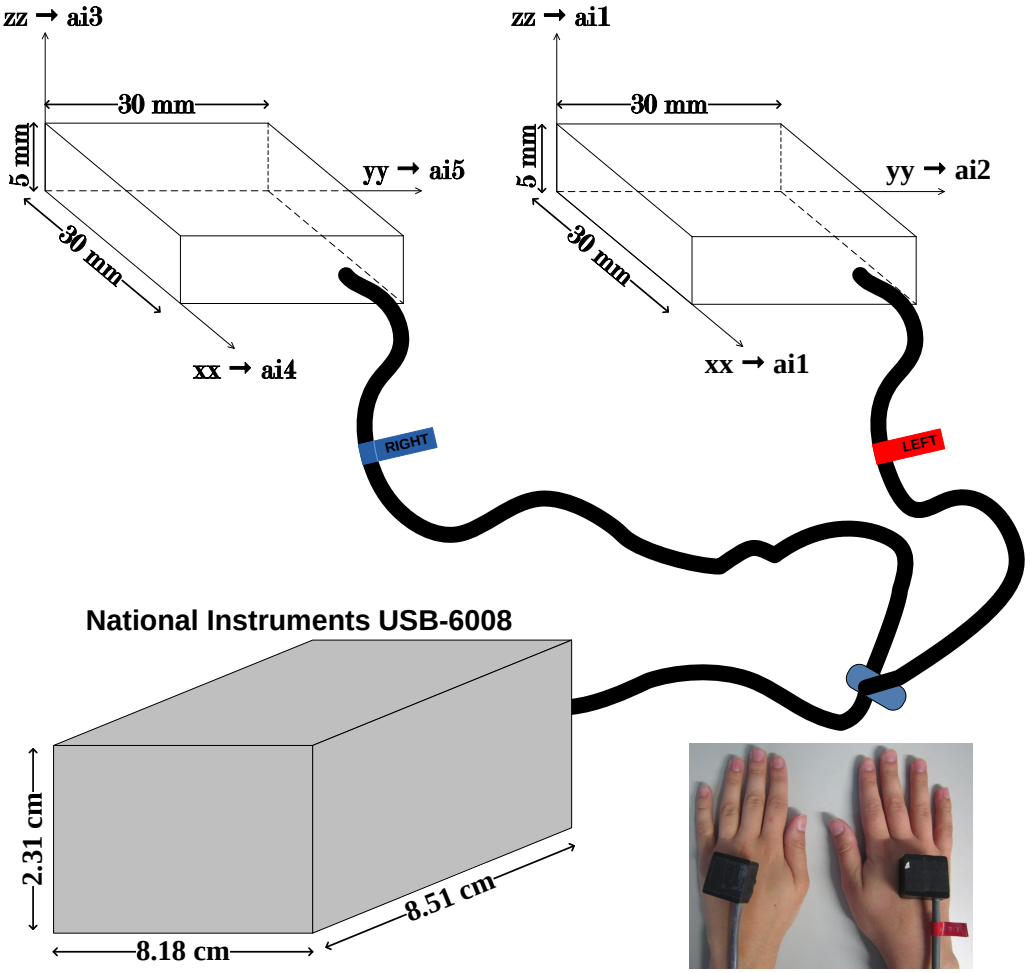

Figure 3.5: Accelerometers configuration: NI USB-6008 channels correspondence to each axis.

should not be applied to Parkinson's Disease (PD) patients since MVC require perfect stabilization and hand supporting which is not the case.[51,56]

3.4 Accelerometry setup

Three-axis accelerometer transducers (sensitivity ± 200 mV/g, range ± 6 g, Mag Design and Engineering, Redwood City, CA, EUA), were attached to the dorsal surface of the hand. Accelerometers were connected to a National Instruments USB-6008 (with 11-bit input single-ended resolution A/D converter), the data acquisition device chosen to sample the analog data to digital values.

The accelerometers themselves are analog devices and do not have an inherent sampling rate, but have a 350 Hz (−3 dB) limit in X and Y axis and 150 Hz (−3 dB) in Z axis. In Matlab acquisition code sampling frequency was set to

50 Hz. Channels were configured for single-ended input and the acquisition range was fixed between −10 to 10 V which yields a 9.8 mV resolution.

3.5 fMRI setup

In the fMRI environment, patients were scanned in a 3T Siemens Magnetom Tim Trio scanner at the Portuguese Brain Imaging Network, using a 12-channel head coil. A series of T2* weighted echo-planar images of the whole brain with a resolution of $4 \times 4 \times 4$ ($3.5 \times 3.5 \times 3.5$) mm^3, a repetition time (TR) of 3 s and a echo time (TE) of 30 ms, depicting blood oxygen level dependent (BOLD) contrast (sensitivity to neural activity), were acquired in each session, together with an anatomical MRI for coregistration purposes. One complete brain

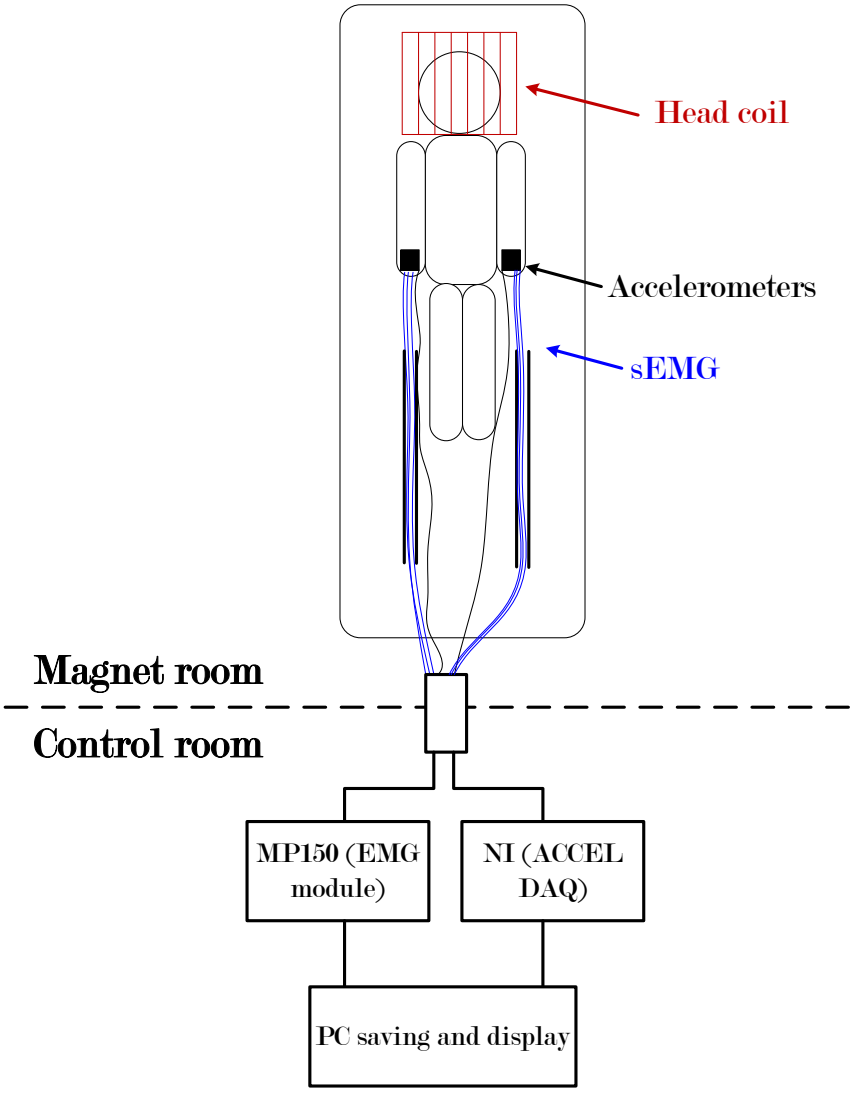

Figure 3.6: fMRI acquisition setup.

volume or scan is acquired every TR. To minimize the motion of the subject's head during the study, foam padding was employed.

Chapter 4

Accelerometry

Accelerometers are widely used to detect and quantify tremor, due to its ability to provide reliable and objective parameters. In this study, capacitance accelerometers were used, which belong to the group of the micro electromechanical systems (MEM) sensors. They are described by two microstructures, a set of fixed plates and a flexible plate attached to an internal spring. Acceleration forces induce a displacement on the movable plate causing a proportional variation of the electric capacitance between the two microstructures that is measured as voltage by the accelerometers.[4,57–59] Additionally, those capacitance accelerometers are considered to have a wide bandwidth, very high impedance, high accuracy and good ruggedness.[4,9,57]

4.1 Pre-processing

The acquired accelerometric raw data consisted of three signals corresponding to three axis. A signal was obtained from the Euclidian normalization of the three acceleration components (see Equation 4.1).[26,40]

$$a = \sqrt{x^2 + y^2 + z^2} \tag{4.1}$$

The accelerometer detects the gravitational component which would ideally appear only in one of the three axis if the sensor was perfectly aligned with the Earth's gravitational field. In practice, a slight misalignment often occurs and will be reflected in the gravity vector contribution to the three axes in addition to the movement acceleration already detected in each axis.[58]

In order to correct for the gravity effects, the normalized signal was segmented in postural and baseline resting segments and the latter were averaged

over time. Assuming the sensor is not rotated significantly, then the average over all previously obtained baseline means was subtracted from the normalized data. Finally, data were detrended.

4.1.1 Bandpass digital filtering

The same filtering procedure applied to the surface electromyography (sEMG) signals (see Section 5.1.1) will be also presented in this section. The signal resulting from the normalization and gravity effect correction was band-pass filtered using a Butterworth and Chebyshev type I infinite impulse response (IIR) filters. High cutoff frequency was set to 16 Hz, since the information related to tremor is located in the low frequencies.[3,40–42,46,60] The low cutoff frequency was set to 1 Hz in order to remove the low-frequency trends caused by the ascending and descending arm movements (see Figure 4.1).[40,42,46,60] Filters were both dual pass, thus filtering data twice (4th order filters) to obtain a zero-shifted signal in comparison to the unfiltered signal.

The bandpass Butterworth filter was chosen to pre-process all accelerometric data, besides being often used in similar studies.[3,46,60] Unlike Chebyshev, Butterworth type filtering does not attenuate the signal in the band frequency of interest (see Figures 4.2 and 4.3).

On the other hand, the roll-off of the Butterworth filter is clearly slower

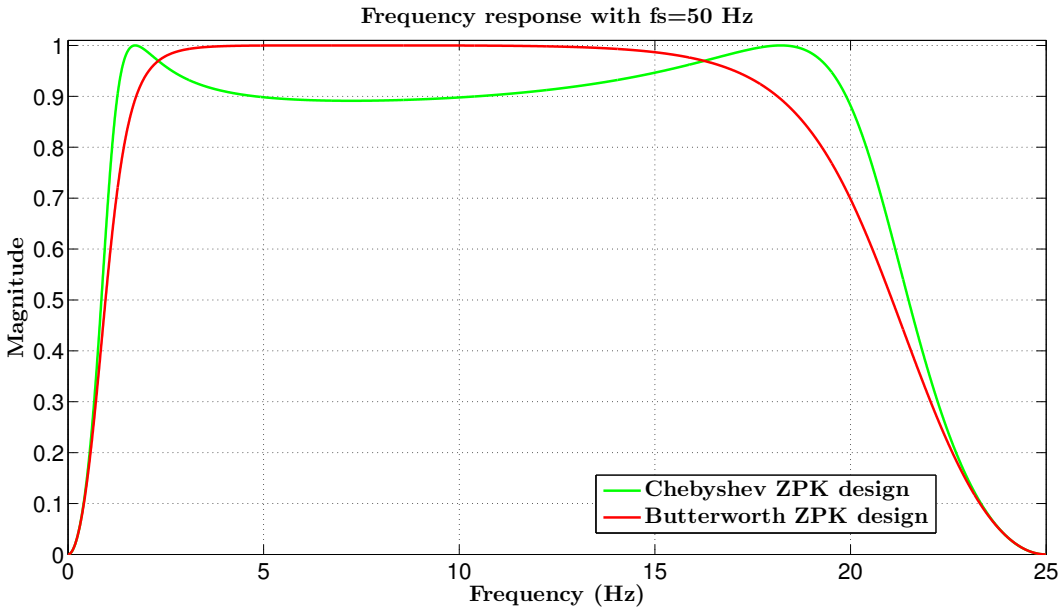

Figure 4.1: Frequency response for the two types of IIR filters using the zero-pole-gain design. In the Chebyshev type I filter design it was used 1 dB of peak-to-peak ripple in the passband.

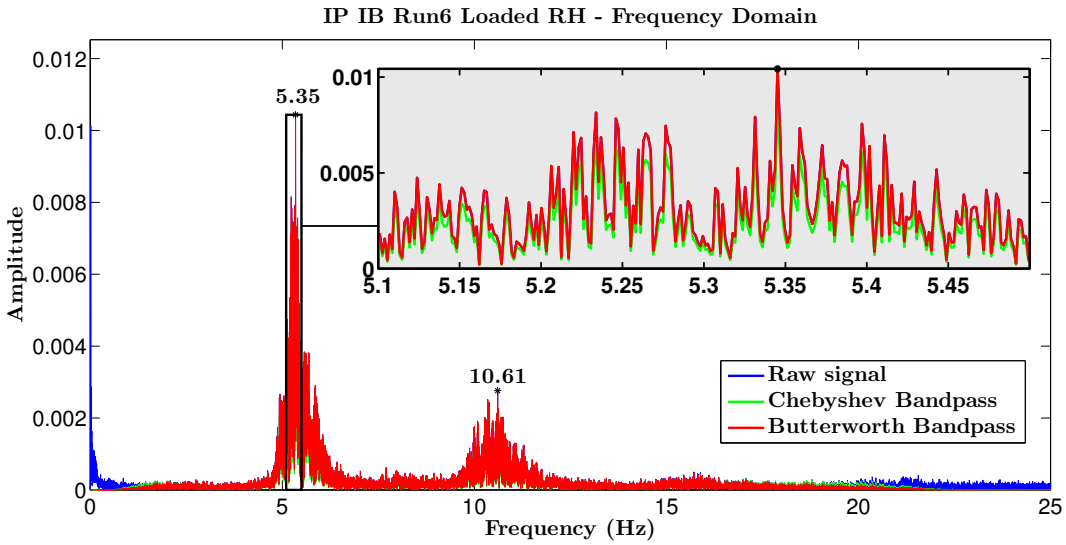

Figure 4.2: Frequency domain representation ($f_s = 50Hz$) of the accelerometry signal after bandpass filtering between 1 and 16 Hz, using zero-pole-gain design. This signal was acquired during the in-bore experiment in PD patient 1 (run 6, loaded, right hand).

compared to the Chebyshev filter.

Peak amplitude and frequency were computed using the whole frequency spectrum (see Figure 4.2).

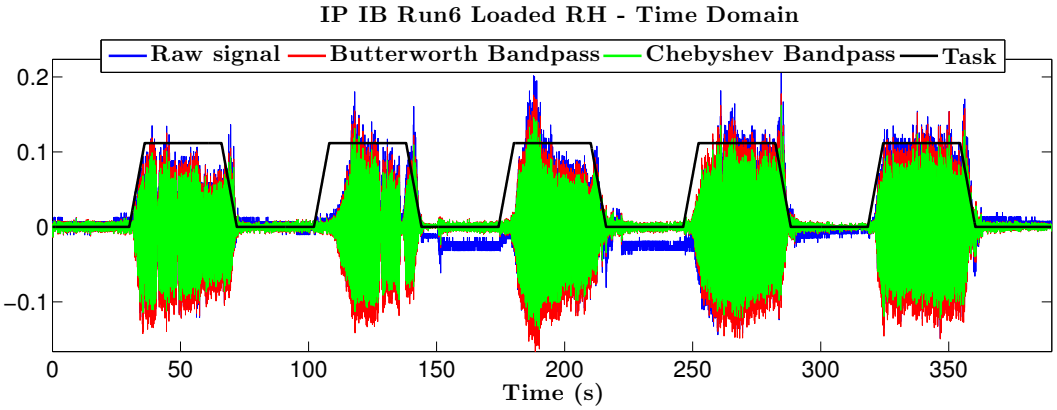

Figure 4.3: Time domain representation ($f_s = 50Hz$) of the accelerometry signal after bandpass filtering between 1 and 16 Hz, using a Butterworth filter (red signal) and a Chebyshev Type I filter (green signal). This signal was acquired during the in-bore experiment in PD patient 1 (run 6, loaded, right hand).

Chapter 5

Surface Electromyography

The function of human neuromuscular system can be assessed using surface electromyography (sEMG) technique.[2,40,51] The control of the muscular contraction process is conducted through the motor units (MU), which ensemble a motor neuron and the muscle fibers innervated. Depolarization and repolarization of the membrane induces action potentials in the muscle fiber that can be recorded in sEMG signals.[26,51] The resultant electromyographic activity can be accessed by placing surface electrodes on the skin above the muscle of interest. Frequency and amplitude of the recorded sEMG signals are modulated by the recruitment of motor units action potentials and the corresponding firing frequency.[51] Evaluation of the muscle performance is a rapid, noninvasive and painless process when using sEMG technique.[4,9,20] It allows studying the neuromuscular activation of muscles within postural tasks, functional movements, work conditions and treatment regimes.[51]

Different type of information can be provided depending on what type of study are we doing. There are static and/or dynamic muscle contractions, i.e., with a constant and/or a varying force and posture, respectively.[40] Typically, static sEMG is analysed using methods based on amplitude and Fourier-based spectral analysis, providing information about the level of muscle activity and fatigue.[3,26,40] On the other hand, there are no suitable methods for dynamic sEMG analysis, existing a lack of knowledge concerning the relation between the signal features and the corresponding physiological mechanisms.[40]

New methods for sEMG analysis have been recently reported and include nonlinear methods and higher order moments. These new approaches have been used to analyse sEMG signals recorded during static muscle contraction and, most recently also during voluntary isometric contractions tasks. Results have shown that nonlinear methods are more effective in the quantification of

differences in sEMG signals between Parkinson's Disease (PD) patients and healthy subjects, when comparing to traditional sEMG analysis methods (i.e., amplitude and median frequencies).[40,55,61,62]

In our study the task performed consists of a block design alternating static posture and resting positions and ascending and descending dynamic segments (see Section 3.2). We are particularly interested in the resting and posture segments rather than ascending and descending movements. The latter last considerably less time than posture and resting segments and are not in the scope of this study. Knowing that, tremor amplitude and frequency and other parameters derived from the spectral analysis will be determined by processing the sEMG signals. Those parameters can be used to quantify and discriminate rest from postural tremor.[3,10,20]

In order to relate brain activity in motor areas and the level of muscle activation, the described task was performed in the magnetic resonance scanner simultaneously with sEMG acquisitions.[25,52] This chapter's focus is mainly the denoising and subsequent analysis of the in-bore sEMG signals. Out-bore sEMG signals presents no image artifacts and thus will be used, when necessary, as control signal to be compared with the cleaned in-bore sEMG signal.[52]

Two cleaning methods were implemented in order to reduce and/or remove the functional magnetic resonance imaging (fMRI) artifacts. One of them used digital filters to eliminate the high frequency content of the sEMG signal. The other was the so-called wavelet analysis and has been proved to be a suitable method to filter signals in different frequency bands.[26] In PD studies, wavelets have been mainly used to extract features from sEMG signals.[63–65] It is the first time this method is used to clean noise of sEMG signals acquired in an fMRI environment.

Signal processing was conducted using Matlab™ (MathWorks Inc.). A diagram of the analysis is depicted in Figure 5.1.

5.1 Pre-processing: IIR Filtering

The raw sEMG signal can present a baseline shift from the true zero line, i.e., when the mean of the signal is different from zero. Knowing that, the first step is to subtract that offset from the signal.[51,54]

Out-bore sEMG signals can be affected by the ground noise from the power net which will be reflected in the increase in the baseline amplitude in the

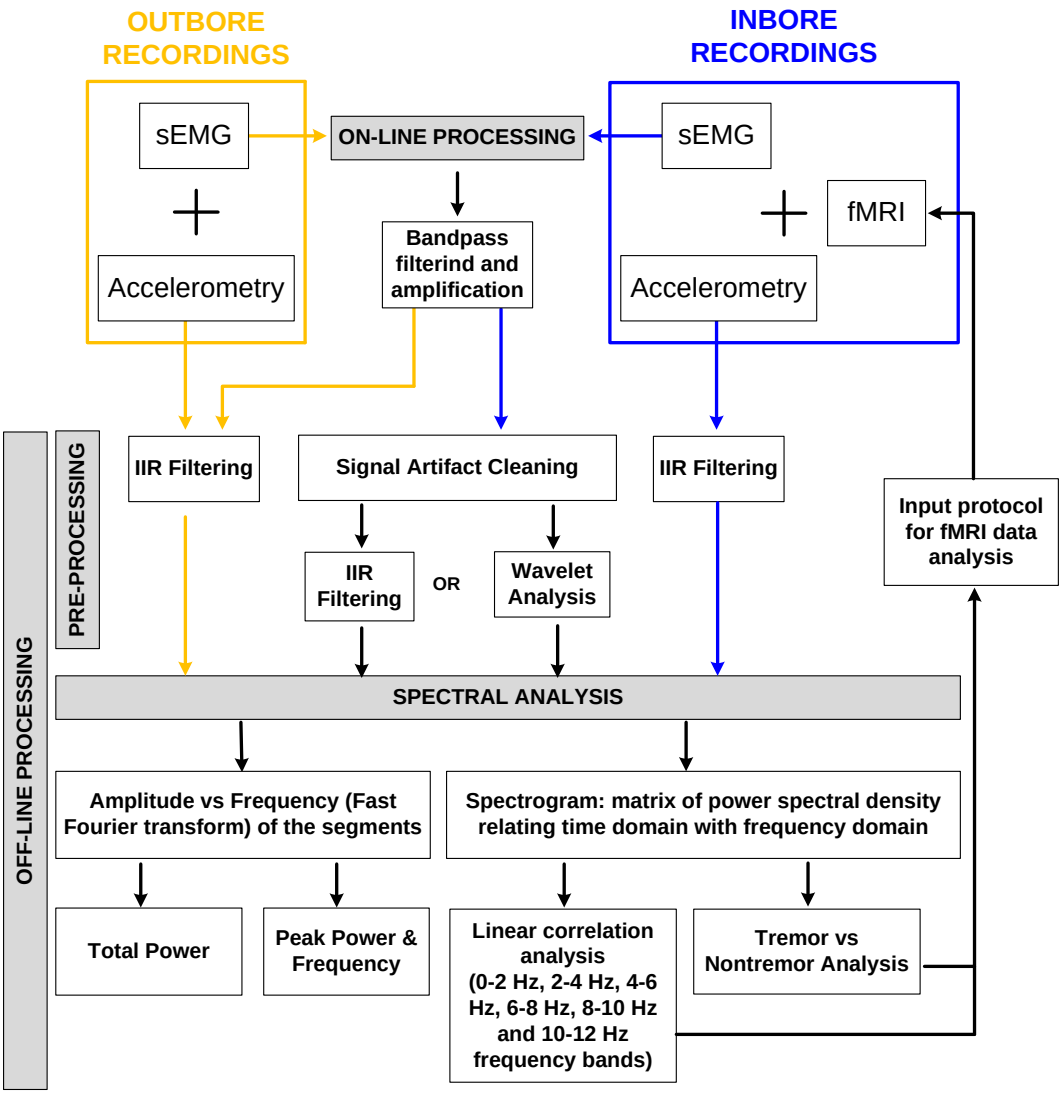

Figure 5.1: Analysis diagram

time domain and can also be seen in the frequency domain as the 50 Hz peak frequency.[51] This kind of interference is due to hardware problems (e.g., poor grounding).

Artifacts originated by different sources can occur in the in-bore sEMG signal. They can be divided in magnetic field gradients (used for proton excitation and spatial localization), the radio frequency (RF) pulse and movement artifacts (see Section 7.1).[25,52] RF pulse artifact presents a much higher frequency than sEMG (typically 64 MHz at 1.5 T) being easily removed using a low-pass filter.[52,66] Movement artifacts are generated by electrode wires movement during the task performance and can be restrained by fixing those wires (see Section 3.3 for more detailed information).

During the in-bore environment, echo-planar imaging (EPI) introduces the

magnetic gradient field artifacts in the sEMG signals (see Section 7.1). Those artifacts span the entire sEMG spectrum, not vanishing after applying a low-pass filter. The gradient fields are applied every time an image slice of the brain is acquired.[52,53] As the image sequence repeats every 138.52 ms, the gradient field artifacts will appear at a slice acquisition frequency of ~ 14.33 Hz and multiples. Peaks at ~ 7 Hz and multiples, of lower amplitude, were also identified (see Figure 5.2).

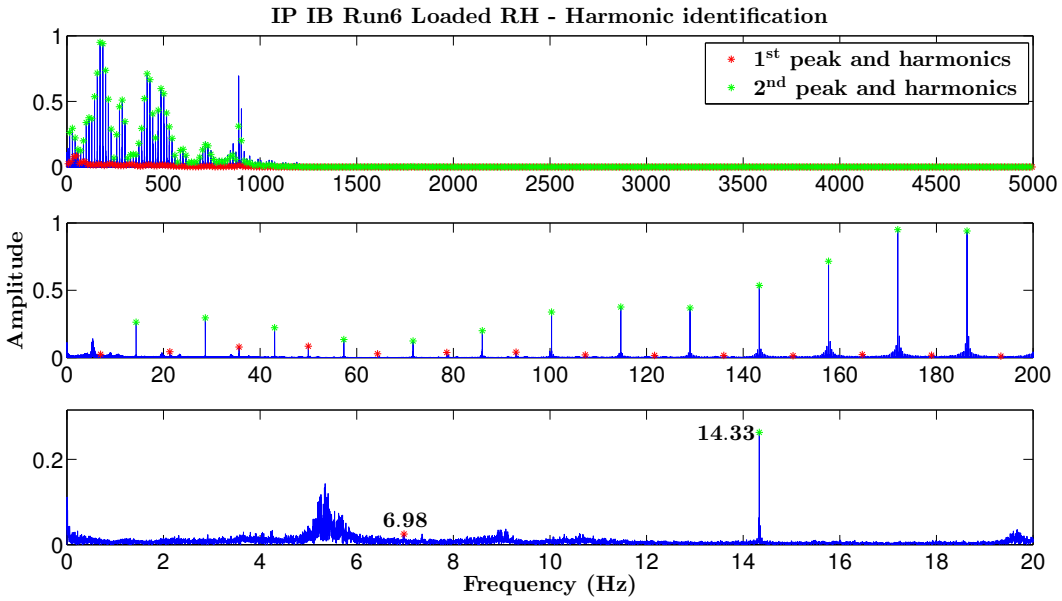

Figure 5.2: Gradient field artifacts identification in sEMG signal recorded in the in-bore experiment in PD patient 1. Noise is clearly present in frequencies in the multiple of 14.33 Hz.

5.1.1 Bandpass digital filtering

Knowing that, the next step was to design a bandpass filter able to, in the first place, remove the high frequencies of the signal and hence the RF pulse artifact and the 50 Hz power hum noise.

There are two types of digital filters, the finite impulse response (FIR) or non-recursive filters and the IIR or recursive filters. The first has a finite impulse response duration and only depends on the input samples. The latter has an infinite response duration and depends on both input and previous output samples.[67] In this work we will use IIR filters since they allow to achieve a set of design specifications with smaller filter order compared to the FIR filters. IIR filters use feedback loops to achieve a steeper response with far less coefficients. The feedback is also responsible for a response that never decays to zero when an impulse is applied to the filter.[68] Two types of IIR

filters, the Butterworth and Chebyshev Type I were analysed in this project and the best suitable filter to our purpose was applied to all sEMG filters.

Both types of filters are characterized by the following transfer function of nth-order:

$$H(z) = \frac{B(z)}{A(z)} = \frac{\sum_{n=0}^{M} b_n z^{-n}}{\sum_{n=0}^{N} a_n z^{-n}} = \frac{b_0 + b_1 z^{-1} + ... + b_M z^{-M}}{1 + a_1 z^{-1} + ... + a_N z^{-N}}; a_0 = 1 \qquad (5.1)$$

with b_n and b_n corresponding to the filter coefficients.

The order of the filter was set knowing that the higher the order, more noticeable will be the Gibbs phenomenon in the output of the filter. This phenomenon is more evident when the signal presents on-off transitions. This is the case of our sEMG signal which presents periods of muscle relaxation and steadiness (during resting position segments) and hence low amplitude.

The `filtfilt` Matlab routine was used to filter data forward and backward, avoiding zero-phase-shift between the original and the filtered signal. However, by using this command, we are running the filter twice, in forward and backward directions (dual-pass method) which doubles the effective order of the filter and removes phase distortion. For example, a dual-pass second order filter is a 4^{th} order filter since at high frequencies the response drops off proportional to frequency to the power -4. Knowing that, the cutoff frequency had to be adjusted for the dual-pass.[54,69] Data were then effectively filtered in the 2 to 24 Hz bandwidth.[3,50]

The frequency response for this two types of IIR filters was compared in order to identify the best filter to apply to sEMG data. As can be seen in Figure 5.3, Butterworth filters are characterized by a magnitude response that is maximally flat (or with no ripple) in the pass-band and monotonic overall. Butterworth filters sacrifice rolloff steepness for monotonicity in the pass- and stop-bands.[68] Chebyshev type I filters are only equiripple in the pass-band and monotonic in the stop-band. On the other hand, type II filters only have ripple in the stop-band. Type I filters achieve faster roll off than type II filters, but at the expense of greater deviation from unity in the pass-band. Concerning type I filters, increasing ripple results in a sharper roll-off.[68,70]

As expected, frequency response for both filters for transfer function design overlap, as well as for the zero-pole-gain design. Differences between the two filter designs could perhaps be seen when increasing the order of the filter. In this situation, using the transfer function design could lead to numerical

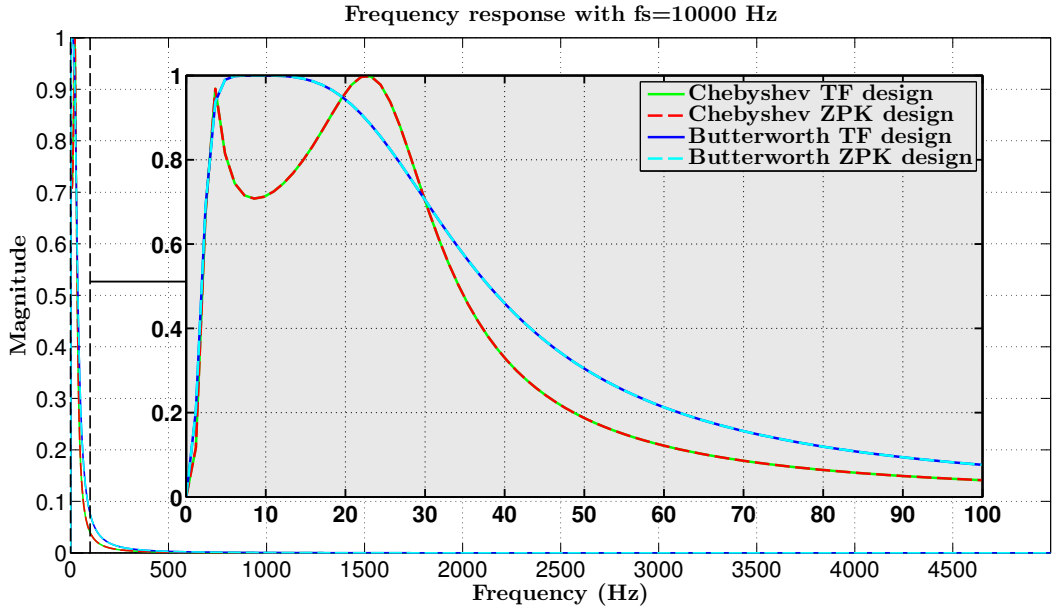

Figure 5.3: Frequency response for the two types of IIR filters and for the two different filter designs, transfer function and zero-pole-gain. In the Chebyshev type I filter design it was used a 3 dB of peak-to-peak ripple in the passband.

problems due to the occurrence of roundoff errors. Then, even though we are using a small filter order, we decided to use the zero-pole-gain syntax to filter all the sEMG signals.

The fast Fourier transform (FFT) was applied to the signal in order to ob-

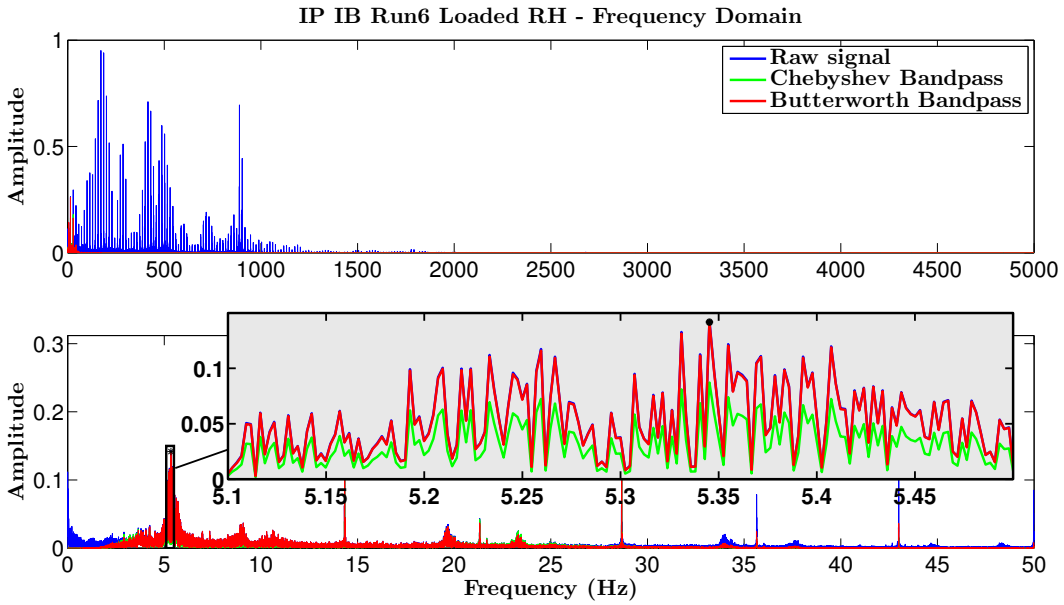

Figure 5.4: Frequency domain representation ($f_s = 10000Hz$) of the sEMG signal after bandpass filtering between 2 and 24 Hz, using zero-pole-gain design. The signal was acquired during the in-bore experiment in PD patient 1 (run 6, loaded, right hand).

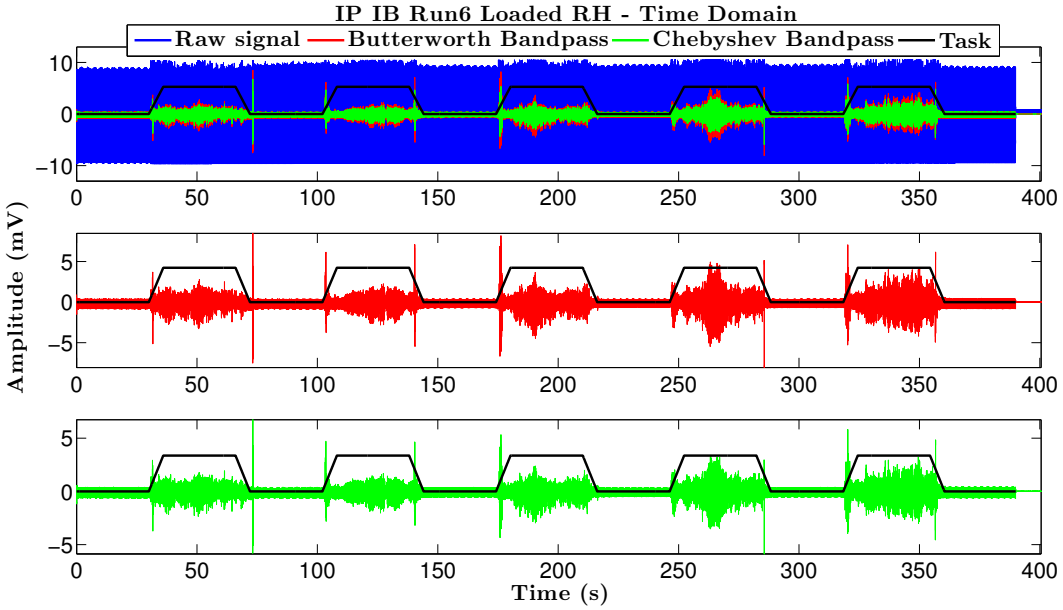

Figure 5.5: Time domain representation ($f_s = 10000Hz$) of the sEMG signal after bandpass filtering between 2 and 24 Hz, using a Butterworth filter (red signal) and a Chebyshev type I filter (green signal). The signal was acquired during the in-bore experiment in PD patient 1 (run 6, loaded, right hand).

serve the results of the IIR filters (see Figure 5.4). As can be seen in the figure and as expected, in our bandwidth of interest (2 to 20 Hz) the Butterworth filter has the better performance. In this interval this filter has a frequency response closer to the unit, with no signal attenuation. On the other hand, the Chebyshev type I filter attenuates about 0.72 at 8 Hz. Knowing that, the Butterworth filter was chosen to bandpass filter all sEMG signals, as selected in other similar studies.[40,46,71]

The resulting signals from bandpass filtering can be see in Figure 5.5, which presents a clearly less noise affected sEMG signal. At this point, the RF pulse artifacts and the baseline noise resulting from the power hum no longer interfere with the signal.

5.1.2 Notch filtering

However, if we take a look at Figure 5.6, it is possible to see that the frequency peaks corresponding to the magnetic gradient field artifacts (14.33 Hz and multiples and 7 Hz and multiples) still remain in the bandpass filtered sEMG signal. Given that, the next step was to implement a IIR notching comb filter in order to attenuate the harmonically related frequencies identified.[52] Filter coefficients were obtained using `iircomb` Matlab command and used to filter data in the backward and forward directions.

The notch filter transfer function is given by

$$H(z) = b\frac{1 - z^{-n}}{1 - \alpha z^{-n}} \tag{5.2}$$

where α and b are positive scalars. n is the order of the filter which corresponds to the number of notches of the filter in the $0 - 2\pi$ range or, in other words, the number of harmonics to eliminate (see Figure 5.7).

In the frequency spectrum it is possible to confirm that the frequency content introduced by the magnetic gradient field artifacts vanished. However, elimination of these interference peaks was achieved at the expense of amplitude loss in its neighbourhood. The bandwidth of the filter depends on a quality factor (Q) that was altered until best compromise between the spectrum loss and the frequency harmonic influence attenuation was achieved. Increasing that Q factor a sharper frequency response was obtained, however harmonic peaks at 14.33 Hz were not efficiently removed. Decreasing Q factor, increased the spectrum loss.

In the time domain, notch filtering lead to a significant decrease in the amplitude of the signal specifically in the periods of muscle relaxation and resting (baseline segments) (see Figure 5.6).

The loss in amplitude in the frequency spectrum can be noticed in the time domain as a slight decrease in the amplitude when the muscle was in the postural position (top segments). The signal was only scaled and this reduction

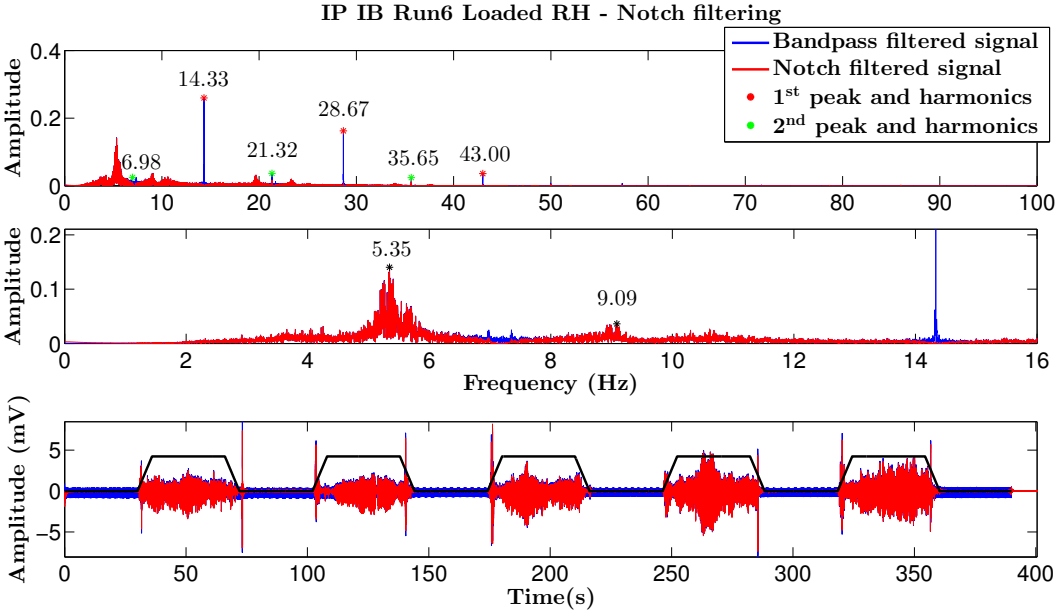

Figure 5.6: Frequency domain representation of the sEMG signal after filtering in the in-bore experiment in PD patient 1 (run 6, right hand).

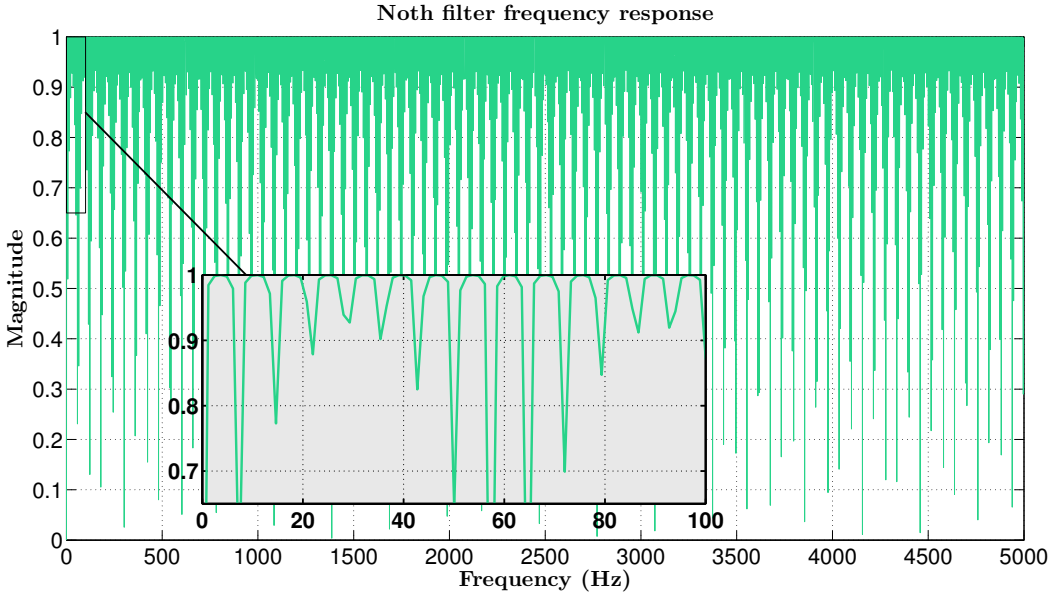

Figure 5.7: Frequency response notch comb filter, with $Q = 15$.

in the signal amplitude did not compromise the performance of the filter. The muscle activity in the frequency band of interest remains preserved.[52]

5.1.3 Downsampling

After bandpass filtering, the sEMG signal was downsampled. High frequency components were filtered before downsampling to prevent its appearance as other frequencies (aliasing) in the downsampled signal.

If we take a look at Figure 5.3 it is possible to see that at 100 Hz only 4 % of the original signal is kept, using Butterworth filter. Neglecting this part of the signal downsampling was performed resulting in a signal sampled at 200 Hz .

5.2 Pre-processing: Wavelet Analysis

Wavelet analysis has been proved to be efficient when applied to nonstationary biosignals. It allows the precise detection of time evolutions in frequency distribution.[26,40] It has been widely used to for noise reduction and/or elimination, data compression and signal classification.[9,64,65,72,73] With this method, a time series can be displayed in multiple resolutions, i.e., in different band of frequencies.

The Wavelet Transform (WT) is preferred to the Fourier transform (FT) analysis. Given a function $f(t)$ the FT $F(\omega)$ is obtained by integration of the whole signal (see Equation 5.3). However this method does not provide

information about temporal occurrence of the spectral components (see Figure 5.11).[20,40,65,74,75] For example, if a signal has two different frequency components, a low frequency component followed by a high frequency component or vice-versa, the FT returns only the identified frequencies and corresponding amplitude, but not the order of its appearance. Or, in other words, a peak in the spectrum and the corresponding frequency can be related, for example, to a period of intense muscle activity or can result from a short period of burst activity.[20,74] This means that it is not possible to distinguish two different signals in time that have the same frequency component.[74] In sum, FT is suitable to the analysis of stationary signals, instead of signals presenting short duration frequency discontinuities as is the case of sEMG.[65]

$$F(\omega) = \int_{-\infty}^{+\infty} f(t)e^{j\omega t}dt \tag{5.3}$$

WT also overcome short-time Fourier transform (STFT). The latter applies the FT to assumed stationary portions of the non-stationary signal. With this method, a temporal window function, which shape is given by $g(t)$ is applied throughout all the signal (see Equation 5.4). STFT provides a good time-frequency representation, although bad resolution is obtained (see Figure 5.11). This is due to the use of the same window, of fixed size, in the whole signal which is characterized by different frequency components in different time intervals. Analogous to the Heisenberg's Uncertainty Principle, with STFT it is not possible to simultaneously know the time and frequency components.[65,74,75]

$$F(\omega, \tau) = \int_{-\infty}^{+\infty} f(t)g^*(t-\tau)e^{j\omega t}dt \tag{5.4}$$

Observing Figures 5.10, 5.9 and 5.8 it is possible to conclude that as the window length increases, the time resolution decreases and the frequency resolution considerably increases. In other words, as the `nfft` value increases, the time intervals lose definition and the frequency is presents more defined and distinguishable values. Hereupon, it can be concluded that STFT is not suitable to the problem in study, since it needs a particular window for each signal segment, in order to obtain the correct resolution in both time and frequency.[65,75,76]

Identification of the frequency components and the corresponding time lo-

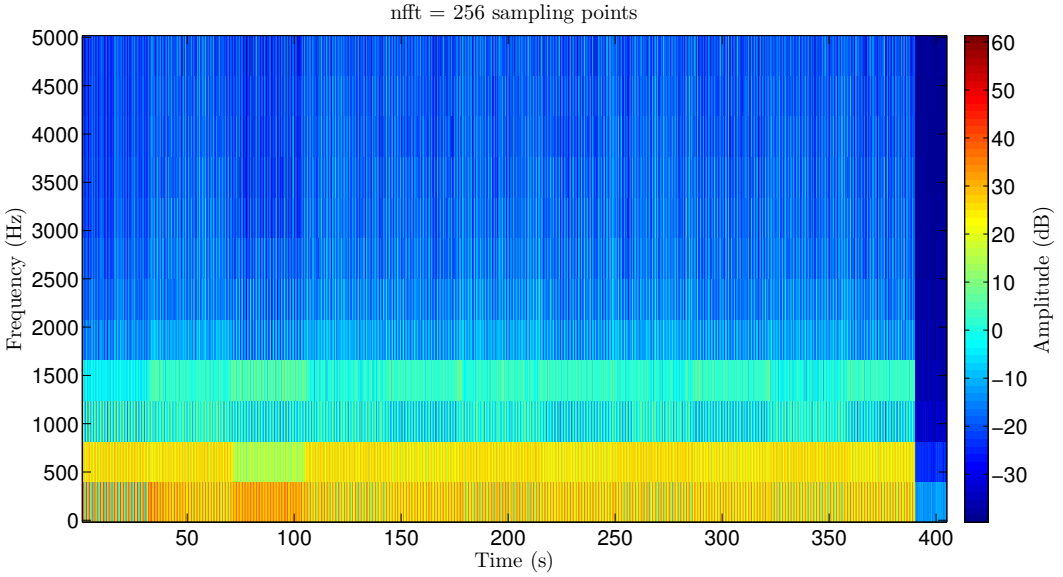

Figure 5.8: Short-time fourier transform for $nfft = 256$ samples of a sEMG signal for patient 1, run 4, unloaded condition and dominant harm.

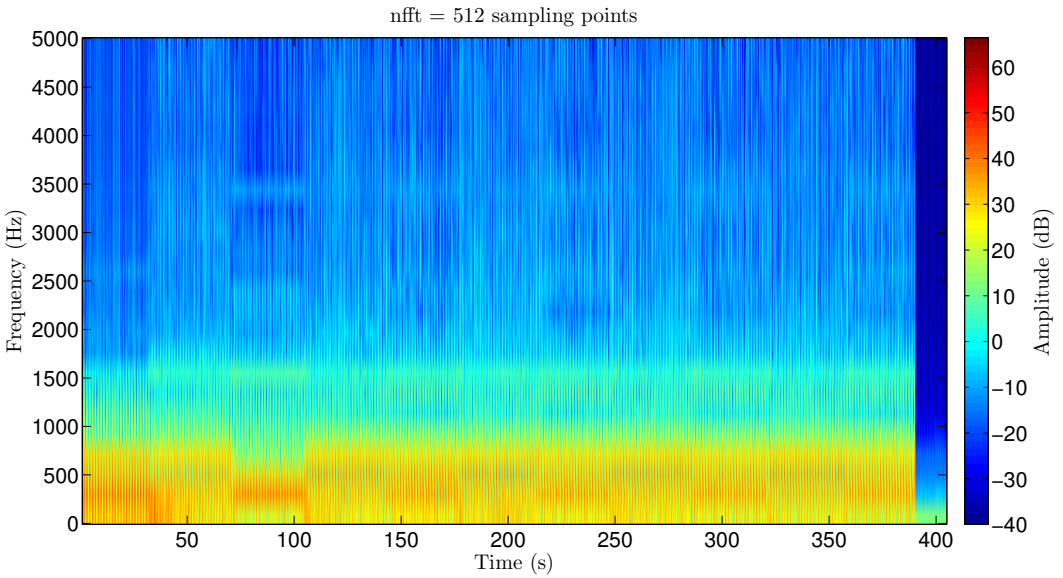

Figure 5.9: Short-time fourier transform for $nfft = 512$ samples of a sEMG signal for patient 1, run 4, unloaded condition and dominant harm.

cations can be achieved using the WT. This method applies a "scale analysis". In other words, generates small parts of the signal during which, frequency and/or amplitude variations occur, allowing the correct analysis of the non-stationary signal. It consists in the choice of a prototype wavelet, the *mother-wavelet*.[65,74,75,77] This function $\Psi(t)$ has variable parameters, that allow *scaling* and translating operations. Temporal resolution can be obtained by shifting the wavelet in time (changing b in Equation 5.5). Frequency resolution results from scale variations, (varying a in Equation 5.5). By varying

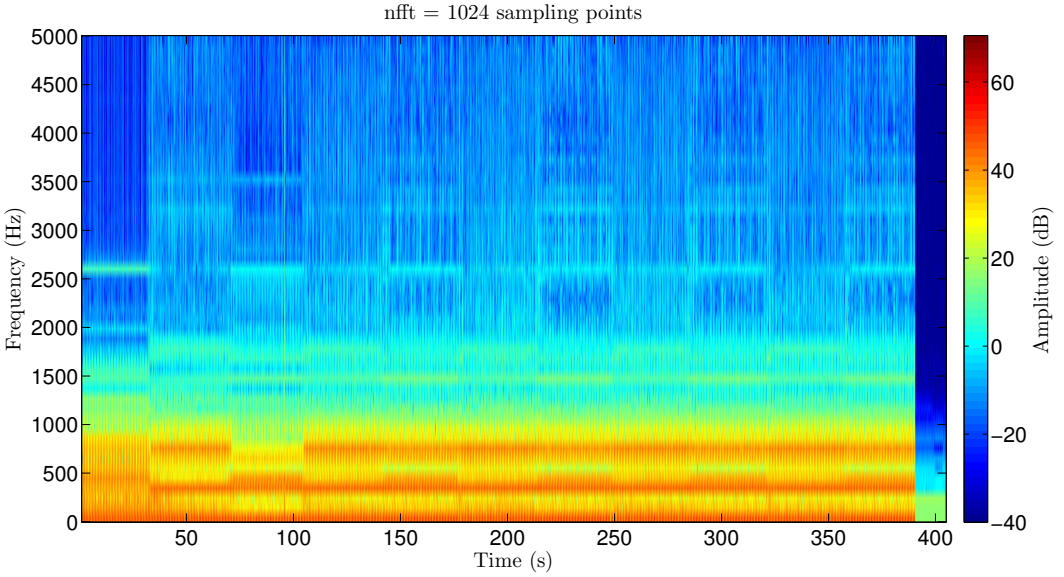

Figure 5.10: Short-time fourier transform for $nfft = 1024$ samples of a sEMG signal for patient 1, run 4, unloaded condition and dominant harm.

the scale parameter, the bandpass is also varied which allows the analysis of a particular frequency band. Then, the resulting shifted functions, given by $\Psi_{a,b}$, are applied to different portions of the signal.[40,65,73,75]

$$\Psi_{a,b}(t) = \frac{1}{\sqrt{a}}\Psi\left(\frac{t-b}{a}\right) \tag{5.5}$$

The normalizing factor $1/\sqrt{a}$ in Equation 5.5, ensures that energy does not change for different values of a.[74]

The WT (see Equation 5.6) is defined as the internal product between the signal of interest $f(t)$ and the basis function $\Psi_{a,b}(t)$ (in Equation 5.5). If a and b are continuous the WT is named continuous wavelet transform (CWT). For a given scale, WT coefficient increases as more similar is frequency content between the signal and the basis function.

$$CWT(a,b) = \int_{-\infty}^{\infty} f(t)\Psi^*_{a,b}(t)dt \tag{5.6}$$

The WT performs a multiresolution analysis, by varying the scale factor a. This method allows to detect the high frequency content (small and detailed signal discontinuities) by setting a low scale, with good time resolution and poor frequency resolution. Conversely the low frequencies (which are usually present in almost the entire signal) can be obtained using a higher scale, with good frequency resolution and poor time resolution (see Figure 5.11).[73,76,78]

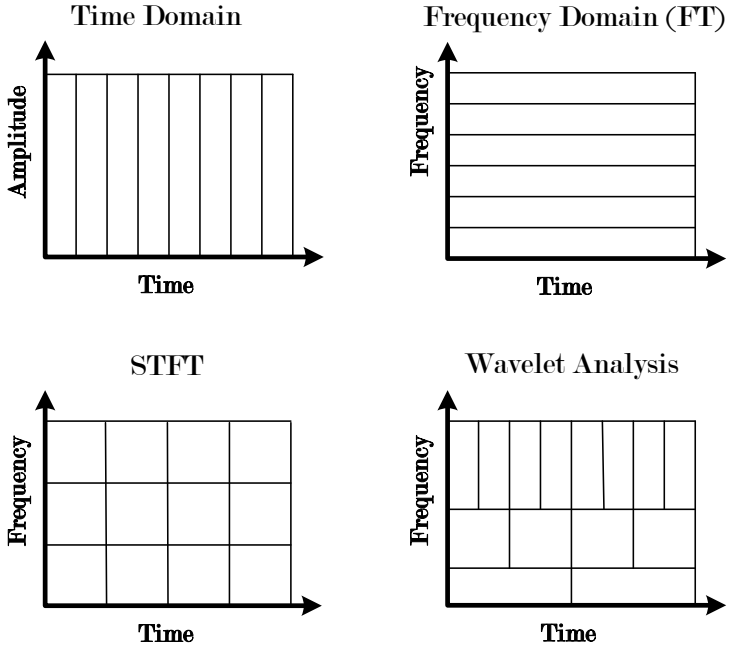

Figure 5.11: Interpretation of the transforms analysed

In this work we will use the discrete version of the WT, the Discrete Wavelet Transform (DWT). The DWT (see Equation 5.7) is then given by the internal product between the continuous function $f(t)$ and the discrete representation of the time-scale wavelet $\Psi_{m,n}$ (see Equation 5.8).[74,78]

$$DWT(m,n) = \int \Psi_{m,n}(t) f(t) dt \tag{5.7}$$

$$\Psi_{m,n}(t) = a_0^{m/2} \Psi(a_0^m t - n b_0) \tag{5.8}$$

The basis function $\Psi_{m,n}$ is still a continuous function of time, but with discrete scaling and translating parameters:

$$a = a_0^{-m}, b = n b_0 a_0^{-m}, m, n \in Z \tag{5.9}$$

The two parameters are related in the way that if the scale value returns a narrow function, the translation operation should correspond to small step and vice versa.[74] In order to effectively compute the DWT, the dyadic scaling function (see Equation 5.10) is obtained by setting $a_0 = 2$ and $b_0 = 1$.[76,78]

$$\Psi_{m,n}(t) = 2^{m/2} \Psi(2^m t - n) \tag{5.10}$$

The DWT provides enough information to the analysis and computation of

the original sEMG signal, without redundant information which implies significantly less computation time and effort when compared to the CWT.[65,76,79]

Similarly to the CWT, DWT also returns a time-scale representation of the desired signal using digital filtering methods. Different scales are obtained by using filters with different cutoff frequencies. Thus yielding different frequency sub-bands, as results of high pass (high frequency analysis) and low pass (low frequency analysis) filtering. The amount of detail information in the signal, given by the resolution, can be changed through the use of filters. The scale can be changed by upsampling and downsampling operations.

DWT transforms the continuous function $f(t)$ (our acquired sEMG signal) in a sequence of wavelets coefficients which represent the decomposition of the original signal.[78] In this work Daubechies wavelet family was used because, besides being one of the most reported in literature, presents an orthonormal basis. This last property allows the reconstruction of the decomposed signal.[26,76]

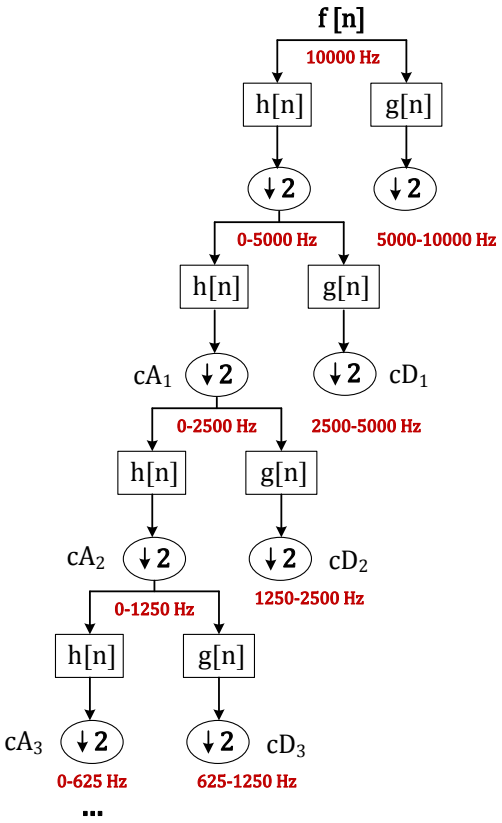

Figure 5.12: DWT decomposition structure. The original signal passes through a half band highpass filter $g[n]$ and a lowpass filter $h[n]$. Then the filters output is downsampled by two thus yielding the first decomposition level. Every level, involves filtering and downsampling operations resulting in half the number of samples (and hence half the time resolution) and half the frequency band spanned (and hence double the frequency resolution).

In each level of decomposition two functions operate. The scaling function (see equation 5.11) which is responsible for the low pass filtering and returns the approximation coefficients. Usually the signals are evaluated using scales that are powers of two.

$$\Phi_{m,n}(t) = 2^{m/2}\Phi(2^m t - n) \tag{5.11}$$

The wavelet function (see Equation 5.7) processes the high pass filter and outputs the detail coefficients. The resolution of the wavelet function, or the frequency band covered, can be varied by changing the scaling function.

In order to decompose the acquired signal, the fist step is to apply a half band digital lowpass filter, removing all frequencies above half of the highest frequency in the signal (according to the Nyquist sampling criterion). Since the signal has now half of the original frequency as its highest frequency, half of the samples are redundant and can be discarded, i.e., a signal with half the number of the points is obtained (downsampled by two). Using the half band lowpass filter results in the loss of the high frequency content and consequently doubles the frequency resolution. Downsampling doubles the scale and halves

Table 5.1: Approximation and detail frequency bands.

cA	**Frequency range (Hz)**	**cD**	**Frequency range (Hz)**
cA_1	$0 - 2500$	cD_1	$2500 - 5000$
cA_2	$0 - 1250$	cD_2	$1250 - 2500$
cA_3	$0 - 625$	cD_3	$625 - 1250$
cA_4	$0 - 312.5$	cD_4	$312.5 - 625$
cA_5	$0 - 156.25$	cD_5	$156.25 - 312.5$
cA_6	$0 - 78.13$	cD_6	$78.13 - 156.25$
cA_7	$0 - 39.06$	cD_7	$39.06 - 78.13$
cA_8	$0 - 19.53$	cD_8	$19.53 - 39.06$
cA_9	$0 - 9.77$	cD_9	$9.77 - 19.53$
cA_{10}	$0 - 4.88$	cD_{10}	$4.88 - 9.77$
cA_{11}	$0 - 2.44$	cD_{11}	$2.44 - 4.88$

cA: approximation coefficients, cD: detail coefficients

the time resolution.[73,76]

The signal is then decomposed into different frequency sub-bands with different resolutions by sequential lowpass (see Equation 5.12) and highpass (see Equation 5.13) filtering operations.

$$d[k] = \sum_{n=-\infty}^{\infty} f[n] \cdot h[2n-k] \tag{5.12}$$

$$h[k] = \sum_{n=-\infty}^{\infty} f[n] \cdot g[2n-k] \tag{5.13}$$

The $2n$ term presented in both filters refers to the downsampling operation.

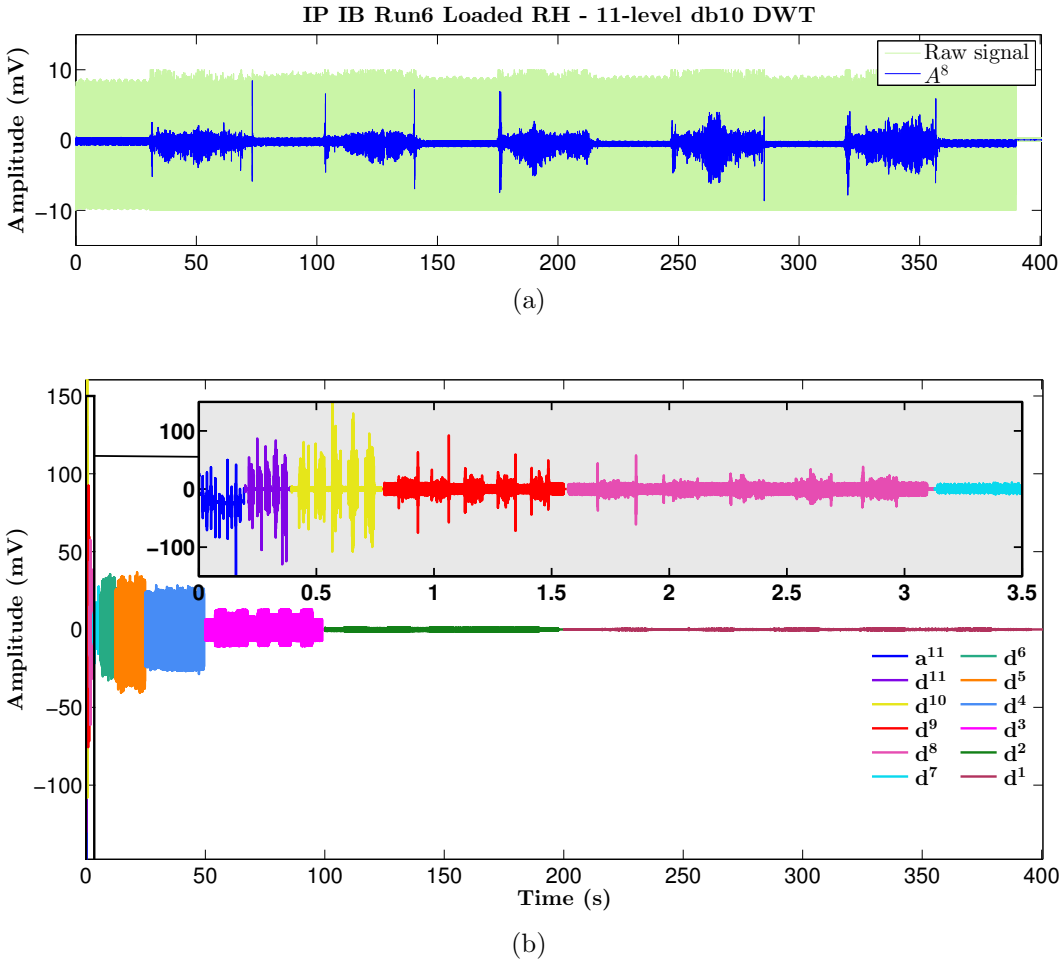

Figure 5.13: 11-level DWT decomposition using daubechie ('db10') mother wavelet. (a) The reconstructed 8^{th} level approximation coefficient $A8$ is superimposed to the original signal. (b) The highest frequency band of the signal corresponds to the non reconstructed detail coefficient d^1 (last 2002662 samples), followed by the second highest frequency band represented by d^2 (previous 1001340 samples) and so on. The lower frequencies, which carry the information of interest (of the PD tremor frequency range), are represented by the last coefficients computed in the zoomed window.

Approximation and detail coefficients are obtained as can be seen in Figure 5.12. DWT is obtained through all coefficient concatenation starting from the last level of decomposition. The most prominent frequencies in the original signal will occur as high amplitudes in the region of the DWT signal where those frequencies can be observed. The temporal resolution will depend in which level those frequencies of interest appear. High frequencies show better time resolution, since they encompass a higher number of samples (see Figure 5.13). Low frequencies are composed by a few samples resulting in low precision in time localization. In other words, good time resolution is obtained at high frequencies and good frequency resolution at low frequencies. As was depicted in Figure 5.11, for lower frequencies the length of the coefficients decreases (lower length of the rectangular areas in the frequency axis). As we are interested in the low frequencies, samples corresponding to the higher frequencies can be then discarded without any loss of information, thus reducing the size of the final data that will be analysed.[73,76]

Due to successive downsampling by two, the signal length must be a power of two, or at least a multiple of power of two (as is our case), allowing the effective application of the method. The number of samples of the signal determines the number of decomposition levels. Theoretically, the signal must be decomposed until getting the level corresponding to the last sample, or, as in our study, until the frequency levels of PD are obtained.

The main purpose of this wavelet analysis was to obtain a new cleaned signal, containing the frequencies of interest and of lower size. The final result would be a more easy to handle signal, with less computational time when computing its characterizing parameters (peak frequency, peak amplitude, linear envelope, etc). However, a significant amplitude difference between the unreconstructed approximation coefficient $\boldsymbol{a}$ at 11th level (see Figure 5.13) and the corresponding reconstructed approximation coefficient $\boldsymbol{A}$ (see Figure 5.14) can be observed. That difference is more evident in Figure 5.15 for the 8th level of decomposition which encompasses the frequency band of interest in this study. The reconstructed signal $\boldsymbol{A}$ has an amplitude that is in the range of the original signal, unlike approximation coefficient $\boldsymbol{a}$ which presents an abnormal high amplitude for a sEMG signal. This amplitude difference in of the unreconstructed approximation coefficient represents a drawback in the further calculations in the time domain, (e.g., the envelope and corresponding area under the curve, see Section 5.4.2). Then the main purpose of this wavelet analysis was not achieved since the returned approximation coefficient, even

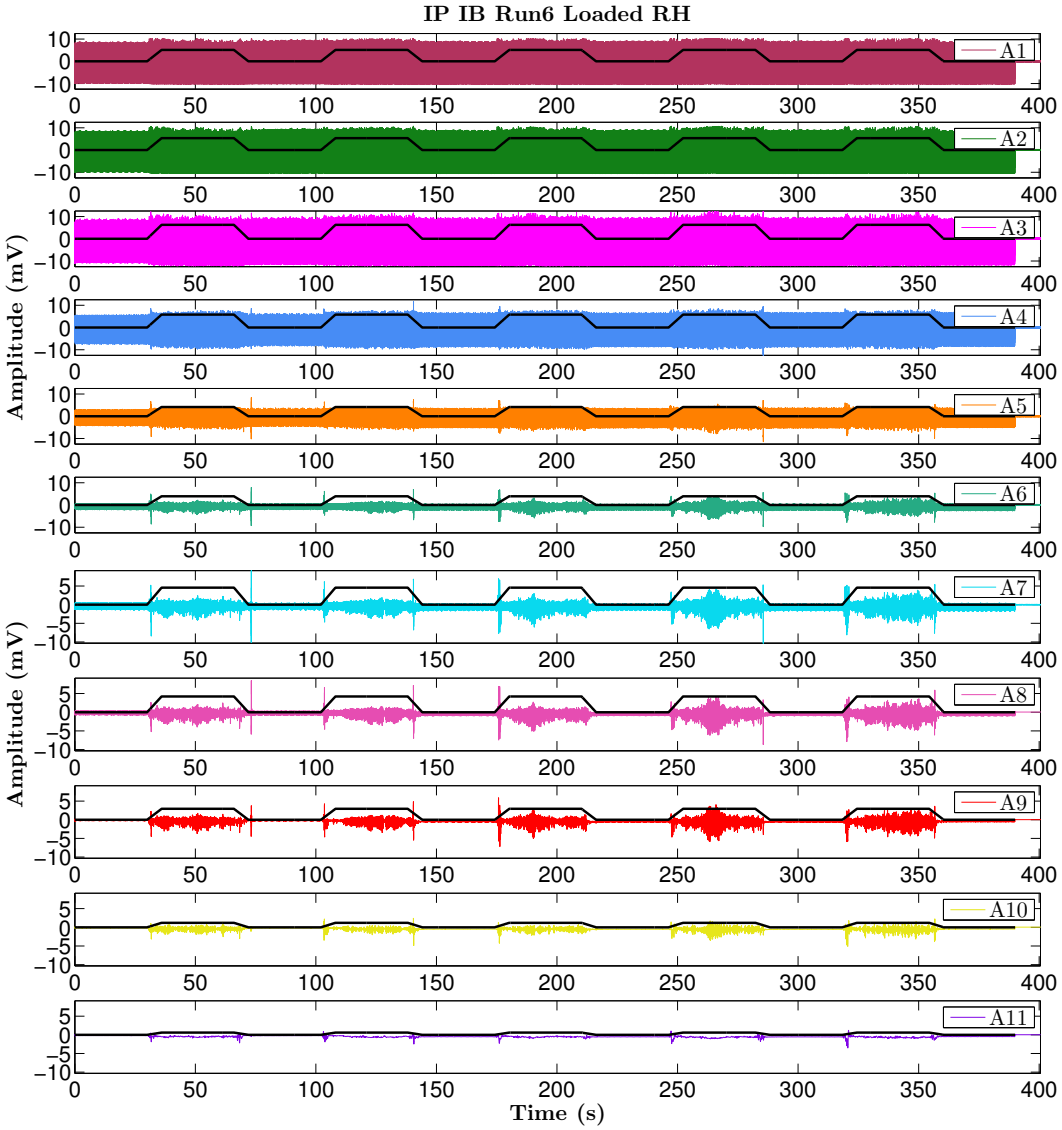

Figure 5.14: Reconstruction of the approximation coefficients. Using the mother wavelet ('db10' in our case) and the decomposition structure parameters (C and L) it is possible to reconstruct the detail and approximation coefficients. A new signal corresponding to the frequency range for each level is obtained, having the same size and sampling frequency as the original sEMG signal.

though being composed of less samples and thus being posteriorly more easy to handle, has an abnormal amplitude not in accordance with the standard sEMG signal.

The spectrum of the unreconstructed and reconstructed approximation coefficient at 8th level was computed in Figure 5.16. The magnetic gradient field artifacts (at 14.33 Hz and multiples and 7 Hz and multiples) are still present in the signal which is reflected in the high amplitude of the baseline segments in Figure 5.15. Instead, the next level of decomposition, the 9th approximation coefficient ($0-10$ Hz) could be used and the noise frequency component would

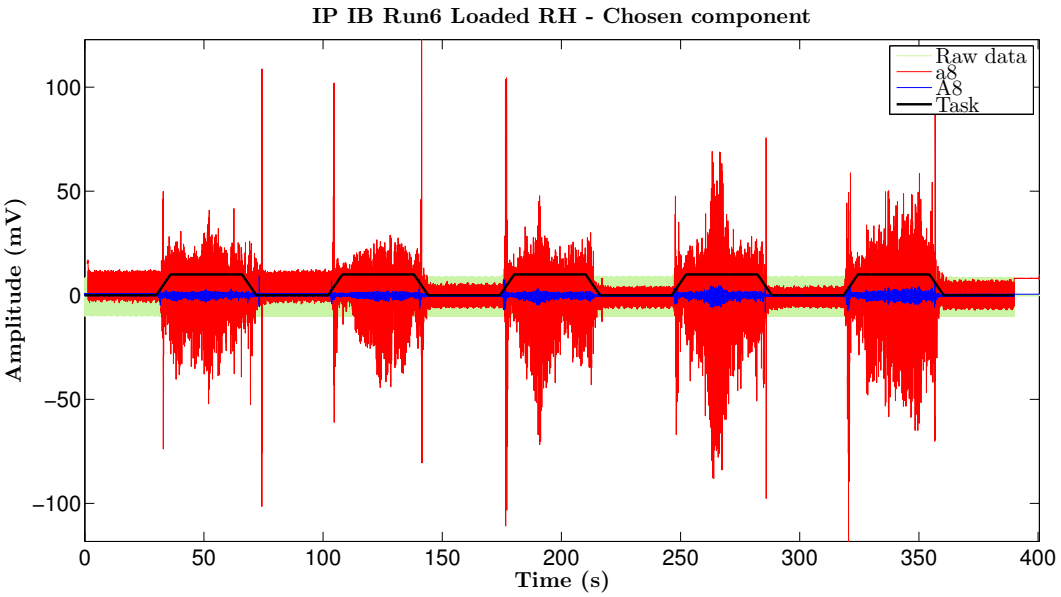

Figure 5.15: Comparison of the reconstructed approximation coefficient $\boldsymbol{A}$ for the 8th level $(0-20$ Hz), with the same size of the original signal, and the corresponding unreconstructed approximation coefficient $\boldsymbol{a}$ of much less length and significantly higher amplitude.

not interfere with the signal. However, the frequency range is too narrow and neglects important information above 10 Hz. The solution could reside in the application of a notch filter to the 8th level approximation coefficient, but that would make this wavelet method redundant, comparing to the IIR filtering method.

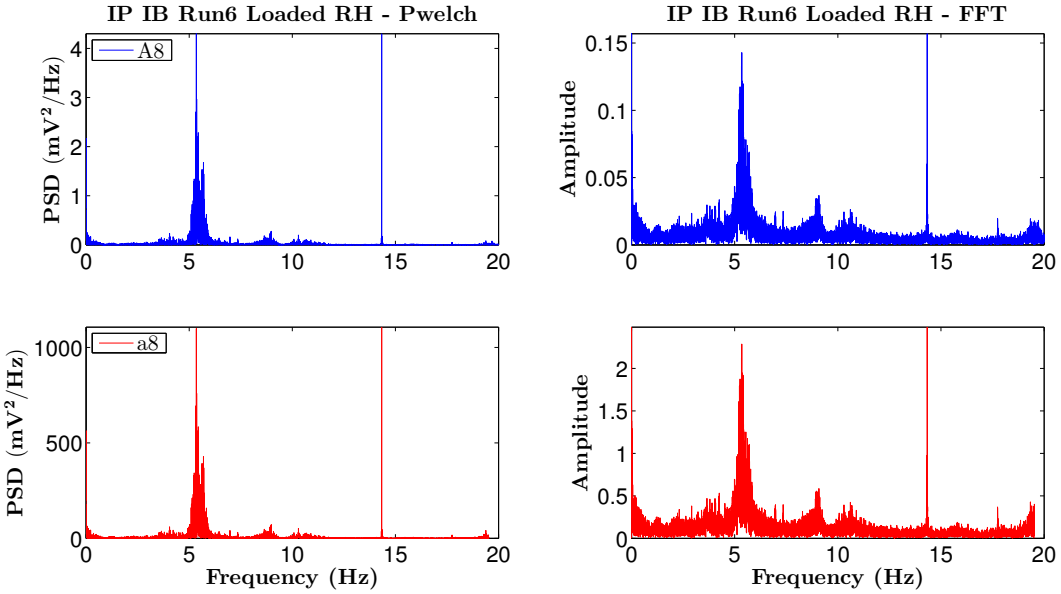

Figure 5.16: Power and amplitude spectrum representation of the approximation coefficient at the 8th level $(0-20$ Hz frequency range), after wavelet analysis.

5.3 Algorithm validation

Both algorithms (IIR filtering and wavelet analysis) tested on the sEMG signals have proven to be effective in artifact removal. In a similar study, during sEMG and fMRI simultaneous recordings, visual inspection of the amplitude spectrum and also of the filtered signal in the time domain were sufficient to validate the cleaning algorithm that makes use of filtering techniques.[53] However, according to another analysis in the same conditions, an accurate validation would imply a correlation between an sEMG signal acquired in an artifact-free environment and the signal resulting from filtering. In other words, a comparison of the distribution properties could be done between out-bore and in-bore signals. Nevertheless, such direct measure is not feasible since each sEMG signal is unique in the way that the pattern activation and force levels hardly will be exactly reproduced in another signal acquired in the same circumstances.[51,52] There is also a reduction in the signal power caused by filtering which does not happen in the artifact-free sEMG signal.[52]

In another study, the cleaning algorithm was validated using the information of joint torque acquired using an optical torque sensor.[52] In the present study, accelerometer signals were used in validation since they were not influenced by fMRI artifacts. Therefore, accelerometric filtered signals can be individually correlated with the corresponding cleaned sEMG signals (see Figure 5.17). However, the sEMG signals was found to be a suboptimal detection

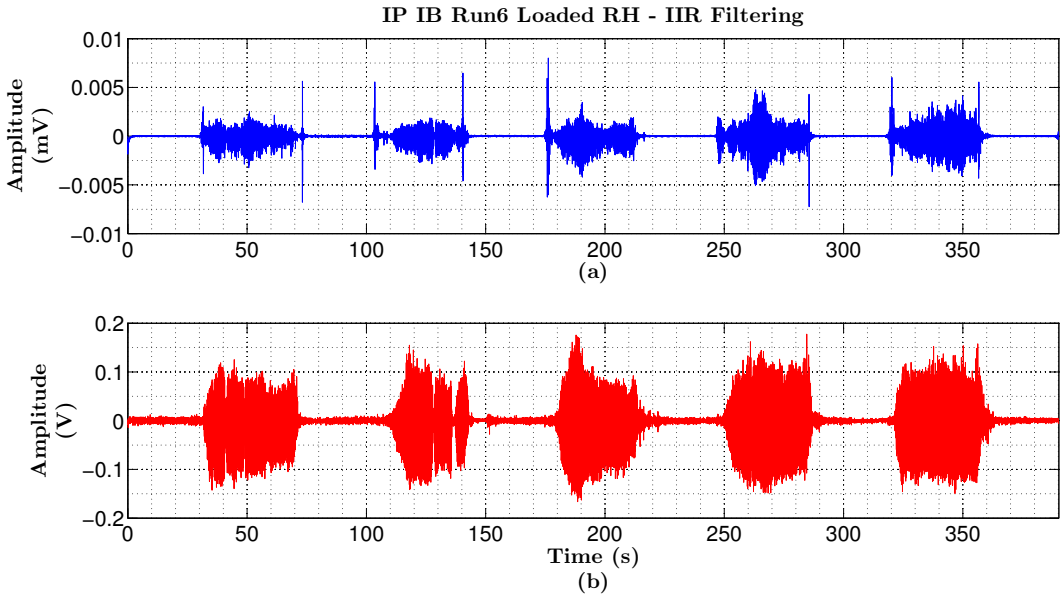

Figure 5.17: (a)Filtered sEMG data. (b)Filtered accelerometric data. Signals were acquired in-bore in patient 1 (run6, loaded, right dominant hand).

technique since rest tremor of patient 3, as an example, was not accurately reproduced in the signal as it was in accelerometric data. Increasing the number of acquisitions in PD patients will allow to confirm the relation between the sEMG and the accelerometric signals behaviour over time. Then validation could be performed using both signals that should be accurately detected during in-bore and out-bore acquisitions.

In sum, two different methods were used to filter the sEMG data. Both were able to remove the fMRI artifacts from the signals. However using wavelet analysis the results were not satisfactory since, even though the output included the frequencies of interest, it also presented the fMRI artifacts resulting from the magnetic field applied during the experiment. The IIR filtering method was then used to remove artifacts from the sEMG data.

5.4 Parameter computation

5.4.1 Full wave rectification

The signal resulting from the filtering process was then rectified, i.e., its absolute value was computed in order to proceed to determination of the shape or "envelope" of the sEMG signal (see Figure 5.19). sEMG signal typically oscillates near zero (zero mean), with either fast negative and positive transitions around zero. So if the next step is, e.g., the smoothing or moving average computation of the signal, when rectification is skipped, the result will be an approximately zero vector.[54]

5.4.2 Signal envelope

In this work the envelope of the sEMG signal was assessed using three different methods: moving average, root mean square (RMS), and a lowpass Butterworth filter.[54]

First, a lowpass IIR filter was applied to the rectified signal in order to obtain the correspondent "linear envelope", called this way due to the filter feature requirement of linearity and signal envelope detection through the lowpass filtering.[54] A zero-phase lowpass Butterworth filter was then applied to the downsampled data. The implementation of the filter and response frequency was similar to the bandpass filter, explained in the Section 5.1.1, with cutoff frequency of 0.5 Hz and filter order of two.

As moving average is a small order, linear lowpass FIR filter (see Equation 5.14). It has a good performance in the time domain, whereas in the frequency domain it is not capable to separate frequency bands. Other similar filters with better performance in the frequency domain (e.g., Gaussian filters) could be used, although at the expense of more computation effort.[80] We are mainly interested in the result in the time domain, i.e., in the envelope of the signal and for that a moving average filter was used.

$$y[i] = \frac{1}{N} \sum_{j=0}^{N-1} x[i+j] \tag{5.14}$$

In this work, moving average was obtained by convolving the input signal with a rectangular impulse with a area of one. The output sample is computed using a centered window, i.e., uses points from both sides of the corresponding input sample (see Equation 5.15), preventing the occurrence of time shifts from the original signal to the signal envelope.[54,80]

$$y(n) = \sum_{k=0}^{N-1} h(k)x(n-k) \tag{5.15}$$

where x and y are the input and output signals, respectively and N is the number of points averaged. N was set in order to achieve a cutoff frequency similar to the lowpass filter, resulting in the same signal attenuation.

The response frequency is given by

$$h(n) = \frac{1}{N} \sum_{k=0}^{N-1} \delta(n-k) \tag{5.16}$$

The discrete-time response frequency is given by

$$H(\omega) = \sum_{n=-\infty}^{\infty} x[n]\mathrm{e}^{-j\omega n} = \frac{1}{N} \sum_{n=0}^{N-1} \mathrm{e}^{-j\omega n} = \frac{1}{N} \left(\frac{1-\mathrm{e}^{-j\omega N}}{1-\mathrm{e}^{-j\omega}} \right) \tag{5.17}$$

Equation 5.17 can be simplified, using Euler's formula, (which demonstration will not be presented here) resulting in the following equation

$$|H(\omega)| = \left| \frac{sin(\frac{\omega N}{2})}{sin(\frac{\omega}{2})} \right| \tag{5.18}$$

Another way to analyse the envelope of the sEMG signals is to compute

the RMS value of the signal within a window which spans the signal for short successive intervals of time. Again, convolution was used to obtain the RMS vector from the non-rectified, squared sEMG signal.

$$RMS = \sqrt{\frac{\sum_{t-T_w/2}^{t+T_w/2} y(t)^2}{Nw}} \tag{5.19}$$

The moving average filter has a zero-phase response frequency, which is flat in the passband, with a slow roll-off and very rippled (non-monotonic) stopband (see Figure 5.18).

The Butterworth frequency response is closer to the unity in the passband and nearly zero in the stopband. Looking at Figure 5.19 it is possible to see that Butterworth filter has a greater smoothing effect comparing to the moving average or the RMS.

Decreasing the cutoff frequency (and increasing the number of samples N), lead to the occurrence of undershoot in the Butterworth envelope (see the zoomed area in see Figure 5.19). The moving average and RMS envelopes also present overshoot but with less smooth effect.

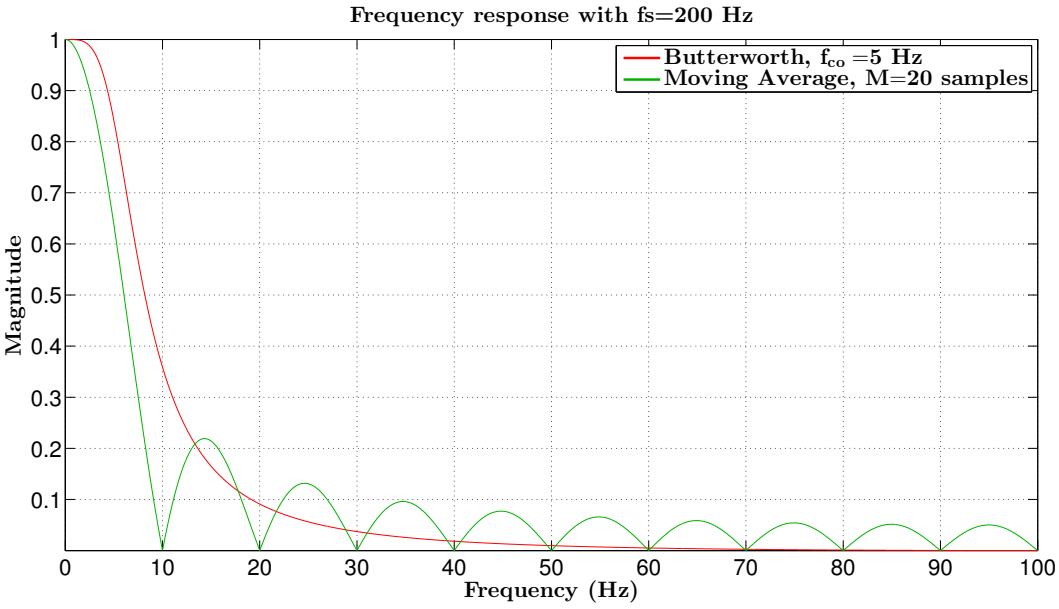

Figure 5.18: Signal envelope response frequency.

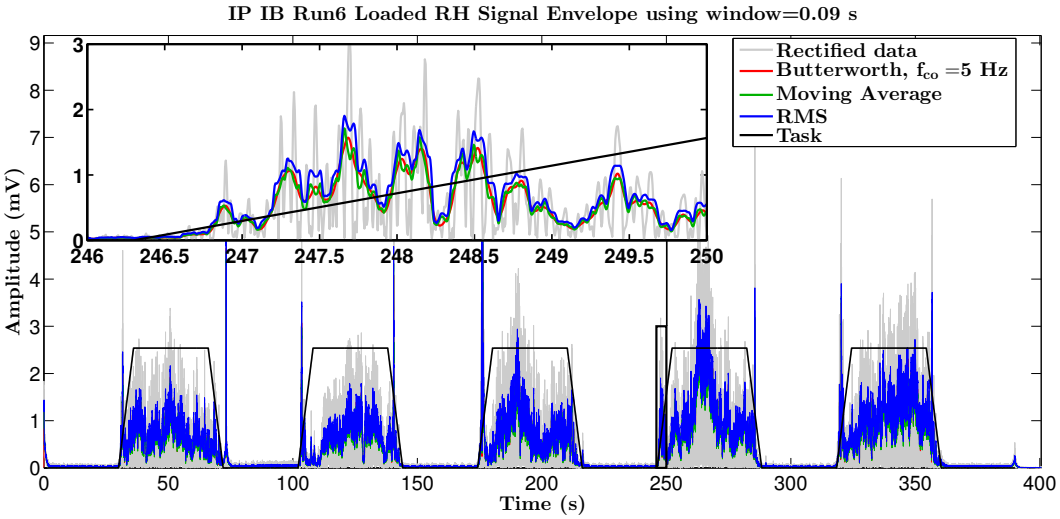

(a)

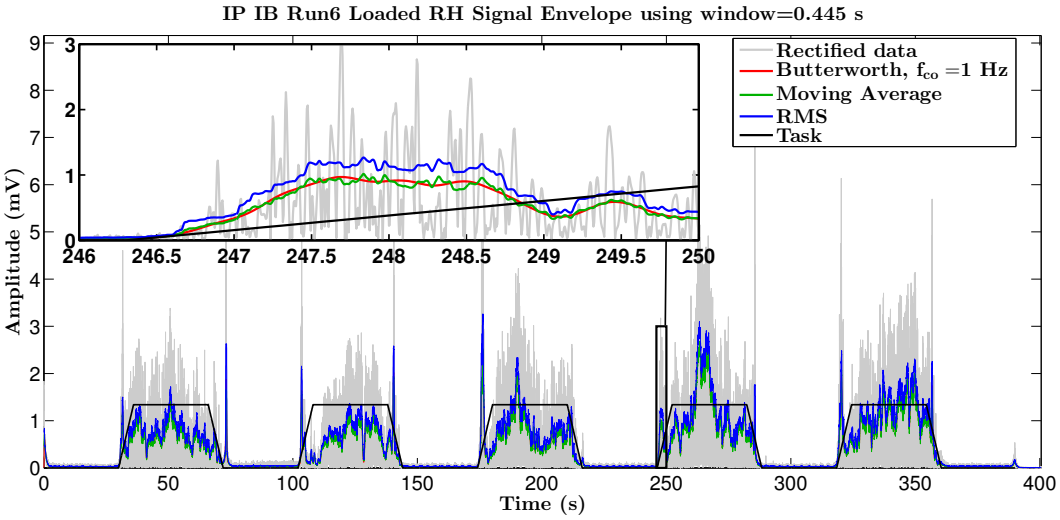

(b)

Figure 5.19: Signal envelope of the downsampled sEMG signal obtained during the in-bore experiment in patient 1 (run 6, loaded, right hand), for (a) 5 Hz and for (b) 1 Hz cutoff frequency.

5.4.3 Area Under the Curve

The area under the curve (AUC) was computed using the output of the moving average filter using a window of 0.45 s. First the signal was divided in the corresponding segments (see Figure 5.20), five posture segments (arms in the postural position) and six rest segments (arms in the rest position). Results indicate a clear difference in the envelope amplitude between rest and postural segments and a higher difference between the dominant and the non-dominant hand.

The AUC was obtained using Matlab routine `trapz` which computes the

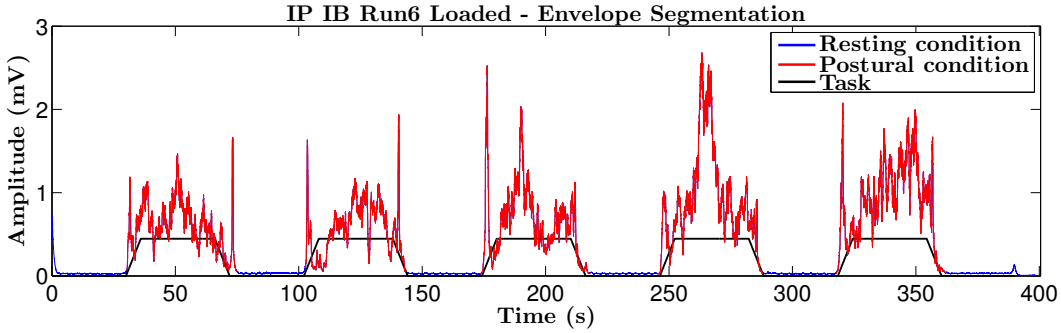

(a) Right hand

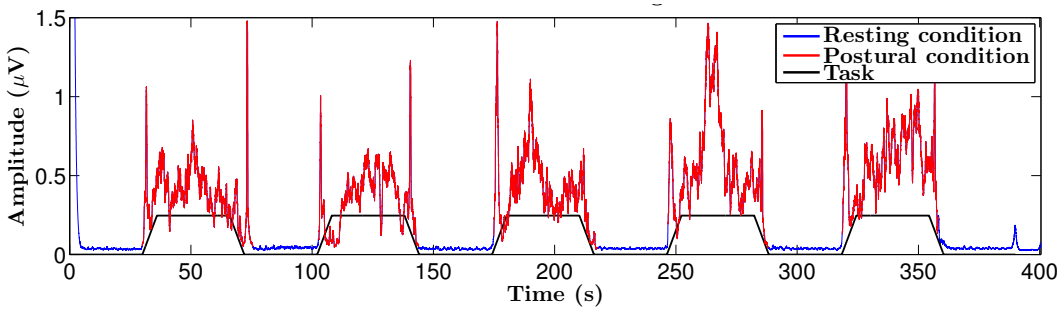

(b) Left hand

Figure 5.20: Identification of the rest and postural segments of the linear envelope of the sEMG signal obtained during the in-bore experiment in patient 1 (run 6, loaded). There is a clear reduction in the envelope amplitude from the right do the left hand (from the millivolts to the microvolts).

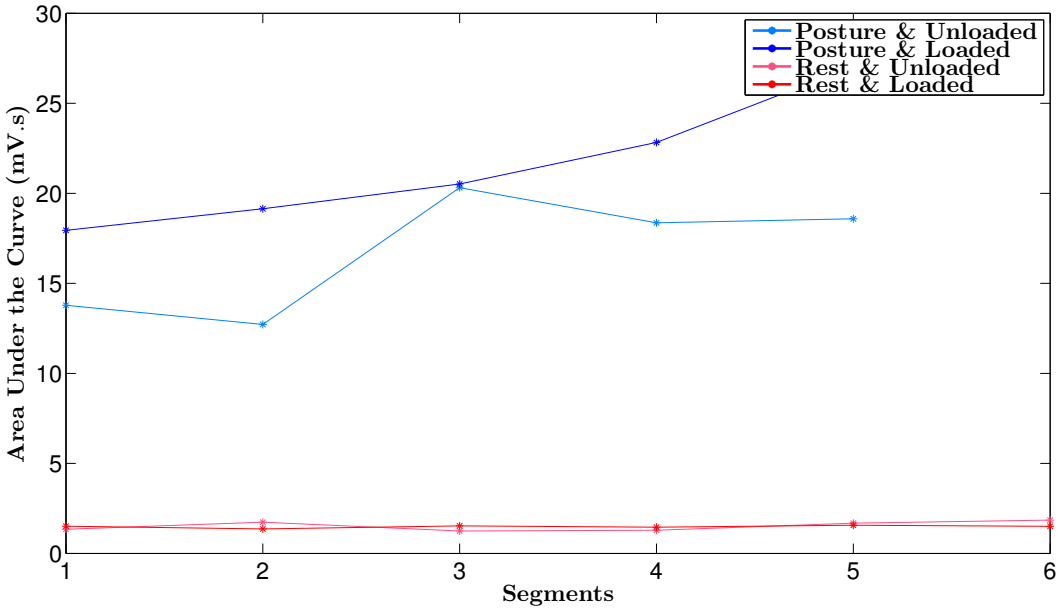

Figure 5.21: The AUC was computed for each segment using the linear envelope of the sEMG signal obtained during the in-bore experiment in PD patient 1.

numerical integration using the trapezoidal method. This parameter was computed for each segment (see Figure 5.21) and the values were stored in order to be ready to the statistical analysis.[51] Posture and rest segments greatly differ in AUC values. Comparing loaded and unloaded tasks results it is possible to conclude that postural condition is able to increase the effect of load. However, only statistical analysis with a larger and homogeneous PD population will make possible to take robust conclusions.

Chapter 6

Spectral Analysis

In this section, methods to analyse both the accelerometric and surface electromyography (sEMG) signals are described. In a first approach spectral analysis, using Fourier transform (FT), was performed in order to identify the peak amplitude (PA) and corresponding peak frequency (PF).[3,42,44,60,81,82]Spectral analysis is the most common method used to obtain tremor parameters such as frequency, amplitude or power.[4,9,20,26,42,81]

This procedure was applied to signals acquired from three patients, all presenting an asymmetric tremor. Patient 1 presents right hand dominant PD tremor. Patients 2 and 3 have PD tremor most prominent in the left hand. Patient 2 continued medication intake before the acquisition. Patients 1 and 3 stopped medication administration 12 hours before the experiment. Patient 3 was diagnosed with rest tremor.

6.1 Peak amplitude and frequency

The first results PA and PF for were obtained using the whole sEMG filtered signal (see Table 6.1). Concerning tremor PA, the highest values are seen for patient 1, with right hand dominant tremor. Tremor PA increases as more runs are performed. Patient 2 reveals lower PA for the dominant left hand, which could be explained by the medication effect.[44] The less affected hands for both patients present, as expected, lower tremor PA, when the latter can even be identified. Contrarily to the tendency seen in the dominant limbs, in the non-dominant hands patient 2 has higher tremor PA than patient 1.

As for the PF, it was present around 5 Hz in the patient 1 results and 7 Hz for patient 2. Once again, differences could be justified by the effect of medication in the attenuation of tremor in patient 2.

Table 6.1: Peak frequency and amplitude in all spectrum computed for accelerometric signals of patients 1 and 2

Parameter	Amplitude (mV)				Frequency (Hz)			
Patient	**1**	**2**	**1**	**2**	**1**	**2**	**1**	**2**
Hand	LH		RH		LH		RH	
Run 1	-	0.99	2.52	-	-	7.02	5.19	-
Run 2	-	0.93	4.31	-	-	7.95	5.19	-
Run 3	0.27	1.27	3.98	-	6.99	6.75	5.11	-
Run 4	0.41	2.53	3.88	0.61	7.00	6.65	5.06	6.85
Run 5	0.56	1.99	5.39	0.87	5.29	6.73	5.15	6.79
Run 6	0.54	2.51	10.44	-	5.35	6.51	5.35	-

LH: left hand, RH: right hand, the '-' indicate that no peak was identified.

Second peaks, which were not inserted in Table 6.1, were observed only in patient 1 accelerometric signals, in all runs of right hand and in the last four runs of left hand. Those frequency peaks located near 10 Hz. The corresponding PA is lower than that observed for the first amplitude peaks, for both hands. Higher PA was seen for the dominant hand comparing to the non-dominant. Second PA increased with the number of runs performed by the patient.

Peak frequency and power were also identified in the segmented filtered

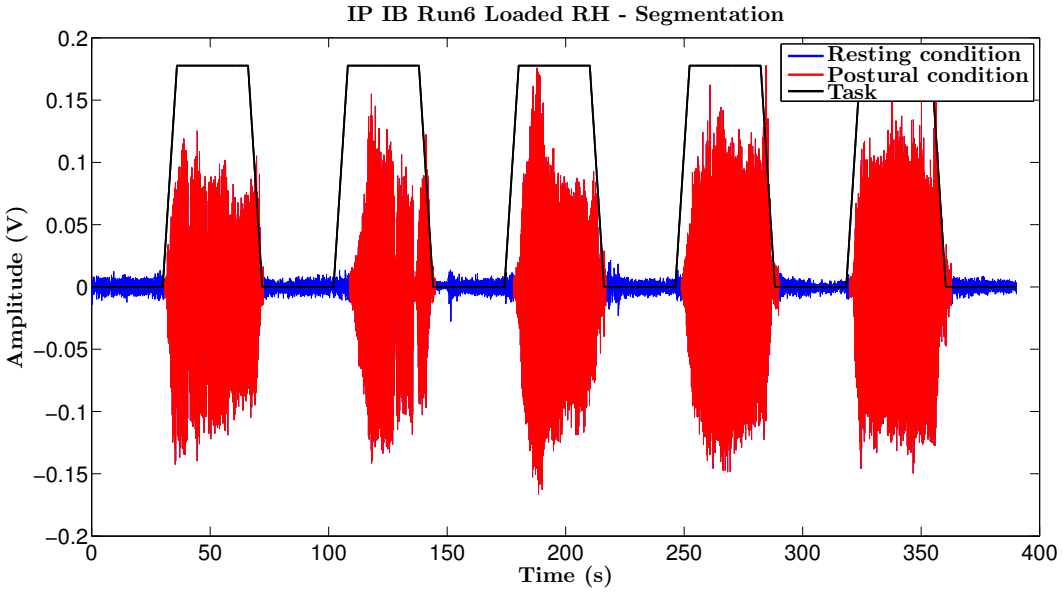

Figure 6.1: Segmentation into rest and postural segments of the accelerometer filtered signal acquired in-bore in PD patient 1 (run 6, loaded, right hand).

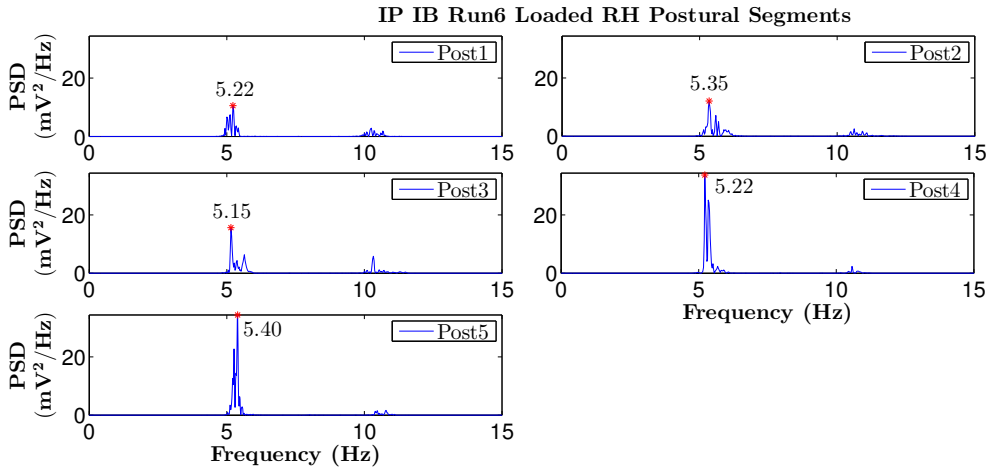

Figure 6.2: Peak amplitude and frequency for each postural segment for the accelerometer filtered signal acquired in-bore in PD patient 1 (run 6, loaded, right dominant hand).

signal (see Figure 6.1). In other words, the signal resulting from the pre-processing stage was divided in postural and rest segments. Then, Welch's power spectral density (PSD) estimate was computed for each segment, using a Hanning window of the length of the signal and a 50% of overlapping of the windows.

In the postural segments of patient 1, during which arms remained outstretched in a postural position, two distinct peaks were often identified, one near 5 Hz and the other, of lower amplitude, near 10 Hz, as reported by another study.[20] Observing the results in Figure 6.2, it is possible to conclude

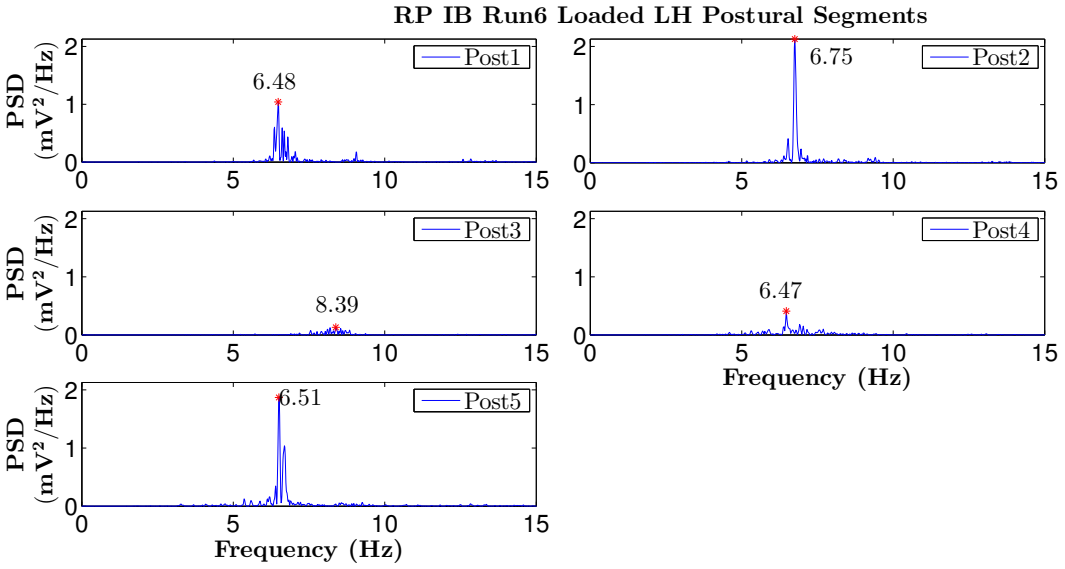

Figure 6.3: Peak amplitude and frequency for each postural segment for the accelerometer filtered signal acquired in-bore in PD patient 2 (run 6, loaded, left dominant hand).

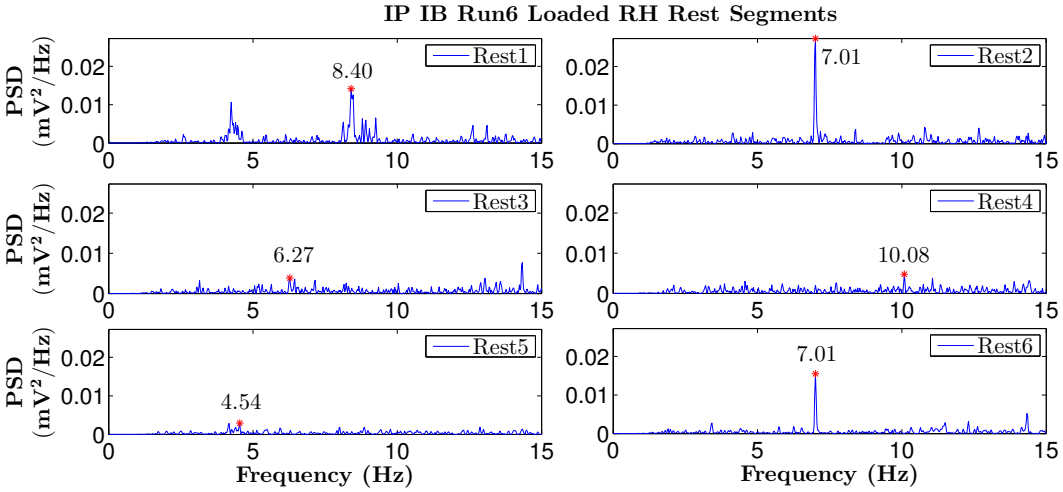

Figure 6.4: Peak amplitude and frequency for each rest segment for the accelerometer filtered signal acquired in-bore in PD patient 1 (run 6, loaded, right dominant hand).

that postural segments power is the most contributive to the peak of amplitude observed for all data (in Figure 4.2). Power peaks in the postural segments are significantly higher than in rest segments and a second peak of about 10 Hz is always seen.

Patient 2 results for the postural segments indicate a constant presence of a power peak between 6 to 7 Hz (see Figure 6.3). Second peak are not seen in the spectrum. This increase in the frequency from patient 1 to patient 2 in the postural segments can be explained by the medication effect or the presence of a different type fo tremor. As refereed in the Subsection 2.1.1, re-emergent tremor typically manifests in the postural condition. A significant difference in terms of power was seen between the two patients in the postural segments. Patient's 2 rest segments (not presented here) are similar to patient 1, being

Table 6.2: Peak frequency (Hz) in signal segments

	Postural Segments					Rest Segments					
Run	**1**	**2**	**3**	**4**	**5**	**1**	**2**	**3**	**4**	**5**	**6**
1	5.59	8.15	6.81	6.47	6.45	2.66	2.25	6.47	10.52	4.13	3.39
2	5.07	5.19	5.27	5.18	5.40	4.25	7.01	7.01	7.01	7.01	4.08
3	4.88	5.11	4.96	5.09	5.00	7.01	4.37	3.27	7.01	11.62	4.61
4	4.92	5.08	5.13	5.05	4.64	4.42	7.01	6.20	7.01	6.98	7.01
5	5.21	4.90	4.96	4.88	5.30	7.01	4.49	10.45	7.01	12.45	8.59
6	5.22	5.35	5.15	5.22	5.40	8.40	7.01	6.45	10.08	4.54	7.01

This data corresponds to PD patient's 1 right dominant hand.

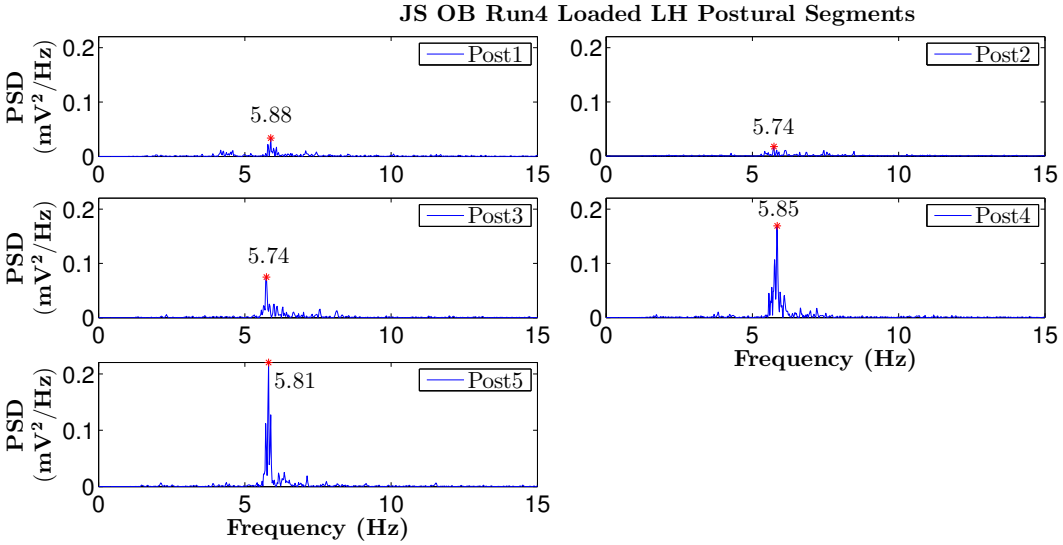

Figure 6.5: Peak amplitude and frequency for each postural segment for the accelerometer filtered signal acquired out-bore in PD patient 3 (run 4, loaded, left dominant hand).

both within the same power range and with no peaks identified.

Results of the spectral analysis for patient 3 in each segment are depicted in Figures 6.5 and 6.6. The significant difference in power seen in the other two patients (which only had postural tremor) between rest and postural segments is no longer present in patient 3. In fact, rest segments have higher power peaks comparing to postural segments. A difference can also be observed concerning peak frequency. Rest segments, during which patients' hands were in a relaxed resting position, showed frequency peaks tending to 5 Hz, as reported in other

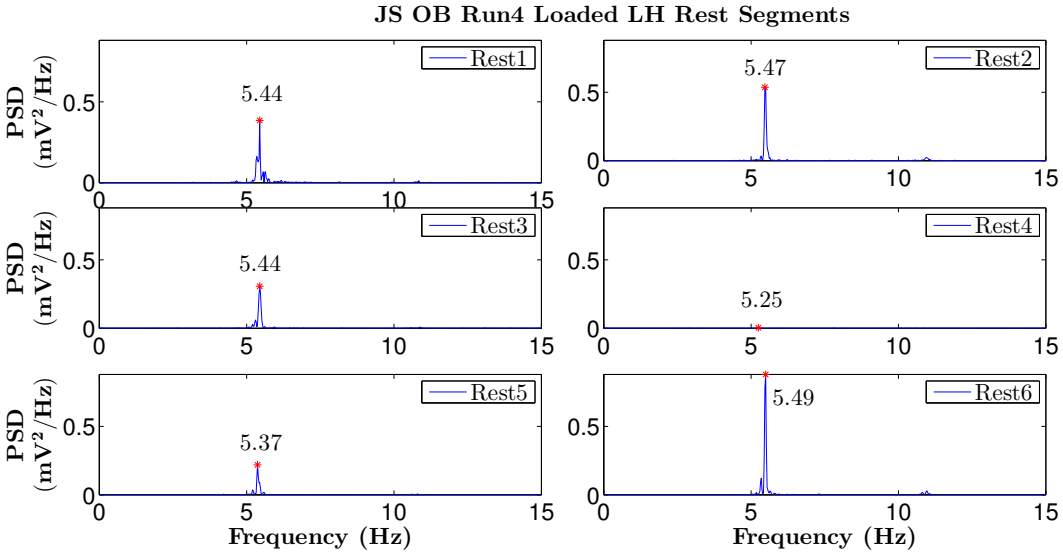

Figure 6.6: Peak amplitude and frequency for each baseline segment for the accelerometer filtered signal acquired out-bore in PD patient 3 (run 4, loaded, left dominant hand).

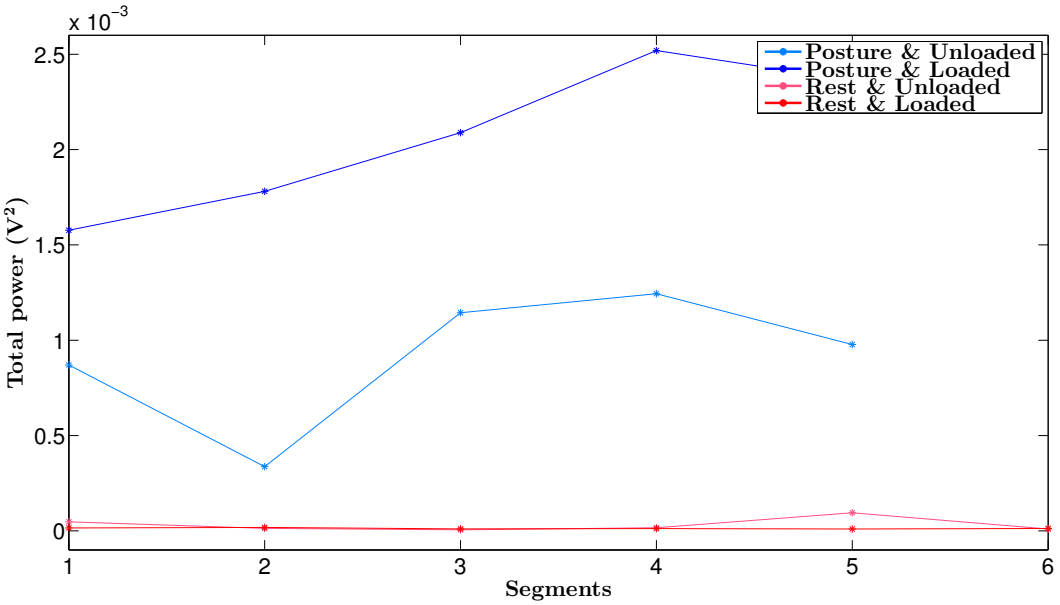

Figure 6.7: Total power in each segment for PD patient 1, right hand from in-bore accelerometric signals.

similar studies.[20,42] In postural segments peak frequency tended to 6 Hz and no second peak was present.[20,42,60]

Total power of the spectra between 1-25 Hz was also computed and considered as a measure of tremor amplitude. Those values were determined using trapezoidal method (using Matlab routine `trapz`). Then the values were averaged over the loaded and unloaded runs for patient 1 (see Figure 6.7). Rest and postural segments present very distinct values of total power. Noteworthy are the results for unloaded and loaded runs, which, unlike for rest segments, greatly differ in the postural segments. However, this results are merely representative, since they are mean of three values of total power per segment for loaded and unloaded conditions. With a more homogeneous and larger PD population, a statistical analysis would provide reliable results.

6.2 Spectrogram

Spectrogram of the filtered data was computed in order to relate time and frequency domains. This method outputs a PSD matrix with the number of lines corresponding to the length of the frequency vector and the number of columns equal to the length of the time vector.

Observing Figure 6.8 in (a), it is possible to see a clear increase in PSD during the postural segments near 5 and 10 Hz. The plot of the frequency corresponding to maximum PSD in each instant also shows a predominance of

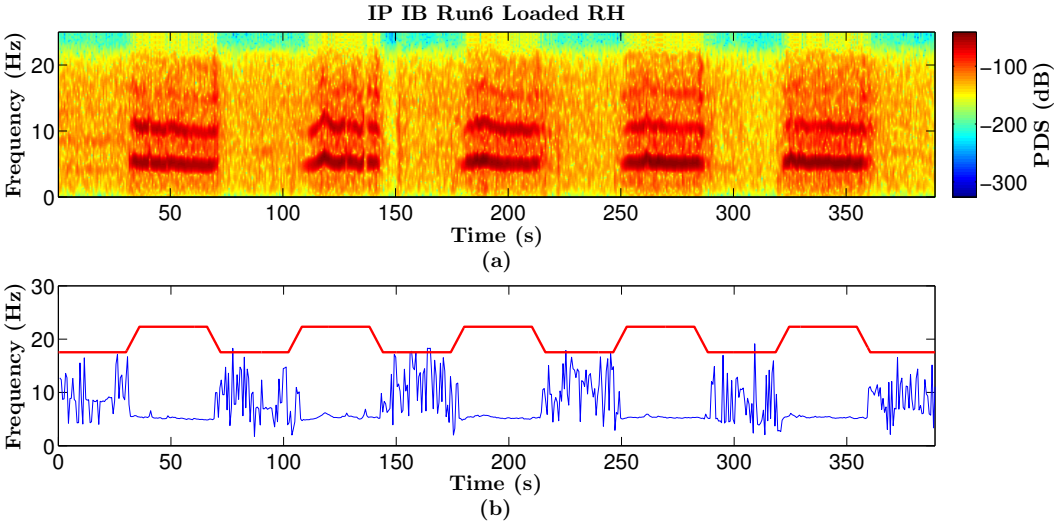

Figure 6.8: (a) Spectrogram plotting of the filtered accelerometric signal acquired during the in-bore experiment in PD patient 1 (run 6, loaded, right hand). (b) Time-frequency representation of the maximum PSD in each time.

the 5 Hz frequency in the postural segments.

6.3 Tremor and nontremor analysis

Using the spectrogram PSD matrix a method was developed in order to provide predictors to analyse the functional magnetic resonance imaging (fMRI) data (see Chapter 7). To obtain the spectrogram averaged data (see Figure 6.9) the mean of the matrix over the time columns was computed. The resulting vector (Spectrogram averaged data in Figure 6.9) was binarized, i.e., values above and below a given threshold (defined by Equation 6.1) were set to one and zero, respectively.[42] Then, using a binary classification intervals of *tremor* and *non tremor* were identified as being one and zero respectively.

$$threshold = MEAN - \frac{2}{3}SD \tag{6.1}$$

An analysis over time will be performed in each run and blocks where tremor exists and will be defined as predictors to input in the fMRI analysis. An automatic algorithm was implemented in order to obtain this block design. However, a close look at the Figure 6.9, at the signal resulting from Equation 6.1 (in blue) will be sufficient to note a misidentified tremor interval in the second top segment. In that segment the non-tremor interval identified below the threshold could be neglected. To avoid this cases a 4th order low-pass Butterworth zero-lag IIR filter was applied to the data using a low-pass cutoff

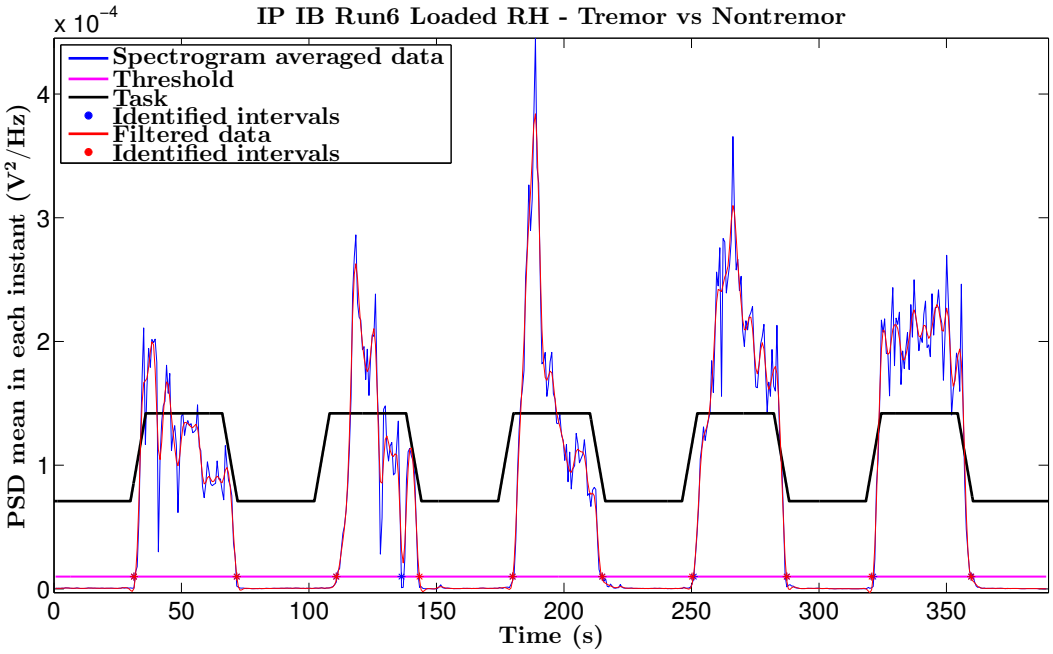

Figure 6.9: Tremor vs Nontremor plot of the filtered accelerometric signal acquired during the in-bore experiment in PD patient 1 (run 6, loaded, right hand)

frequency of 6 Hz. The result is a well identified tremor block. A moving average filter was also tested, but with less number of well identified tremor intervals and the results were not presented here.

6.4 Frequency bands analysis

The spectrogram PSD matrix was again used to determine the mean PSD vector for the following frequency bins: $0-2$, $2-4$, $4-6$, $6-8$, $8-10$ and $10-12$ Hz.[60] Another frequency division was also adopted, taking into account the frequency bands characteristic of the rest ($3-7$ Hz) and postural ($7-12$ Hz) tremors. Each frequency band was obtained by averaging the spectrogram matrix for the chosen frequency band. In other words, a given frequency band vector was obtained by computing the mean in each time (each column) over the two frequencies of the range.

In all runs performed by patient 1, frequency band $4-6$ Hz showed the greatest power comparing to the other bands, followed by the $6-8$ Hz band. On the other hand, patient 2 presented $6-8$ Hz as the most powerful frequency band across the runs, followed by the $8-10$ Hz band, as seen in other similar study during which patients remained on medication.[3] Comparing the results between the two patients, the patient 2 presents frequency bands with

considerably less power (of about one unit bellow) than patient 1. Once more, this could be the result of the on medication state.[60]

Both the tremor vs nontremor and frequency bands analysis will be used to analyse the functional images. The latter analysis has the advantage of retaining the whole frequency band information, unlike the tremor vs nontremor intervals analysis.

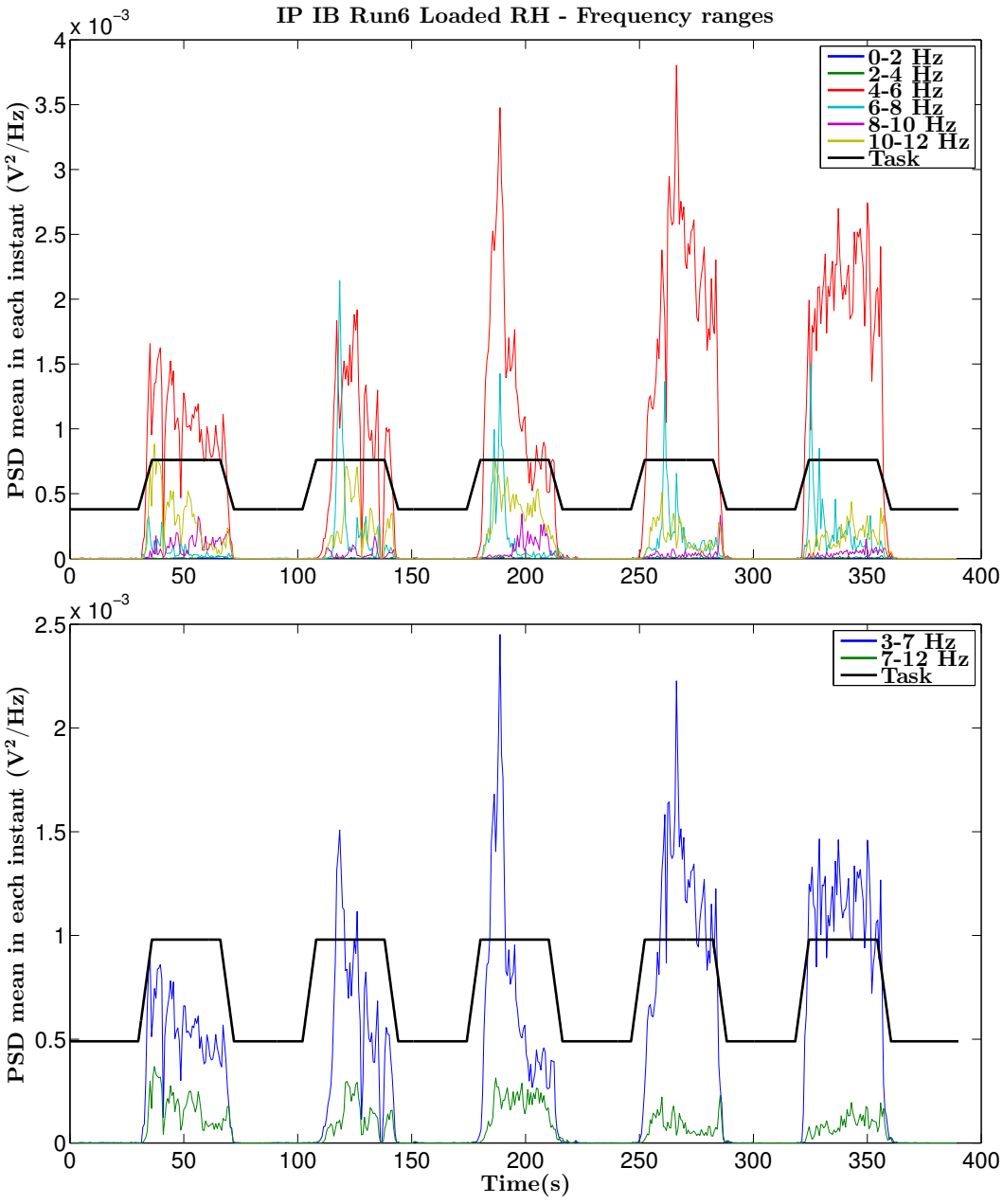

Figure 6.10: Frequency bands

6.5 Discussion

In this section signal processing was used to analyse the accelerometric data. Namely, spectral analysis was performed and tremor changes in amplitude and frequency were assessed, during the two different task conditions. All methods proved to be efficient. However, the small and non-homogeneous PD population were considered the main drawbacks of this work. Variability in the PD tremor results were the reflex of different levels of disease progression, medication state and type of diagnosed PD tremor (see Table 3.1).

Postural condition tended to increase the PD tremor.[46] As the runs were performed an increase in amplitude of the peak was observed that could be explained by the fatigue.

In all patients it was reported a power increase in the $4 - 12$ Hz and lower power in the remaining spectrum. Vaillancourt & Newell[3] assigned that increase in power from the higher to the lower frequencies to the change of the level of contribution of the peripheral feedback oscillator to the central neural oscillator. Namely, in the postural segments, power peaks were identified for patient 1 near 5 Hz and a second peak was also detected about 10 Hz. The 5 Hz peak can be assign to the presence of re-emergent tremor, which shares the same frequency range with rest tremor but usually occurs in the postural condition. On the other hand, the patient tested on medication presented a reduced tremor amplitude and a shift in PF to higher frequencies (between $6 - 7$ Hz),[46] which can be explained or be the medication effect or by the manifestation of a tremor type within another distinct frequency range. Second peaks were not seen both in postural and rest segments in patients 2 and 3 results. The results for the patient diagnosed with PD rest tremor showed the existence of one peak in both postural and rest segments, but located at slightly different frequencies in the spectrum.

A quick look at the results (see Table 6.2) is sufficient to note a slight decrease in the tremor PF during the loaded runs.[20] However, both the effect of load and the difference between postural and rest segments can only be accurately assessed by applying statistical analysis in a larger and homogeneous population.

Chapter 7

fMRI

Functional magnetic resonance imaging (fMRI) arose as a useful functional and non-invasive brain imaging technique. Namely, it has been widely used to understand the pathophysiology of PD, including functional connectivity.[25,36,52,53,83]

The main purpose of this chapter is to determine the circuits modulating Parkinson tremor and understand the functional connectivity of the involved brain areas (i.e., describe the connections and 'synchrony' between and within brain regions).

7.1 Physical basis of fMRI

Herein a brief description of the physical principle of the fMRI technique is presented. This technique relies on the intrinsic magnetic properties of the water protons, which behave as a magnet if its spin is different from zero. When no external magnetic field is applied, the spins and their nuclear magnetic moments are randomly oriented. However, is the presence of a strong magnetic field, the nuclei align with the field. The nuclei precess around the field with an angular frequency (Larmor frequency), but at a random phase. Then, in order to align the phase and increase the flip angle of the spin, a radio frequency (RF) pulse can be applied. Consequently, the longitudinal magnetization (parallel to the magnetic field) decreases and a new transversal magnetization (perpendicular to the field) is established. When the RF pulse ceases, the equilibrium is replaced, i.e., the transverse magnetization decreases and disappears (transversal relaxation) and the longitudinal magnetization increases to its original size (longitudinal relaxation). The time constant T1 describes longitudinal relaxation (exponential growth) or restoration of net

magnetization along the longitudinal direction as spins return to their parallel state. The time constant T2 corresponds to the transverse relaxation (exponential decay) or loss of net magnetization in the transverse plane due to loss of phase coherence. T1 and T2 are tissue properties that can be differently weighted, originating different image contrasts and consequently varying the specificity of the study. Pulse sequences are then manipulated by tuning three parameters: the frequency of the RF pulses, or repetition time (TR), how soon after the excitation pulse we begin data collection, or echo time (TE) and the flip angle. In the end of this process a signal is created that can be measured using a receiver coil. In order to localize the voxels (single volume elements containing protons), spatial information needs to be encoded into the magnetic resonance signal. This is the so called spatial encoding process which relies on successively applying magnetic field gradients. To image a given slice (containing the voxels), a magnetic gradient is added along the slice direction. Therefore, a slice frequency acquisition corresponds to the frequency of the magnetic gradient interference.[84–86]

Performance of certain sensory, motor or cognitive tasks induces local changes in oxygen consumption, cerebral blood flow and blood volume which can be related to increases or decreases of activity in specific regions of the brain.[25,36,52,53,83] An increase in neural activity originates a growing demand for oxygen which results in a blood flow increase in the activated regions. Hemoglobin, a protein responsible to deliver oxygen to the neurons, exists in two different states, each characterized by different magnetic properties that will producing different local magnetic fields. The oxyhemoglobin is diamagnetic and, when it delivers the oxygen to the cells, it becomes deoxyhemoglobin, which is paramagnetic. Deoxyhemoglobin creates an inhomogeneity in the magnetic field which causes the nuclei to dephase quicker and therefore to suppress the magnetic resonance signal. As the concentration of deoxyhemoglobin decreases the signal intensity increases. Then, the combined effect of T2 and the distinct mechanism of transverse relaxation induced by the magnetic field is described by another property, the T2*. Being sensitive to flow and oxygenation makes T2* suitable to be used in image brain function. The gradient-echo pulse sequence was used in the study and is weighted in T2*.[86] BOLD signals are taken from the ratio in T2* between oxygenated and deoxygenated hemoglobin in the blood. In sum, BOLD fMRI measures the neuronal activity indirectly, by measuring the metabolic demands (oxygen consumption) of active neurons. Instantaneous neuronal activity will change the magnetic

resonance signal resulting in a hemodynamic response function (HRF). This response reflects the variations in T2* and, consequently, it reflects the energy demands and the neural activity. In the present study, the task paradigm is composed of segments of alternating postural and resting periods during which BOLD signal was acquired.[36,52,53]

7.2 Analysis

The imaging data analysis was performed using the Brain Voyager Software (QX version 2.4; Brain Innovation, Maastricht, The Netherlands). Before applying statistical analysis, data needed to be pre-processed. First, slice scan time correction was performed, followed by head motion correction, spatially smoothed with a 4 −mm full-width at half-maximum (FWHM) Gaussian filter and three-dimensional temporal filtering.[53,83,87] The functional data were co-registered with the structural images and the data collected was then automatically registered into the standard Tailarach space.

In the first-level, data were analysed for each subject separately using general linear models (GLM) to identify significantly activated voxels. The predictors model was obtained by convolution of the time course belonging to each condition with a two-gamma hemodynamic response function. After model estimation, contrast maps derived from each participant were calculated and analysed individually. A second-level analysis with the total number of participants, using one-way repeated measures ANOVAs, was performed correcting

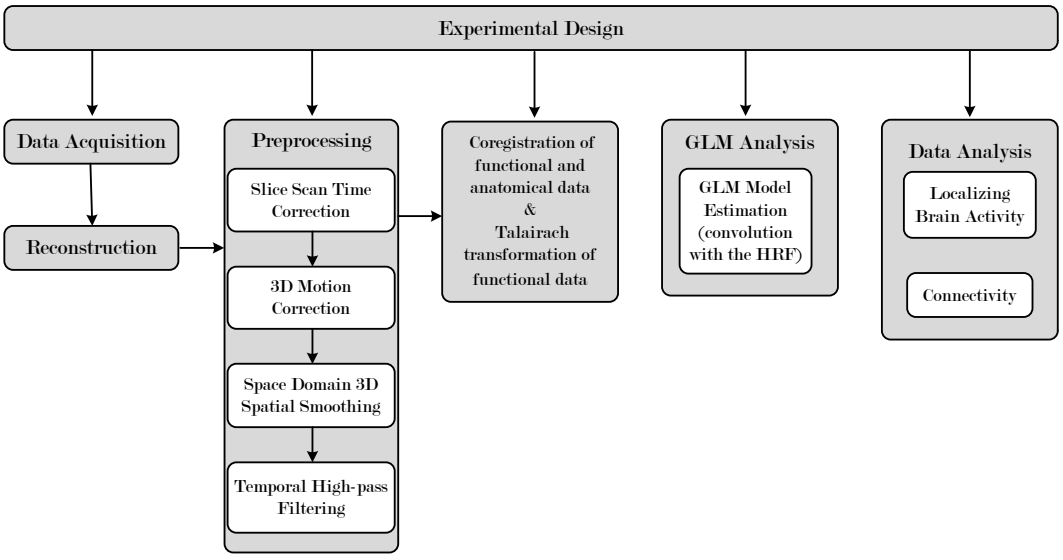

Figure 7.1: Data processing pipeline

for temporal serial correlations.

Data will be analysed using a multivariate statistical general linear model (GLM) (see Equation 7.1) of the experiment, voxel-by-voxel, with one predictor for the *tremor* condition.

$$\mathbf{X} = \mathbf{G} \cdot \beta + \varepsilon \tag{7.1}$$

X is the observation matrix for single voxel, which columns corresponds to the response variables (each one corresponding to one run) and the rows correspond to the number of scans. G is called the design matrix with each row corresponding to a scan and each column to an predictor variable. The column vector β stands for the unknown parameters corresponding to each predictor variable, with the rows corresponding to each voxel and ε are the unknown errors, i.e., the independent and identically distributed normal random variables with zero mean and variance. The GLM explains the response variable X through the linear combination of the explanatory variables plus the error term.[53,87,88]

In the present study, the explanatory variables are the tremor and non-tremor periods, which are the effects of interest that will be modelled by a boxcar function and convolved with the canonical HRF in Brain Voyager Software.[50,53]

7.3 Multi-study results

Multi session/subject experiments allow to increase sensitivity of the overall experiment since more data is available. This kind of study is important to determine if the observed effects are common and stable across, or between, groups and allows generalization of the individual conclusions to the whole population of subjects. Since the experiment is composed of only three PD patients, each one presenting different characteristics concerning presence of rest tremor and medication withdrawal (see Section 3.1), intra-subject multi-study was not performed. A multi-study between runs for patient 1, for the unloaded conditions (runs 1, 4 and 5) is presented in Figure 7.2. Tremor vs nontremor blocks were defined as predictors using sEMG or accelerometry data (see Section 6.3).

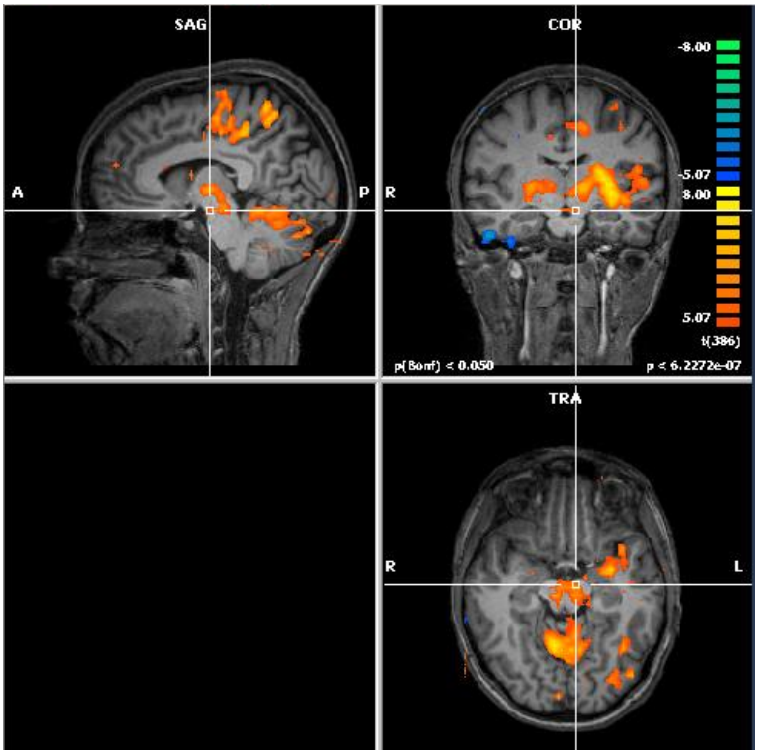

Figure 7.2: GLM multistudy of unloaded runs for patient 1 for the right dominant hand. Gray Matter nearest to (-5,-14,-11) Talairach coordinates: Left Brainstem, Midbrain, Gray Matter, Substantia Nigra.

7.4 Discussion

In this chapter the physical principles and context of fMRI were presented. This technique will allow to identify the neural circuits of the subcortical and cortical regions that are associated with tremor modulation. The GLM analysis can only be conducted having the time intervals of tremor vs nontremor obtained using the accelerometric or the sEMG signal. Comparing blocks with and without tremor (see Figure 7.2) it is possible to see activation in the substantia nigra and in areas related to motor control in the dominant hand. This approach is then able to return important and meaningful results concerning the brain oscillatory circuits responsible for PD tremor occurrence.

This preliminary analysis was important to define new steps towards a deep investigation of the PD tremors. For example, the neural loops behind rest and postural tremors generation could be determined by defining periods of tremor vs nontremor in each postural and rest segments, using a binary approach.

Another analysis called linear correlation maps could be done using the frequency band analysis (see Section 6.4), which return non binarized predictors. This analysis allows to ascertain if there are differences between the frequency

bands in terms of activation and what are the neuronal networks responsible for those activations.

Chapter 8

Conclusions

In this research signal processing tools were used to process and analyse signals acquired with two distinct and also widely used techniques, surface electromyography (sEMG) and accelerometry. Parkinson's disease (PD) tremor was assessed by acquiring the two aforementioned signals during the performance of a block defined task, in which PD patients alternated between resting and postural arm positions. In order to understand which areas activate during the performance of the task, the patients neuronal circuits were assessed in the fMRI environment. However, the acquisition characteristics inside the scanner interfere with the electromyographic signals, adding easily identifiable frequency components in the signal spectrum. Then, one of the main purposes of this study was to develop an algorithm capable of eliminate in-bore artifacts from the sEMG signal. Accelerometric signals were also pre-processed. The next step consisted in the PD tremor parameter computation, which aimed to assess the frequency spectrum and identify frequency and amplitude peaks, in each rest and postural condition, in both accelerometric and sEMG signals. Simultaneous acquisition of functional images will allow to determine which areas activate during postural and rest segments and identify the PD tremor generators. This project has clinical interest, namely in diagnosis and therapeutics. Combining the three techniques, accelerometry, sEMG and fMRI has the potential to distinguish different types of PD tremor, which can have different responses to different treatments and can evolve in different ways over the disease course.

8.1 Surface EMG artifact cleaning

Surface electromyographic signals obtained inside the scanner presented artifacts originated by the magnetic field gradient introduced during scanning process, by the radio frequency pulse (RF) and also movement artifacts.

Two algorithms were tested in order to ascertain which one had the optimal performance in a de-noising the sEMG signals.

The first developed algorithm tested different band-pass IIR filters intended to remove the high frequency content. Butterworth type returned the best results. A notch comb filter was then applied to the previous band-pass filtered signal to specifically eliminate or attenuate the interference of the magnetic field gradient seen as individual harmonically related frequencies in the spectrum. The result is a cleaned sEMG signal, with no baseline noise. Validation of the in-bore sEMG cleaning algorithm can be done by correlating the sEMG and the accelerometric signals recorded out-bore and also correlating another set of those signals acquired in-bore. High correlation between both signals for both sets of in-bore and out-bore signals will yield the validity of the algorithm. The second algorithm made use of the wavelet frequency decomposition analysis. The frequency band of interest was easily obtained however, even though the high frequency content has been correctly filtered, the magnetic field gradient artifact is still present in the signal (the frequency harmonics are still present) and would only be removed using a notch filter. This procedure was performed in the aforementioned first algorithm using the IIR filters. This wavelet approach was then considered not useful for accurately clean the sEMG signal, even though a fast and efficient frequency band discrimination has been attained.

Other studies applied IIR filters to clean sEMG signals acquired in a fMRI environment in healthy subjects[25,52,53,83] and in a PD population.[50] In the present research methods were combined in order to obtain a new method that quickly removes the fMRI artifacts from the electromyographic signals.

8.2 Parameter computation

The purpose of this chapter was to construct algorithms to investigate the effect of a task comprising rest and postural arm positions in PD tremor. Segmentation of the accelerometric and sEMG signals in the rest and postural blocks and inspection of the frequency spectrum was sufficient to be aware

of the clear differences between the two types of arm positions in PD tremor. Peak power and frequency and the total power of the spectrum were computed for accelerometry and sEMG filtered signals. The area under the curve of the sEMG envelope was also computed for each segment. Spectrogram was used to inspect the accelerometry and sEMG signals and blocks of tremor vs nontremor were identified. A frequency band analysis was also performed in order to determine the most contributing frequencies to the signals.

During postural segments it was possible to identify a distinct peak of power about 5 Hz in one patient, which could evidence the presence of reemergent rest tremor in the postural segments. A second peak of lower amplitude about 10 Hz was also found which falls in the frequency range characteristic of this postural condition. Rest segments were of considerably less power and did not presented a clear peak across the runs.

Results for the postural segments of a second patient, which did not fulfil the requirement for medication washout before the session, showed a clear peak between 6 and 7 Hz of less power comparing to the same results for the previously mentioned patient. The absence of a second peak was noted.

In the patient diagnosed with rest PD tremor, both rest and postural segments presented identifiable peaks for all runs, but second peaks were not detected. Rest segments peak power was higher comparing to postural ones. During rest segments power peaks were found near 5 Hz. On the other hand, frequency peaks for the postural segments were identified near 6 Hz.

8.3 Functional MRI analysis

Principles of this technique were described and its utility to the study of the PD tremor activated brain areas was underlined. A preliminary within runs multi-study using the identified intervals from the tremor vs nontremor analysis was performed. The sample size did not allow for a deep analysis and a larger population needs to be studied to increase the statistical power. However, a preliminary analysis of a multi-study for one of the patients showed an activation of the substantia nigra, in which dopamine-producing neurons are degenerated in PD. This analysis have the potential to together with the accelerometry and sEMG results, return important conclusions about the rest and postural tremors characterization (enabling tremor separation) and also about the correspondent generators in the brain.

8.4 Limitations & Future Work

Starting with the acquisition protocol, it must be noted that sEMG signals need to be carefully detected. Electrodes should be precisely attached to the cleaned muscle skin and the wires disposition should be thoroughly assessed. Otherwise, interferences will influence the signal and even invalidate it.

Distinguish rest from postural tremor using the spectral parameters returned through the analysis of the filtered accelerometric and sEMG signals would be possible by performing a statistical analysis in a larger, homogeneous and preferably disorder duration matched population. In order to obtain consistent results, all patients should also be in the same medication state, i.e., in pharmacological washout condition since at least 12 h before the beginning of the session. More parameters can also be computed to help distinguishing between rest and postural tremors. Furthermore, coherence studies can be performed between sEMG and accelerometric data. Future work with higher sample sizes and statistical power are also expected to confirm the preliminary observations obtained in the fMRI study and should further elucidate the about the dynamics of tremor modulation.

Finally, a feature space could be build with the tremor parameters determined in this research for a larger population. Then the best classifier would be selected and used in the classification of postural or rest tremor.

Bibliography

[1] J. Jankovic and S. Fahn, "Physiologic and pathologic tremors. Diagnosis, mechanism, and management.," *Annals of internal medicine*, vol. 93, pp. 460–5, Sept. 1980.

[2] C. W. Hess and S. L. Pullman, "Tremor: clinical phenomenology and assessment techniques.," *Tremor and other hyperkinetic movements (New York, N.Y.)*, vol. 2, Jan. 2012.

[3] D. E. Vaillancourt and K. M. Newell, "The dynamics of resting and postural tremor in Parkinson's disease.," *Clinical neurophysiology : official journal of the International Federation of Clinical Neurophysiology*, vol. 111, pp. 2046–56, Nov. 2000.

[4] P. H. G. Mansur, L. K. P. Cury, A. O. Andrade, A. a. Pereira, G. A. a. Miotto, A. B. Soares, and E. L. M. Naves, "A review on techniques for tremor recording and quantification.," *Critical reviews in biomedical engineering*, vol. 35, pp. 343–62, Jan. 2007.

[5] J. Jankovic, "Parkinson's disease: clinical features and diagnosis.," *Journal of neurology, neurosurgery, and psychiatry*, vol. 79, pp. 368–76, Apr. 2008.

[6] R. Bhidayasiri, "Differential diagnosis of common tremor syndromes.," *Postgraduate medical journal*, vol. 81, pp. 756–62, Dec. 2005.

[7] P. Crawford and E. E. Zimmerman, "Differentiation and diagnosis of tremor.," *American family physician*, vol. 83, pp. 697–702, Mar. 2011.

[8] G. Deuschl, F. Papengut, and H. Hellriegel, "The phenomenology of parkinsonian tremor.," *Parkinsonism & related disorders*, vol. 18 Suppl 1, pp. S87–9, Jan. 2012.

[9] G. Grimaldi and M. Manto, "Neurological tremor: sensors, signal processing and emerging applications.," *Sensors (Basel, Switzerland)*, vol. 10, pp. 1399–422, Jan. 2010.

[10] A. W. G. Buijink, M. F. Contarino, J. H. T. M. Koelman, J. D. Speelman, and A. F. van Rootselaar, "How to tackle tremor - systematic review of the literature and diagnostic work-up.," *Frontiers in neurology*, vol. 3, p. 146, Jan. 2012.

[11] R. C. Helmich, M. Hallett, G. Deuschl, I. Toni, and B. R. Bloem, "Cerebral causes and consequences of parkinsonian resting tremor: a tale of two circuits?," *Brain : a journal of neurology*, vol. 135, pp. 3206–26, Nov. 2012.

[12] J. M. Beitz, "Parkinson's disease: a review.," *Frontiers in bioscience (Scholar edition)*, vol. 6, pp. 65–74, Jan. 2014.

[13] M. A. Thenganatt and J. Jankovic, "Parkinson disease subtypes.," *JAMA neurology*, vol. 71, pp. 499–504, Apr. 2014.

[14] T. B. Sherer, S. Chowdhury, K. Peabody, and D. W. Brooks, "Overcoming obstacles in Parkinson's disease.," *Movement disorders : official journal of the Movement Disorder Society*, vol. 27, pp. 1606–11, Nov. 2012.

[15] W. J. Elias and B. B. Shah, "Tremor.," *JAMA*, vol. 311, pp. 948–54, Mar. 2014.

[16] M. Edwards, N. Quinn, and K. Bhatia, "Parkinson's disease," in *Parkinson's Disease and Other Movement Disorders (Oxford Specialist Handbooks in Neurology)*, ch. 3, pp. 17–80, Oxford: Oxford University Press, 2008.

[17] J. Jankovic, K. S. Schwartz, and W. Ondo, "Re-emergent tremor of Parkinson's disease," *Journal of Neurology, Neurosurgery & Psychiatry*, vol. 67, pp. 646–650, Nov. 1999.

[18] E. D. Louis, S. L. Pullman, D. Eidelberg, and V. Dhawan, "Re-emergent tremor without accompanying rest tremor in Parkinson's disease," *Canadian Journal of Neurological Sciences*, vol. 35, pp. 513–515, 2008.

[19] C. Duval, "Rest and postural tremors in patients with Parkinson's disease.," *Brain research bulletin*, vol. 70, pp. 44–8, June 2006.

[20] N. Maurits, "Tremor, Polymyography, and Spectral Analysis," in *From Neurology to Methodology and Back: An Introduction to Clinical Neuroengineering*, ch. 3, pp. 33–66, New York, NY: Springer New York, 2012.

[21] P. Faria, M. Patrício, G. Philipiak, F. Caramelo, C. Januário, A. Freire, and M. Castelo-Branco, "Tremor modulations across periods with and without voluntary motion and limb load task demands using movement quantification.," *Conference proceedings : ... Annual International Conference of the IEEE Engineering in Medicine and Biology Society. IEEE Engineering in Medicine and Biology Society. Annual Conference*, vol. 2013, pp. 4338–41, Jan. 2013.

[22] P. Faria, A. Leal, A. Freire, C. Januário, M. Patrício, and M. Castelo-Branco, "Quantification and Modulation of Tremor in Rapid Upper Limb Movements," in *The International Conference on Health Informatics SE - 86* (Y.-T. Zhang, ed.), vol. 42 of *IFMBE Proceedings*, pp. 339–342, Springer International Publishing, 2014.

[23] P. Pascoal-Faria, M. Patrício, A. Leal, F. Caramelo, A. Freire, C. Januário, and M. Castelo-Branco, "Understanding Tremor in Rapid Upper Limb Movements Using 3D Accelerometers Data," *Neuroscience & Medicine*, vol. 05, pp. 205–213, Oct. 2014.

[24] a. J. Stoessl, W. W. Martin, M. J. McKeown, and V. Sossi, "Advances in imaging in Parkinson's disease.," *Lancet neurology*, vol. 10, pp. 987–1001, Nov. 2011.

[25] H. van Duinen, I. Zijdewind, H. Hoogduin, and N. Maurits, "Surface EMG measurements during fMRI at 3T: accurate EMG recordings after artifact correction.," *NeuroImage*, vol. 27, pp. 240–6, Aug. 2005.

[26] G. Grimaldi and M. Manto, "Tremor: From Pathogenesis to Treatment," *Synthesis Lectures on Biomedical Engineering*, vol. 3, pp. 1–212, Jan. 2008.

[27] M. Hallett, "Tremor: pathophysiology.," *Parkinsonism & related disorders*, vol. 20 Suppl 1, pp. S118–22, Jan. 2014.

[28] M. Hallett, "Parkinson's disease tremor: pathophysiology.," *Parkinsonism & related disorders*, vol. 18 Suppl 1, pp. S85–6, Jan. 2012.

[29] M. Edwards, N. Quinn, and K. Bhatia, "Tremor," in *Parkinson's Disease and Other Movement Disorders (Oxford Specialist Handbooks in Neurology)*, ch. 5, pp. 101–118, Oxford: Oxford University Press, 2008.

[30] E. D. Louis, G. Levy, L. J. Côte, H. Mejia, S. Fahn, and K. Marder, "Clinical correlates of action tremor in Parkinson disease.," *Archives of neurology*, vol. 58, pp. 1630–4, Oct. 2001.

[31] J. a. Massano and K. P. Bhatia, "Clinical approach to Parkinson's disease: features, diagnosis, and principles of management.," *Cold Spring Harbor perspectives in medicine*, vol. 2, p. a008870, June 2012.

[32] J. a. Burne, T. Blanche, and J. J. Morris, "Muscle loading as a method to isolate the underlying tremor components in essential tremor and Parkinson's disease.," *Muscle & nerve*, vol. 30, pp. 347–55, Sept. 2004.

[33] K. C. Veluvolu and W. T. Ang, "Estimation of physiological tremor from accelerometers for real-time applications.," *Sensors (Basel, Switzerland)*, vol. 11, pp. 3020–36, Jan. 2011.

[34] C. R. Baumann, "Epidemiology, diagnosis and differential diagnosis in Parkinson's disease tremor.," *Parkinsonism & related disorders*, vol. 18 Suppl 1, pp. S90–2, Jan. 2012.

[35] A. J. Lees, J. Hardy, and T. Revesz, "Parkinson's disease.," *Lancet*, vol. 373, pp. 2055–66, June 2009.

[36] F. J. A. Meijer and B. Goraj, "Brain MRI in Parkinson's disease.," *Frontiers in bioscience (Elite edition)*, vol. 6, pp. 360–9, Jan. 2014.

[37] I.-S. Hwang, C.-C. K. Lin, and P.-S. Wu, "Tremor modulation in patients with Parkinson's disease compared to healthy counterparts during loaded postural holding.," *Journal of electromyography and kinesiology : official journal of the International Society of Electrophysiological Kinesiology*, vol. 19, pp. e520–8, Dec. 2009.

[38] M. Conn, *Neuroscience in Medicine*. Humana Press, 3 ed., 2008.

[39] M. Edwards, N. Quinn, and K. Bhatia, "Approach to patients," in *Parkinson's Disease and Other Movement Disorders (Oxford Specialist Handbooks in Neurology)*, ch. 1, pp. 1–7, Oxford: Oxford University Press, 2008.

[40] S. M. Rissanen, M. Kankaanpää, M. P. Tarvainen, A. Y. Meigal, J. Nuutinen, I. M. Tarkka, O. Airaksinen, and P. A. Karjalainen, "Analysis of dynamic voluntary muscle contractions in Parkinson's disease.," *IEEE transactions on bio-medical engineering*, vol. 56, pp. 2280–8, Sept. 2009.

[41] J. I. Hoff, E. a. Wagemans, and B. J. van Hilten, "Ambulatory Objective Assessment of Tremor in Parkinson's Disease," *Clinical Neuropharmacology*, vol. 24, pp. 280–283, Sept. 2001.

[42] M. Smeja, F. Foerster, G. Fuchs, D. Emmans, A. Hornig, and J. Fahrenberg, "24-h Assessment of Tremor Activity and Posture in Parkinson's Disease by Multi-Channel Accelerometry," *Journal of Psychophysiology*, vol. 13, pp. 245–256, Oct. 1999.

[43] R. Oldfield, "The assessment and analysis of handedness: The Edinburgh inventory," *Neuropsychologia*, vol. 9, pp. 97–113, Mar. 1971.

[44] V. Rajaraman, D. Jack, S. V. Adamovich, W. Hening, J. Sage, and H. Poizner, "A novel quantitative method for 3D measurement of Parkinsonian tremor.,"

Clinical neurophysiology : official journal of the International Federation of Clinical Neurophysiology, vol. 111, pp. 338–43, Feb. 2000.

[45] J. Kulisevsky, A. Avila, M. Barbanoj, R. Antonijoan, J. Torres, and R. Arcelus, "Levodopa does not aggravate postural tremor in Parkinson's disease.," *Clinical neuropharmacology*, vol. 18, pp. 435–42, Oct. 1995.

[46] M. M. Sturman, D. E. Vaillancourt, L. V. Metman, R. A. E. Bakay, and D. M. Corcos, "Effects of subthalamic nucleus stimulation and medication on resting and postural tremor in Parkinson's disease.," *Brain : a journal of neurology*, vol. 127, pp. 2131–43, Sept. 2004.

[47] V. Hömberg, H. Hefter, K. Reiners, and H. J. Freund, "Differential effects of changes in mechanical limb properties on physiological and pathological tremor.," *Journal of neurology, neurosurgery, and psychiatry*, vol. 50, pp. 568–79, May 1987.

[48] R. Wenzelburger, J. Raethjen, K. Löffler, H. Stolze, M. Illert, and G. Deuschl, "Kinetic tremor in a reach-to-grasp movement in Parkinson's disease.," *Movement disorders : official journal of the Movement Disorder Society*, vol. 15, pp. 1084–94, Nov. 2000.

[49] H. Makabe and K. Sakamoto, "Judgment of disability stages in Parkinson disease patients due to pathological tremor of index finger.," *Electromyography and clinical neurophysiology*, vol. 40, no. 7, pp. 397–409, 2000.

[50] L. Subramanian, J. V. Hindle, S. Johnston, M. V. Roberts, M. Husain, R. Goebel, and D. Linden, "Real-time functional magnetic resonance imaging neurofeedback for treatment of Parkinson's disease.," *The Journal of neuroscience : the official journal of the Society for Neuroscience*, vol. 31, pp. 16309–17, Nov. 2011.

[51] P. Konrad, *The ABC of EMG - A Practical Introduction to Kinesiological EMG*. No. March, version 1. ed., 2006.

[52] G. Ganesh, D. W. Franklin, R. Gassert, H. Imamizu, and M. Kawato, "Accurate real-time feedback of surface EMG during fMRI.," *Journal of neurophysiology*, vol. 97, pp. 912–20, Jan. 2007.

[53] A.-F. van Rootselaar, N. M. Maurits, R. Renken, J. H. T. M. Koelman, J. M. Hoogduin, K. L. Leenders, and M. A. J. Tijssen, "Simultaneous EMG-functional MRI recordings can directly relate hyperkinetic movements to brain activity.," *Human brain mapping*, vol. 29, pp. 1430–41, Dec. 2008.

[54] W. Rose, "Mathematics and Signal Processing for Biomechanics . EMG (electromyogram) analysis.," 2014.

[55] A. I. Meigal, S. Rissanen, M. P. Tarvainen, P. A. Karjalainen, I. A. Iudina-Vassel, O. Airaksinen, and M. Kankaanpää, "Novel parameters of surface EMG in patients with Parkinson's disease and healthy young and old controls.," *Journal of electromyography and kinesiology : official journal of the International Society of Electrophysiological Kinesiology*, vol. 19, pp. e206–13, June 2009.

[56] M. Halaki and G. Karen, "Normalization of EMG Signals: To Normalize or Not to Normalize and What to Normalize to?," in *Computational Intellience in Electromyography Analysis - A Perspective on Current Applications and Future Challenges* (G. R. Naik, ed.), ch. 7, pp. 175–194, InTech, Oct. 2012.

[57] F. Büsching, U. Kulau, M. Gietzelt, and L. Wolf, "Comparison and validation of capacitive accelerometers for health care applications.," *Computer methods and programs in biomedicine*, vol. 106, pp. 79–88, May 2012.

[58] J. J. Kavanagh and H. B. Menz, "Accelerometry: a technique for quantifying movement patterns during walking.," *Gait & posture*, vol. 28, pp. 1–15, July 2008.

[59] M. Andrejasic, "MEMS ACCELEROMETERS," 2008.

[60] C. Poon, J. A. Robichaud, D. M. Corcos, J. G. Goldman, and D. E. Vaillancourt, "Combined measures of movement and force variability distinguish Parkinson's disease from essential tremor.," *Clinical neurophysiology : official journal of the International Federation of Clinical Neurophysiology*, vol. 122, pp. 2268–75, Nov. 2011.

[61] L. Fattorini, F. Felici, G. C. Filligoi, M. Traballesi, and D. Farina, "Influence of high motor unit synchronization levels on non-linear and spectral variables of the surface EMG.," *Journal of neuroscience methods*, vol. 143, pp. 133–9, Apr. 2005.

[62] S. M. Rissanen, M. Kankaanpää, A. Meigal, M. P. Tarvainen, J. Nuutinen, I. M. Tarkka, O. Airaksinen, and P. A. Karjalainen, "Surface EMG and acceleration signals in Parkinson's disease: feature extraction and cluster analysis.," *Medical & biological engineering & computing*, vol. 46, pp. 849–58, Sept. 2008.

[63] V. Lantz, "A Framework for Hand Gesture Recognition Based on Accelerometer and EMG Sensors," *IEEE Transactions on Systems, Man, and Cybernetics - Part A: Systems and Humans*, vol. 41, pp. 1064–1076, Nov. 2011.

[64] S.-K. Strambi, B. Rossi, G. De Michele, and S. Sello, "Effect of medication in Parkinson's disease: a wavelet analysis of EMG signals.," *Medical engineering & physics*, vol. 26, pp. 279–90, May 2004.

[65] G. De Michele, S. Sello, M. C. Carboncini, B. Rossi, and S.-K. Strambi, "Cross-correlation time-frequency analysis for multiple EMG signals in Parkinsons disease: a wavelet approach," *Medical Engineering & Physics*, vol. 25, pp. 361–369, June 2003.

[66] D. Abi-Abdallah, E. Chauvet, L. Bouchet-Fakri, A. Bataillard, A. Briguet, and O. Fokapu, "Reference signal extraction from corrupted ECG using wavelet decomposition for MRI sequence triggering: application to small animals.," *Biomedical engineering online*, vol. 5, p. 11, Jan. 2006.

[67] W. Y. Yang, "Analog and Digital Filters," in *Signals and Systems with MATLAB*, ch. 7, pp. 307–360, Berlin, Heidelberg: Springer Berlin Heidelberg, 2009.

[68] R. A. Losada, "Digital Filters with MATLAB," 2008.

[69] D. A. Winter, "Kinematics," in *Biomechanics and Motor Control of Human Movement*, ch. 3, p. 370, John Wiley & Sons, 4 ed., 2009.

[70] S. W. Smith, "Chebyshev Filters," in *The Scientist and Engineer's Guide to Digital Signal Processing*, ch. 20, pp. 333–342, California Technical Pub, 1st ed., 1997.

[71] D. Flament, D. Vaillancourt, T. Kempf, K. Shannon, and D. Corcos, "EMG remains fractionated in Parkinson's disease, despite practice-related improvements in performance," *Clinical Neurophysiology*, vol. 114, pp. 2385–2396, Dec. 2003.

[72] L. Ai, J. Wang, and X. Wang, "Multi-features fusion diagnosis of tremor based on artificial neural network and DS evidence theory," *Signal Processing*, vol. 88, pp. 2927–2935, Dec. 2008.

[73] I. M. Dremin, O. V. Ivanov, and V. A. Nechitailo, "Wavelets and their uses," *Physics-Uspekhi*, vol. 44, pp. 447–478, May 2001.

[74] K. Sayood, "Wavelet-Based Compression," in *Introduction to Data Compression* (K. B. T. I. t. D. C. T. E. Sayood, ed.), ch. 15, pp. 473–514, Burlington: Morgan Kaufmann, 3 ed., 2006.

[75] J. Issartel, L. Marin, P. Gaillot, T. Bardainne, and M. Cadopi, "A practical guide to time-frequency analysis in the study of human motor behavior: the contribution of wavelet transform.," *Journal of motor behavior*, vol. 38, pp. 139–59, Mar. 2006.

[76] R. Polikar, "The Wavelet Tutorial."

[77] A. Merlo, D. Farina, and R. Merletti, "A fast and reliable technique for muscle activity detection from surface EMG signals.," *IEEE transactions on biomedical engineering*, vol. 50, pp. 316–23, Mar. 2003.

[78] Y. Sheng, "Wavelet Transform," in *Transforms and Applications Handbook*, Electrical Engineering Handbook, ch. 10, CRC Press, 3 ed., Jan. 2010.

[79] J. Taelman, S. Van Huffel, and A. Spaepen, "Wavelet-independent component analysis to remove electrocardiography contamination in surface electromyography.," *Conference proceedings : ... Annual International Conference of the IEEE Engineering in Medicine and Biology Society. IEEE Engineering in Medicine and Biology Society. Annual Conference*, vol. 2007, pp. 682–5, Jan. 2007.

[80] S. W. Smith, "Moving Average Filters," in *The Scientist and Engineer's Guide to Digital Signal Processing*, ch. 15, pp. 277–284, California Technical Pub, 1st ed., 1997.

[81] N. Mamorita, T. Iizuka, A. Takeuchi, M. Shirataka, and N. Ikeda, "Development of a system for measurement and analysis of tremor using a three-axis accelerometer.," *Methods of information in medicine*, vol. 48, pp. 589–94, Jan. 2009.

[82] P. Schwingenschuh, P. Katschnig, S. Seiler, T. a. Saifee, M. Aguirregomozcorta, C. Cordivari, R. Schmidt, J. C. Rothwell, K. P. Bhatia, and M. J. Edwards, "Moving toward "laboratory-supported" criteria for psychogenic tremor.," *Movement disorders : official journal of the Movement Disorder Society*, vol. 26, pp. 2509–15, Dec. 2011.

[83] M.-G. Knuttinen, T. B. Parrish, C. Weiss, K. S. LaBar, D. R. Gitelman, J. M. Power, M.-M. Mesulam, and J. F. Disterhoft, "Electromyography as a recording system for eyeblink conditioning with functional magnetic resonance imaging.," *NeuroImage*, vol. 17, pp. 977–87, Oct. 2002.

[84] M. J. Sands and A. Levitin, "Basics of magnetic resonance imaging.," *Seminars in vascular surgery*, vol. 17, pp. 66–82, June 2004.

[85] R. J. van Geuns, P. A. Wielopolski, H. G. de Bruin, B. J. Rensing, P. M. van Ooijen, M. Hulshoff, M. Oudkerk, and P. J. de Feyter, "Basic principles of magnetic resonance imaging.," *Progress in cardiovascular diseases*, vol. 42, pp. 149–56, Jan.

[86] E. M. Haacke, R. W. Brown, M. R. Thompson, and R. Venkatesan, *Magnetic Resonance Imaging: Physical Principles and Sequence Design*. Wiley-Liss, 1st ed., 1999.

[87] S. Kiebel and A. Holmes, "The General Linear Model," in *Human Brain Function* (R. S. J. Frackowiak, K. J. Friston, C. D. Frith, R. J. Dolan, C. J. Price, S. Zeki, J. T. Ashburner, and W. D. B. T. H. B. F. S. E. Penny, eds.), ch. 37, pp. 725–760, Burlington: Academic Press, 2 ed., 2004.

[88] K. J. Friston, A. P. Holmes, K. J. Worsley, J.-P. Poline, C. D. Frith, and R. S. J. Frackowiak, "Statistical parametric maps in functional imaging: A general linear approach," *Human Brain Mapping*, vol. 2, pp. 189–210, Oct. 1994.

Appendix A

UPDRS Section III: Motor Examination

18. **Speech**

0 = Normal.
1 = Slight loss of expression, diction and/or volume.
2 = Monotone, slurred but understandable; moderately impaired.
3 = Marked impairment, difficult to understand.
4 = Unintelligible.

19. **Facial Expression**

0 = Normal.
1 = Minimal hypomimia, could be normal 'poker face'.
2 = Slight but definitely abnormal diminution of facial expression.
3 = Moderate hypomimia; lips parted some of the time.
4 = Masked or fixed facies with severe or complete loss of facial expression;lips parted 1/4 inch or more.
5 = Tremor at rest (head, upper and lower extremities)

20. **Tremor at rest (head, upper and lower extremities)**

0 = Absent.
1 = Slight and infrequently present.
2 = Mild in amplitude and persistent. Or moderate in amplitude, but only intermittently present.
3 = Moderate in amplitude and present most of the time.
4 = Marked in amplitude and present most of the time.

21. **Action or Postural Tremor of hands**

0 = Absent.
1 = Slight; present with action.

2 = Moderate in amplitude, present with action.
3 = Moderate in amplitude with posture holding as well as action.
4 = Marked in amplitude; interferes with feeding.

22. **Rigidity (Judged on passive movement of major joints with patient relaxed in sitting position. Cogwheeling to be ignored.)**

0 = Absent.
1 = Slight or detectable only when activated by mirror or other movements.
2 = Mild to moderate.
3 = Marked, but full range of motion easily achieved.
4 = Severe, range of motion achieved with difficulty.

23. **Finger Taps (Patient taps thumb with index finger in rapid succession.)**

0 = Normal.
1 = Mild slowing and/or reduction in amplitude.
2 = Moderately impaired. Definite and early fatiguing. May have occasional arrests in movement.
3 = Severely impaired. Frequent hesitation in initiating movements or arrests in ongoing movement.
4 = Can barely perform the task.

24. **Hand Movements (Patient opens and closes hands in rapid succession.)**

0 = Normal.
1 = Mild slowing and/or reduction in amplitude.
2 = Moderately impaired. Definite and early fatiguing. May have occasional arrests in movement.
3 = Severely impaired. Frequent hesitation in initiating movements or arrests in ongoing movement.
4 = Can barely perform the task.

25. **Rapid Alternating Movements of Hands (Pronation-supination movements of hands, vertically and horizontally, with as large an amplitude as possible, both hands simultaneously.)**

0 = Normal.
1 = Mild slowing and/or reduction in amplitude.
2 = Moderately impaired. Definite and early fatiguing. May have occasional arrests in movement.
3 = Severely impaired. Frequent hesitation in initiating movements or arrests in ongoing movement.
4 = Can barely perform the task.

26. **Leg Agility (Patient taps heel on the ground in rapid succession picking up entire leg. Amplitude should be at least 3 inches.)**

0 = Normal.
1 = Mild slowing and/or reduction in amplitude.
2 = Moderately impaired. Definite and early fatiguing. May have occasional arrests in movement.
3 = Severely impaired. Frequent hesitation in initiating movements or arrests in ongoing movement.
4 = Can barely perform the task.

27. **Arising from Chair (Patient attempts to rise from a straightbacked chair, with arms folded across chest.)**

0 = Normal.
1 = Slow; or may need more than one attempt.
2 = Pushes self up from arms of seat.
3 = Tends to fall back and may have to try more than one time, but can get up without help.
4 = Unable to arise without help.

28. **Posture**

0 = Normal erect.
1 = Not quite erect, slightly stooped posture; could be normal for older person.
2 = Moderately stooped posture, definitely abnormal; can be slightly leaning to one side.
3 = Severely stooped posture with kyphosis; can be moderately leaning to one side.
4 = Marked flexion with extreme abnormality of posture.

29. **Gait**

0 = Normal.
1 = Walks slowly, may shuffle with short steps, but no festination (hastening steps) or propulsion.
2 = Walks with difficulty, but requires little or no assistance; may have some festination, short steps, or propulsion.
3 = Severe disturbance of gait, requiring assistance.
4 = Cannot walk at all, even with assistance.

30. **Postural Stability (Response to sudden, strong posterior displacement produced by pull on shoulders while patient erect with eyes open and feet slightly apart. Patient is prepared.)**

0 = Normal.
1 = Retropulsion, but recovers unaided.

2 = Absence of postural response; would fall if not caught by examiner.
3 = Very unstable, tends to lose balance spontaneously.
4 = Unable to stand without assistance.

31. **Body Bradykinesia and Hypokinesia (Combining slowness, hesitancy, decreased arm swing, small amplitude, and poverty of movement in general.)**

0 = None.
1 = Minimal slowness, giving movement a deliberate character; could be normal for some persons. Possibly reduced amplitude.
2 = Mild degree of slowness and poverty of movement which is definitely abnormal. Alternatively, some reduced amplitude.
3 = Moderate slowness, poverty or small amplitude of movement.
4 = Marked slowness, poverty or small amplitude of movement.

Appendix B

Hoehn & Yahr staging

Stage 1 Symptoms on one side of the body only.

Stage 1.5 Symptoms on one side of the body only and axial symptoms.

Stage 2 Symptoms on both sides of the body; no impairment of balance.

Stage 2.5 Symptoms on both sides of the body plus recovery on the pull test.

Stage 3 Balance impairment; mild to moderate disease; physically independent.

Stage 4 Severe disability, but still able to walk or stand unassisted .

Stage 5 Wheelchair-bound or bedridden unless assisted.